Design and Analysis of Magnetic Hydrocyclones

Gang Shen

A thesis submitted to the Faculty of Graduate Studies
and Research in partial fulfillment of the requirements
for the degree of Master of Engineering

Department of Mining and Metallurgical Engineering
McGill University

ABSTRACT

The magnetic hydrocyclone is a combined centrifugal and magnetic separator which consists of a hydrocyclone and an electromagnet. The emphasis in this thesis is focussed on the design of the magnetic circuitry.

Numerical analysis is used for the evaluation of the magnetic circuitry. Five indices of the magnetic field are developed for evaluating efficiency of the magnetic circuitry.

The distribution of the magnetic field in both Fricker's and Watson's magnetic hydrocyclones is analyzed. The relationship between the index of the magnetic field and the particle (e.g. magnetite) separation is investigated.

A new design of the Watson magnetic hydrocyclone is developed. The numerical analysis shows that the new magnetic circuitry is an improvement on that of Watson's original design. Based on computed data, an optimum 16 pole magnetic circuitry is obtained.

A possible use of magnetic hydrocyclones is for recovering heavy media (e.g. magnetite or ferrosilicon) in coal washing plants. A mathematical simulation shows that a single stage Fricker magnetic hydrocyclone may recover magnetite very efficiently from either washed coal or waste provided there is a large size difference in size between media and coal. When both Fricker and the 16 pole Watson magnetic hydrocyclones are used in combination, reasonably efficient media recovery is possible, even with a 50% passing size of magnetite and coal finer than 75μm.

RESUME

L'hydrocyclone magnétique marie le séparateur magnétique à l'hydrocyclone et est constitué d'un hydrocyclone et d'un électro -aimant. On a, dans cette thèse, mis l'emphase sur l'élaboration du circuit magnétique.

On a utilisé l'analyse numérique pour évaluer le circuit magnétique. Pour évaluer l'efficacité du circuit magnétique on a mis au point cinq indices du champ magnétique.

La distribution des champs magnétiques pour les hydrocyclones de Fricker et de Watson est analysée et on a aussi étudié la relation entre l'indice du champ magnétique et la séparation de particules (e.g. magnetite).

L'hydrocyclone magnétique de Watson a été redessiné et l'analyse numérique prouve que le nouveau circuit magnétique est supérieur à l'original. Grâce aux données informatisées, on a pu obtenir une optimisation avec un circuit magnétique à 16 pôles.

Une des utilisations possibles de l'hydrocyclone magnétique consiste à récupérer du matériel utilisé en milieu dense (e g. magnetite ou ferrosilice) lors du traitement (du charbon) par voie humide.

Une simulation mathématique montre qu'une passe simple par un hydrocyclone magnétique de Fricker peut fort efficacement recupérer la magnetite du charbon traité ou des rejets pourvu qu'il y ait une différence granulométique importante entre la matière alourdissante et le charbon. Lorsque les deux unités, soit le Fricker et l'hydrocyclone magnétique à 16 pôles de Watson, sont utilisés en série, on peut raisonablement récupérer la matière alourdissante, même si la granulométrie de cette dernière et du charbon montre un 50% passant 75 μm.

ACKNOWLEDGEMENTS

I wish to acknowledge Professor J.A.Finch, my supervisor, for his excellent advice, indefatigable help and financial support in my study.

I also wish to acknowledge all members in the mineral processing group for helpful discussions.

TABLE OF CONTENTS

ABSTRACT i

RESUME ii

ACKNOWLEDGEMENTS iii

TABLE OF CONTENTS iv

LIST OF SYMBOLS viii

LIST OF FIGURES xii

LIST OF TABLES xv

CHAPTER 1 INTRODUCTION 1

1.1. GENERAL INFORMATION ON MAGNETIC HYDROCYCLONES 5

1.1.1. Flow Patterns in The Hydrocyclone Chamber 5

1.1.2. Magnetic Field in The Hydrocyclone Chamber 5

1.1.3. Forces Acting on A Particle 7

1.1.4. Behavior of Particles 8

1.1.5. Equilibrium Orbit Hypothesis and Cut Size 9

1.2. FRICKER'S MAGNETIC HYDROCYCLONE 11

1.2.1. Main Design Features 11

1.2.2. Experiments and Results 13

1.3. WATSON'S MAGNETIC HYDROCYCLONE 13

1.3.1. Main Design Features 13

1.3.2. Experiments and Results 17

CHAPTER 2 NUMERICAL ANALYSIS METHOD 18

2.1. MATHEMATICAL FUNDAMENTALS 18

2.1.1. Simplification of The Three Dimensional Magnetic Field 18

2.1.2. Laplace's Equation 18

2.1.3. Finite Difference Method 20

2.2. COMPUTER PROGRAM 24

CHAPTER 3 INDICES OF A MAGNETIC FIELD 27

3.1. TWO COMPONENTS OF A FORCE FACTOR 27

3.2. INDICES OF A MAGNETIC FIELD 29

3.2.1. Indices For Magnetic Force Factor 29

3.2.2. Index For Magnetic Energy 31

3.3. CRITERION FOR EVALUATING MAGNETIC CIRCUITRY 32

CHAPTER 4 ANALYSIS OF FRICKER AND WATSON DESIGNS OF MAGNETIC HYDROCYCLONES 34

4.1. ANALYSIS OF FRICKER'S MAGNETIC HYDROCYCLONE 34

4.1.1. Features of Magnetic Field 35

4.1.2. Evaluation of Magnetic Field 39

4.1.3. Comparison Between Computed and Measured Data of Magnetic Field 41

4.1.4. Relationships Between A.R.F., Magnetic Energy and Cyclone Diameter 42

4.1.5. Forces on a Magnetite Particle 44

4.1.6. Discussion 48

4.2. ANALYSIS OF WATSON'S MAGNETIC HYDROCYCLONE 53

4.2.1. Features of Magnetic Field 53

4.2.2. Evaluation of Magnetic Field 55

4.2.3. Forces on a Magnetite Particle 59

4.2.4. Discussion 60

CHAPTER 5 THE NEW DESIGN OF WATSON MAGNETIC HYDROCYCLONE 66

5.1. A NEW DESIGN USING FOUR MAGNETIC POLES 66

5.1.1. Design Variations 66

5.1.2. Features of Magnetic Field 68

5.1.3. Comparison with Fricker's and Watson's (2-pole) Magnetic Hydrocyclones 72

5.1.4. Gradient of Magnetic Field 74

5.1.5. Effect of Design Variables 75

5.1.6. Forces on a magnetite particle and d50c,m 78

5.2. DESIGNS OF MULTIPOLE MAGNETIC CIRCUITRY 80

5.2.1. Magnetic flux patterns 82

5.2.2. Features of Magnetic Field 86

5.2.3. Effects of Design Variables 89

5.2.4. Relationship between d50c,m and cyclone diameter .. 95

CHAPTER 6 MATHEMATICAL SIMULATION OF MAGNETITE RECOVERY 105

6.1. FUNDAMENTALS OF SIMULATION 106

6.1.1. Corrected Performance Curves of Magnetic Hydrocyclones 106

6.1.2. Mathematical Model of Simulation 106

6.2. CONDITIONS OF SIMULATION 110

6.3. SIMULATION OF MEDIA (MAGNETITE) RECOVERY USING MAGNETIC HYDROCYCLONES AS SEPARATORS IN COAL WASHING PLANT 111

6.3.1. A Single Stage Fricker Magnetic Hydrocyclone 111

6.3.2. A Single Stage 16 pole Watson Magnetic Hydrocyclone 116

6.3.3. Simulation of Combination of Magnetic Hydrocyclones For Fine particles 116

CHAPTER 7 CONCLUSIONS AND SUGGESTIONS FOR FUTURE WORK 122

7.1. CONCLUSIONS 122

7.1.1. Numerical Analysis Has Been Applied to The Study of The Magnetic Hydrocyclones 122

7.1.2. Simulation Using Two Types of Magnetic Hydrocyclone Has Been Conducted 122

7.2. SUGGESTIONS FOR FUTURE WORK 123

7.2.1. Experimental Work 123

7.2.2. Numerical Analysis 123

REFERENCES 124

APPENDIX A Units and Conversions 126

APPENDIX B Cut Sizes d50 and d50c 127

LIST OF SYMBOLS

A	total area of cyclone chamber in Eq.3.1, m^2
A.A.R.F.	absolute average radial force factor, T^2/m
A.A.T.F.	absolute average tangential force factor, T^2/m
A.R.F.	average radial force factor, T^2/m
A.T.F.	average tangential force factor, T^2/m
$area_i$	area of element i, m^2
B	magnetic flux density, Tesla
Ci	function to underflow of class i, dimensionless
Ci_A	fraction reporting to underflow of class i of mineral A, dimensionless
Ci_B	fraction reporting to underflow of class i of mineral B, dimensionless
D	cyclone diameter, m
d	spherical particle diameter, m
di	characteristic size of particle size class i, μm
d*	maximum magnetite particle diameter in Eq.6.12, μm
d50c	corrected cut size of hydrocyclone, μm
$d50c,m$	corrected cut size of magnetic hydrocyclone, μm
E	magnetic energy in cyclone chamber with a unit length of 1 meter, J
Ec	magnetic energy in cyclone chamber in Eq.3.9, J
$Err_{i,n}$	relative error of the n th iteration at point i in Eq.2.19, dimensionless
Ev	magnetic energy in volume v in Eq.3.7, J
FA	fraction of mineral A in feed, dimensionless
FB	fraction of mineral B in feed, dimensionless

F_c	centrifugal force on a particle, N
F_d	drag force on a particle, N
F_m	magnetic force on a particle, N
fA_i	fraction of mineral A in size class i of feed, dimensionless
fB_i	fraction of mineral B in size class i of feed, dimensionless
f_i	force factor at point i in Fig.10, T^2/m
fr_i	radial component of f_i, T^2/m
ft_i	tangential component of f_i, T^2/m
GoA	grade of mineral A in overflow, dimensionless
GoB	grade of mineral B in overflow, dimensionless
GuA	grade of mineral A in underflow, dimensionless
GuB	grade of mineral B in underflow, dimensionless
gradH	gradient of magnetic field intensity H, A/m^2
H	magnetic field intensity, A/m
HgradH	force factor, T^2/m
H_i	H at center of element i in Fig.10, A/m
h	length of mesh. m
ha	length of arc 3-0 or arc 0-1 in Eq.2.18, m
hr	length of sector mesh on radial direction in Eq.2.18, m
$\vec{i}$	X axial unit vector in Cartesian coordinates, m
$\vec{j}$	Y axial unit vector in Cartesian coordinates, m
K	parameter in Eq.2.18
L	length of cyclone chamber, m
m	sharpness of separation coefficient, dimensionless
n	total number of area elements, dimensionless

O_A	component of mineral A in overflow, dimensionless
O_B	component of mineral B in overflow, dimensionless
P	parameter in Eq.2.18
Q	parameter in Eq.2.18
R_f	recovery of feed water to underflow, (= 0.2)
R_{OA}	recovery of mineral A in overflow, dimensionless
R_{OB}	recovery of mineral B in overflow, dimensionless
R_{UA}	recovery of mineral A in underflow, dimensionless
R_{UB}	recovery of mineral B in underflow, dimensionless
r	instantaneous distance of the particle from center of cyclone in Eq.1.1, m;
	radial variable in Eq.2.2;
	distance from point O to the origin in Eq.2.18, m
$\vec{r}$	radial unit vector in polar coordinates, m
U_A	component of mineral A in underflow, dimensionless
U_B	component of mineral B in underflow, dimensionless
v	volume of cyclone chamber in Eq.3.8, m^3
v_r	radial velocity component of flow in magnetic hydrocyclone, m/s
v_t	tangential velocity component of flow in magnetic hydrocyclone, m/s
X	coal size in Eq.6.7, mm
Y	cumulative mass fraction in Eq.6.7, %
Y'	cumulative mass fraction of magnetite finer than d in Eq.6.12, %
Y_O	yield of overflow, dimensionless
Y_U	yield of underflow, dimensionless

Greek letters

α	angular variable in Eq.2.2
$\vec{\alpha}$	angular unit vector in polar coordinates, m
ϕ	magnetic scalar potential, dimensionless
$\phi_{i,n}$	ϕ of the n th iteration at point i, dimensionless
$\phi_{i,n-1}$	ϕ of the (n - 1) th iteration at point i, dimensionless
κ	$= \kappa_p - \kappa_l$, dimensionless
κ_l	susceptibility of liquid, dimensionless
κ_p	susceptibility of particle, dimensionless
μ	viscosity of liquid, kg/m·s
μ_o	permeability of free space, $(= 4\pi \times 10^{-7}$ T*m/A)
ρ_s	density of solid, kg/m^3
ρ_l	density of liquid, kg/m^3

LIST OF FIGURES

Figure 1 Diagram of a hydrocyclone 2

Figure 2 Fricker magnetic hydrocyclone 3

Figure 3 Watson magnetic hydrocyclone 4

Figure 4 Flow patterns in a hydrocyclone 6

Figure 5 Forces acting on an orbiting particle in a magnetic hydrocyclone 10

Figure 6 Magnetic field in Fricker's magnetic hydrocyclone .. 12

Figure 7 Effect of current on magnetite recovery of overflow in Fricker magnetic hydrocyclone 15

Figure 8 The field meshes in Cartesian and polar coordinates 21

Figure 9 The flow - chart of program 25

Figure 10 The effective and ineffective component of a force factor in the magnetic hydrocyclone 28

Figure 11 Magnetic flux density B between inner pole and outer pole in Fricker magnetic hydrocyclone 36

Figure 12 Force factor between inner pole and outer pole in Fricker magnetic hydrocyclone 37

Figure 13 Comparison of computed and measured data of magnetic field in Fricker's magnetic hydrocyclone 43

Figure 14 Forces and force ratios as functions of magnetite particle size in Fricker magnetic hydrocyclone 46

Figure 15 Recovery of magnetic media by particle size from simulated dilute medium slurry 49

Figure 16 Effect of current on grade and recovery 51

Figure 17 Effect of pulp density on grade and recovery 52

Figure 18 Magnetic flux density B between two poles in Watson magnetic hydrocyclone 54

Figure 19 Force factor between two poles in Watson magnetic hydrocyclone 56

Figure 20 Forces and force ratios as functions of magnetite particle size in Watson magnetic hydrocyclone 61

Figure 21 Performance curves of magnetite and dolomite without magnetic field 62

Figure 22 Performance curves of magnetite and dolomite without magnetic field 64

Figure 23 Grade and recovery curves for separation with varying magnetic flux density 65

Figure 24 Top view of a new design for Watson magnetic hydrocyclone 67

Figure 25 Magnetic flux density B between N and S pole 69

Figure 26 Force factors between N and S pole 70

Figure 27 Forces and force ratios as functions of magnetite particle size in 4 pole design 79

Figure 28 Magnetic flux patterns of two magnetic circuitries . 83

Figure 29 Magnetic flux patterns of the 6 pole magnetic circuitry 84

Figure 30 Magnetic flux patterns of the 8 pole magnetic circuitry 85

Figure 31 Average radial force factor in cyclone chamber as a function of width ratio in new designs 90

Figure 32 Average tangential force factor in cyclone chamber as a function of width ratio in new designs 91

Figure 33 Magnetic energy in cyclone chamber as a function of width ratio in new designs 93

Figure 34 Magnetic energy in total volume as a function of width ratio in new designs 94

Figure 35 Average radial force factor in cyclone chamber as a function of cyclone diameter in new designs ... 98

Figure 36 Average tangential force factor in cyclone chamber as a function of cyclone diameter in new designs ... 99

Figure 37 Magnetic energy in cyclone chamber as a function of cyclone diameter in new designs 101

Figure 38 Magnetic energy in total volume as a function of cyclone diameter in new designs 102

Figure 39 Corrected performance curves in the Fricker magnetic hydrocyclone 107

Figure 40 Corrected performance curves in the 16 pole design of the Watson magnetic hydrocyclone 108

Figure 41 Simulation of a Fricker magnetic hydrocyclone for recovering heavy media (magnetite) in coal washing plant 114

Figure 42 Simulation of the 16 pole design of Watson magnetic hydrocyclone for recovering heavy media (magnetite) in coal washing plant 115

Figure 43 Simulation of magnetic hydrocyclones with a feed of fine magnetite and coal particles 117

Figure 44 Simulation of magnetic hydrocyclones with a feed of fine magnetite and shale particles 118

Figure 45 Simulation of a magnetic hydrocyclone circuit with a feed of fine magnetite and coal particles .. 119

Figure 46 Simulation of a magnetic hydrocyclone circuit with a feed of fine magnetite and shale particles . 120

LIST OF TABLES

Table 1 Summary of results with Fricker's magnetic hydrocyclone [3] 14

Table 2 Magnetic field distribution on pole center line in Watson's magnetic hydrocyclone [4] 16

Table 3 Computed results of B and force factor in Fricker's magnetic hydrocyclone 38

Table 4 Computed results of force factor and magnetic energy in Fricker magnetic hydrocyclone 40

Table 5 The relative error of the regressions in Fricker magnetic hydrocyclone 45

Table 6 The distribution of force factors in Watson magnetic hydrocyclone 57

Table 7 Computed results of force factor and magnetic energy in Watson's magnetic hydrocyclone 58

Table 8 The distribution of force factors in the new design . 71

Table 9 Comparison of three magnetic hydrocyclones 73

Table 10 Indices of force factor in 4 pole design 76

Table 11 Indices of magnetic energy in 4 pole design 77

Table 12 Effect of cyclone diameter on cut size in 4 pole design 81

Table 13 Indices of force factor in 8, 12 and 16 pole designs with various width of poles 87

Table 14 Indices of magnetic energy in 8, 12 and 16 pole designs with various width of poles 92

Table 15 Indices of force factor in 8, 12 and 16 pole designs with various diameter of cyclone 96

Table 16 Indices of magnetic energy in 8, 12 and 16 pole designs with various diameter of cyclone ... 100

Table 17 Effect of cyclone diameter on cut size in 16 pole design 104

Table 18 Size distribution of coal in the feed of dense-medium cyclone [7] 112

CHAPTER ONE

INTRODUCTION

The magnetic hydrocyclone is a combined centrifugal and magnetic separator consisting of a hydrocyclone and an electromagnet. A commercial hydrocyclone is shown in Fig.1. The cylindrical part is closed at the top by a cover, through which the vortex finder protrudes some distance into the cyclone body. The slurry enters the hydrocyclone through a tangential inlet which is located near the top cover The overflow carries the fine and / or low density particles through the vortex finder. The underflow, which carries the coarse and / or high density particles, leaves through the opening in the apex of the cone [1,2].

By incorporating an electromagnet a static magnetic field is generated in the hydrocyclone chamber. Depending on the design of the magnet poles, the magnetic force acting on a particle in the cyclone chamber may be radially inward or outward. Fig.2 shows a design where the magnetic force is inward and attracts particles to the overflow; this is referred to as Fricker's design since he proposed it in 1984 [3]. Fig.3 shows another design where the magnetic force is outward and attracts particles to the underflow; this is Watson's design proposed by him in 1983 [4]. Both designs have been considered in isolation; a novel aspect here is to consider them in combination to obtain high recovery and grade. The particular interest is their use for heavy media (e.g.

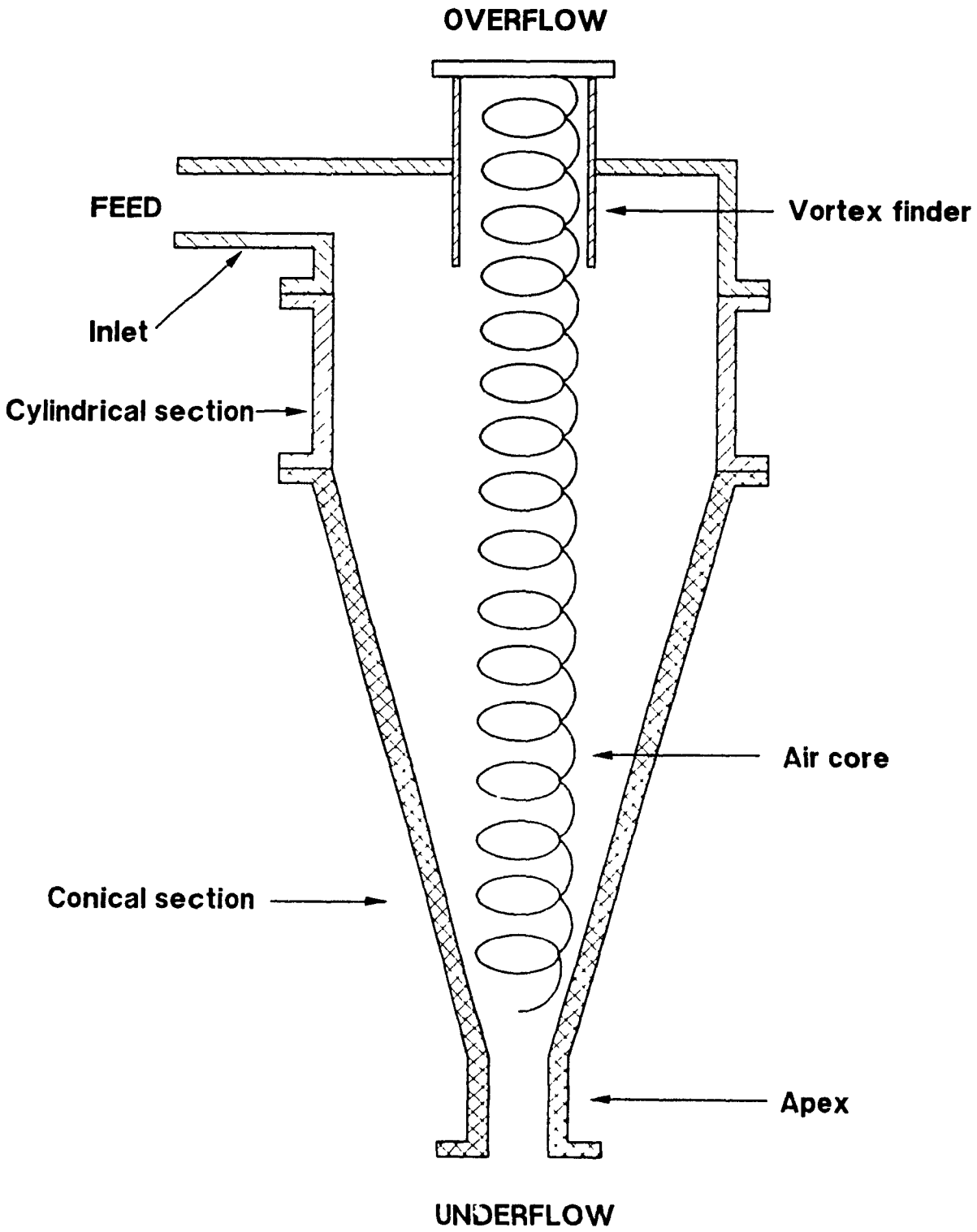

Figure 1. Diagram of a hydrocyclone

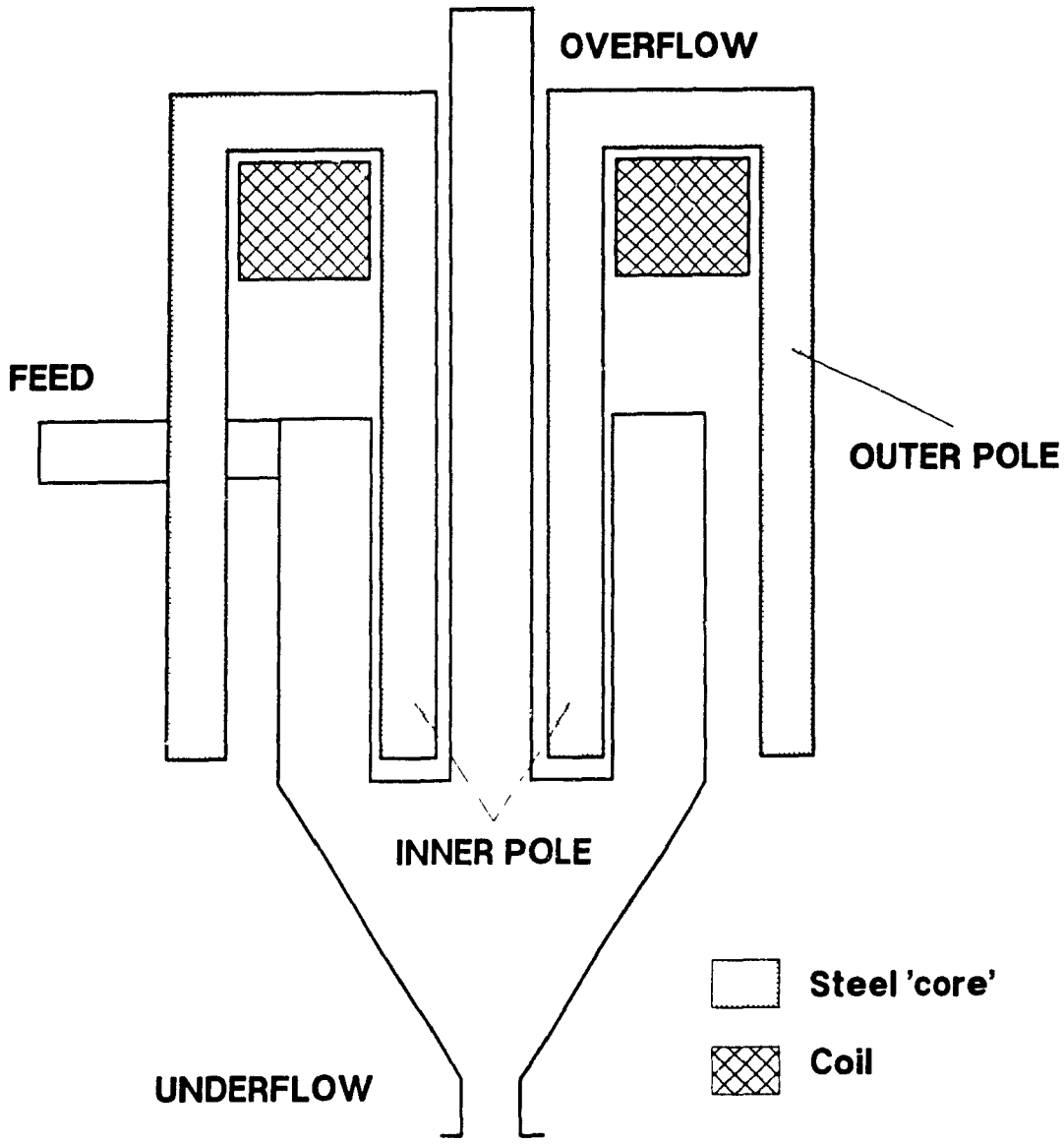

Figure 2. Fricker's magnetic hydrocyclone (After Fricker [3])

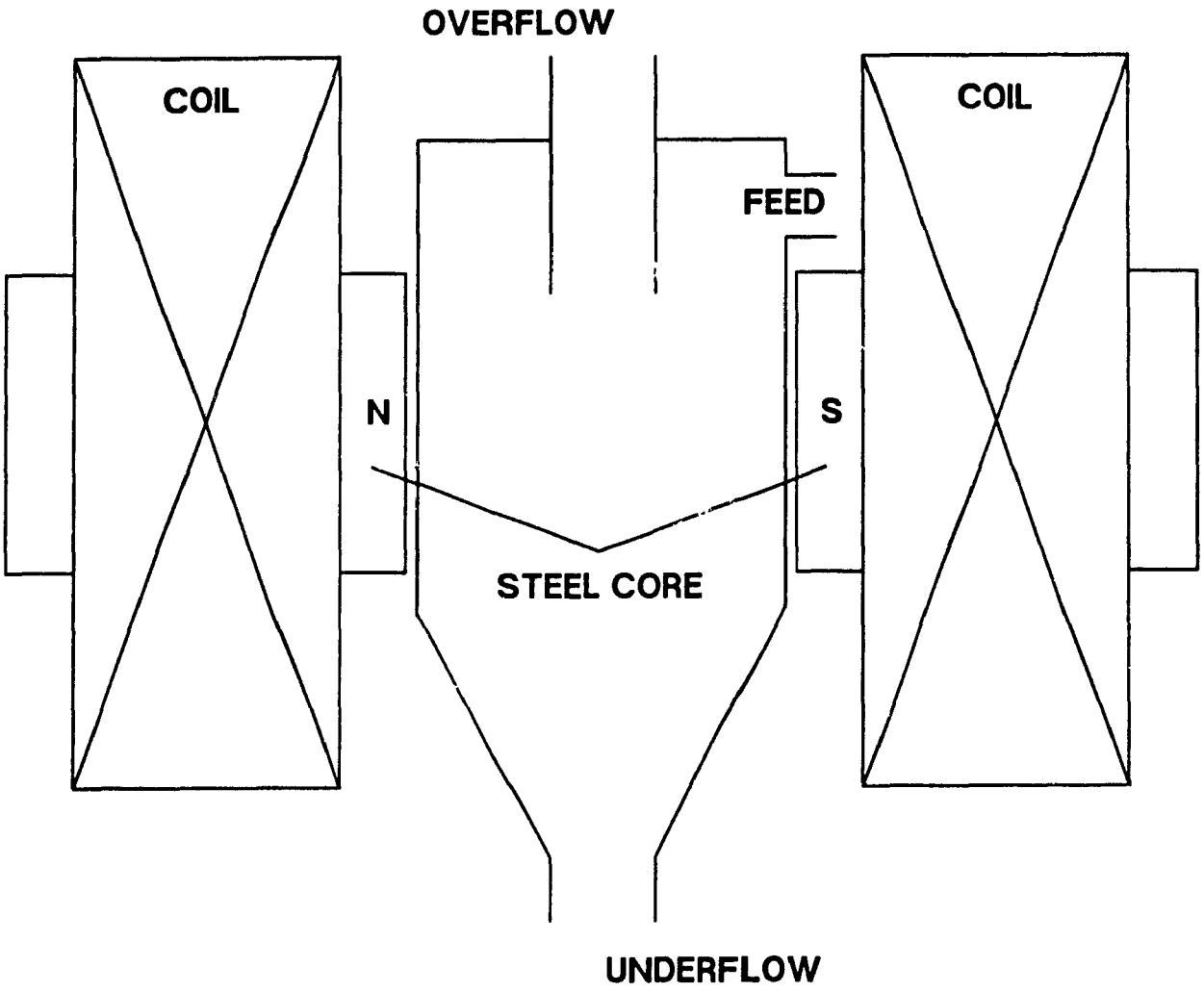

Figure 3. Watson's magnetic hydrocyclone (After Watson [4])

magnetite or ferrosilicon) recovery, for example, in coal washing plants.

1.1. GENERAL INFORMATION ON MAGNETIC HYDROCYCLONES

1.1.1. Flow Patterns in The Hydrocyclone Chamber

The most significant flow pattern in a hydrocyclone is the "spiral within a spiral". Two spirals are generated by the tangential feed and revolve in the same direction on the horizontal plane. However, along the vertical axis, the inner spiral is upwards and the outer spiral is downwards.

As shown in Fig.4, there are four features of flow patterns in the vertical plane of the hydrocyclone. The first is an air core passing through the body of the hydrocyclone, rising from the apex and passing out the vortex finder. The second is a short circuit flow against the roof. The third is eddy flows which exist in the upper section of the hydrocyclone. The fourth, an important feature of the flow patterns, is the envelope of zero vertical velocity.

1.1.2. Magnetic Field in The Hydrocyclone Chamber

Depending on the design of the magnet poles, principally the shape and the location relative to the cyclone chamber, the magnetic force acting on a particle may be radially inward or outward.

In this thesis, the magnetic hydrocyclones are divided into two types by the direction of magnetic force in the cyclone

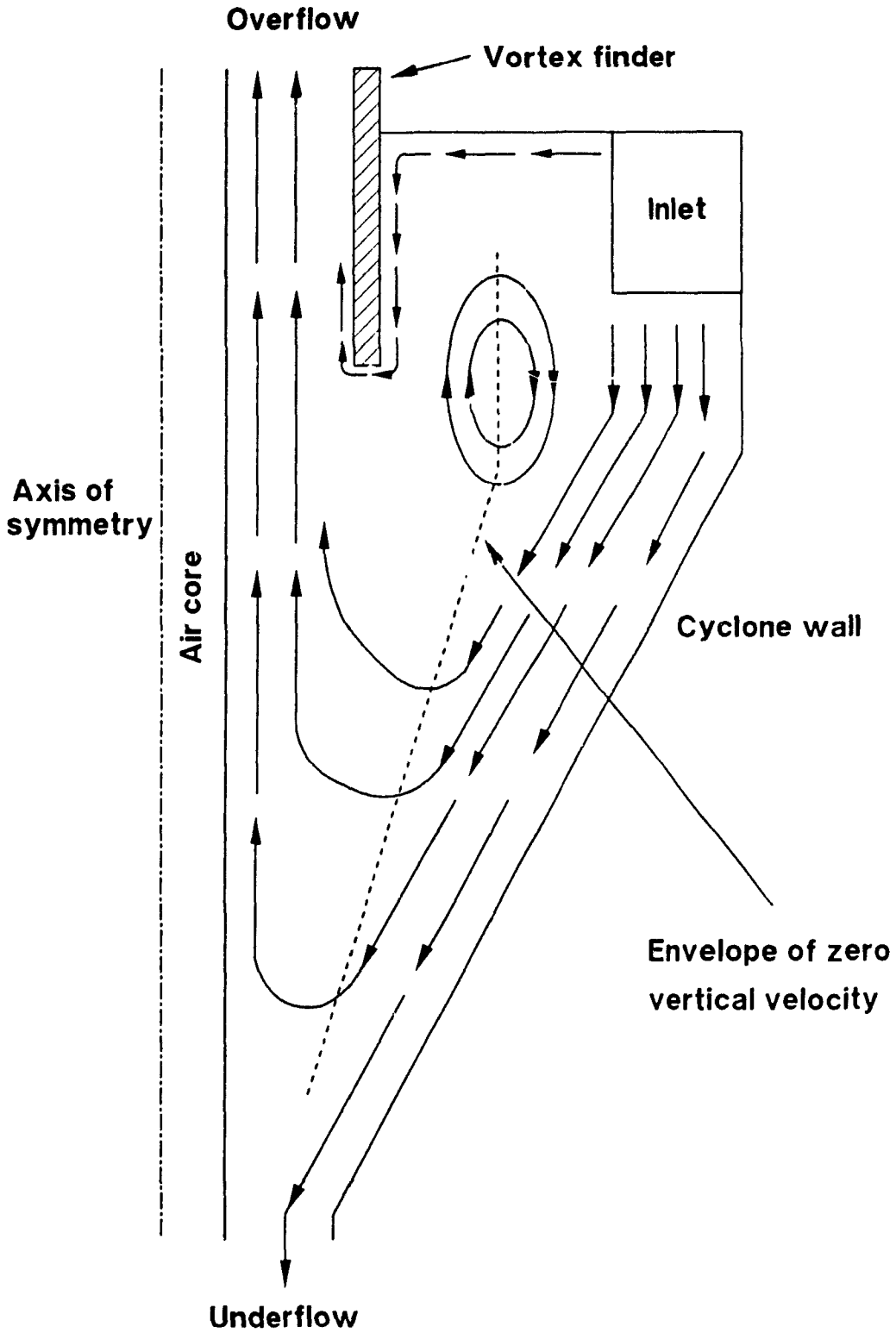

Figure 4. Flow patterns in a hydrocyclone

chamber:

A. Fricker magnetic hydrocyclone - the magnetic force is inward to the vortex finder of the cyclone.

B. Watson magnetic hydrocyclone - the magnetic force is outward to the cylindrical wall of the cyclone.

The characteristics of the two kinds of magnetic field will be discussed in detail in the following chapters.

1.1.3. Forces Acting on A Particle

In general, there are three forces acting on a particle in the magnetic hydrocyclone: an outward centrifugal force F_c, an inward drag force F_d and a magnetic force F_m [1]. Assuming the particle is spherical and flow is laminar relative to the particle, F_c and F_d are given by (unit: N):

$$F_c = \frac{\pi d^3}{6} \frac{\rho_s - \rho_l}{r} v_t^2 \qquad (1.1)$$

$$F_d = 3\pi d\mu v_r \qquad (1.2)$$

where d = the spherical particle diameter, m;

r = the instantaneous distance of the particle from the center of the cyclone, m;

μ = the viscosity of liquid, kg/m·s;

ρ_s , ρ_l = the density of solid and liquid, respectively, kg/m^3;

v_t , v_r = tangential and radial velocity components of flow in the magnetic hydrocyclone, m/s;

F_m (unit: N) is given by (see Appendix A for magnetic units):

$$F_m = \frac{\pi d^3}{6} \mu_o \kappa H \, gradH \qquad (1.3)$$

Where μ_o = the permeability of free space, $4\pi \times 10^{-7} T*m/A$;

$\kappa = \kappa_p - \kappa_l$, the susceptibility of the particle minus the susceptibility of the liquid, dimensionless;

H = the magnetic field intensity, A/m;

$gradH$ = the gradient of magnetic field intensity H, A/m^2;

The product of H and gradH (HgradH) is the most important characteristic for describing the performance of the magnetic separator, and is called the "magnetic force factor" or "force factor" for short. It can be seen that F_m is determined by the direction and magnitude of the force factor.

1.1.4. Behavior of Particles

Behavior of non - magnetic particles

Compared with F_c and F_d, F_m acting on a non - magnetic particle ($|\kappa| < 0.001$) is very small so that it can be ignored. Such particles are subjected only to two opposing forces, F_c and F_d.

Behavior of strongly magnetic particles

In the case of a ferrimagnetic particle such as a magnetite particle, the magnetic force F_m acting on it is greater than either F_c or F_d. For example, in Fricker's magnetic hydrocyclone, F_m on a 30 μm spherical magnetite particle is about 100 times greater than F_c and 80 times greater than F_d when the magnetic

flux density B is 1 Tesla on the inner pole of the magnet.

In the Fricker magnetic hydrocyclone, F_m combines with F_d. When the combined force of F_m and F_d is larger than Fc, the particle moves inward and goes to the overflow; if the combined force is less than Fc, the particle moves outward and goes to the underflow.

In the Watson magnetic hydrocyclone, F_m combines with F_c. When the combined force of F_m and F_c is larger than F_d, the particle moves outward and goes to the underflow; if the combined force is less than F_d, the particle moves inward and goes to the overflow.

1.1.5. Equilibrium Orbit Hypothesis and Cut Size

In order to avoid the confusion with d_{50c} used in the normal hydrocyclone (see Appendix B for the definition of d_{50c}), $d_{50c,m}$ is used to designate the cut size in the magnetic hydrocyclone.

The fundamental equation which calculates the cut size $d_{50c,m}$ is based on the concept of the equilibrium orbit (Fig.5) [2,8]. The force balance on a cut size particle is:

$$F_c - F_d \pm F_m = 0 \qquad (1.4)$$

Then, $d_{50c,m}$ is derived as

$$d_{50c,m} = \left[\frac{18\mu r\, v_r}{(\rho_s - \rho_l)\, v_t^2 \pm r\, \mu_o\, \kappa\, \mathrm{HgradH}} \right]^{\frac{1}{2}} \qquad (1.5)$$

In the case of the Fricker magnetic hydrocyclone, the symbol (±)

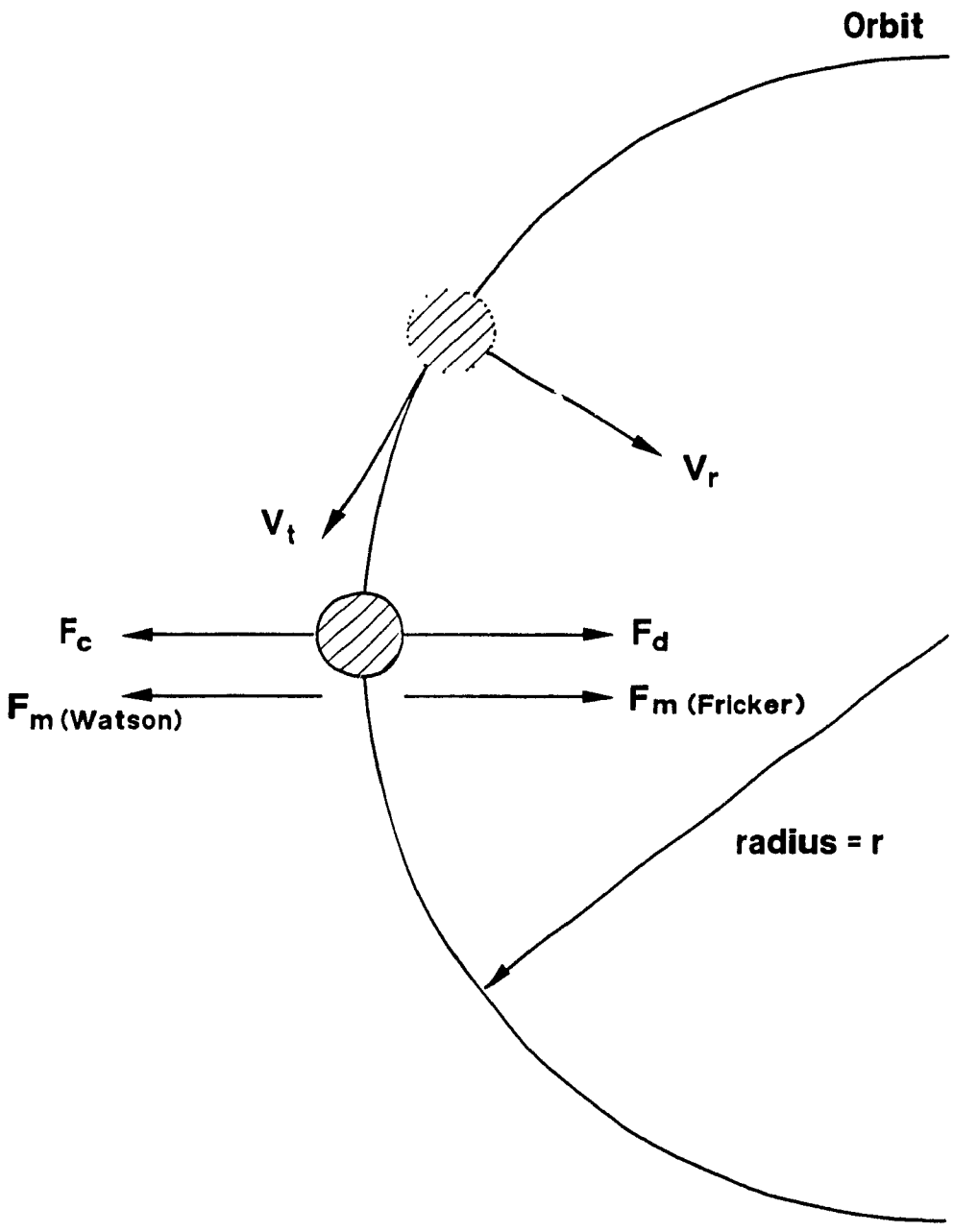

Figure 5. Forces acting on an orbiting particle in a magnetic hydrocyclone

is negative; in the case of Watson's design, it is positive.

From Eq.1.5, it can be seen that upon increasing the force factor the cut size of a ferrimagnetic particle will be increased in Fricker's magnetic hydrocyclone and decreased in Watson's. Meanwhile, the cut size of non - magnetic particles, like silica, will not be changed. Consequently separation can be changed.

1.2. FRICKER'S MAGNETIC HYDROCYCLONE

1.2.1. Main Design Features

Electromagnet design

As shown in Fig.2, an electromagnet of horseshoe section in a circumference of revolution was used. The inner pole and outer pole, which were of hollow bar and connected at one end, were concentric.

The coil was in a plane perpendicular to the axis of the poles. It was made by 400 turns of 2.0 mm copper wire and powered by a variable transformer and rectifier.

The distribution of magnetic field in the cyclone chamber is shown in Fig.6 [3].

Hydrocyclone design

From Fig.2, it can be seen that the vortex finder of the Fricker magnetic hydrocyclone is slightly longer than that of a conventional hydrocyclone, because it has to be fitted into the gap of the magnetic poles.

The test hydrocyclone was brass, 160 mm long and the cone

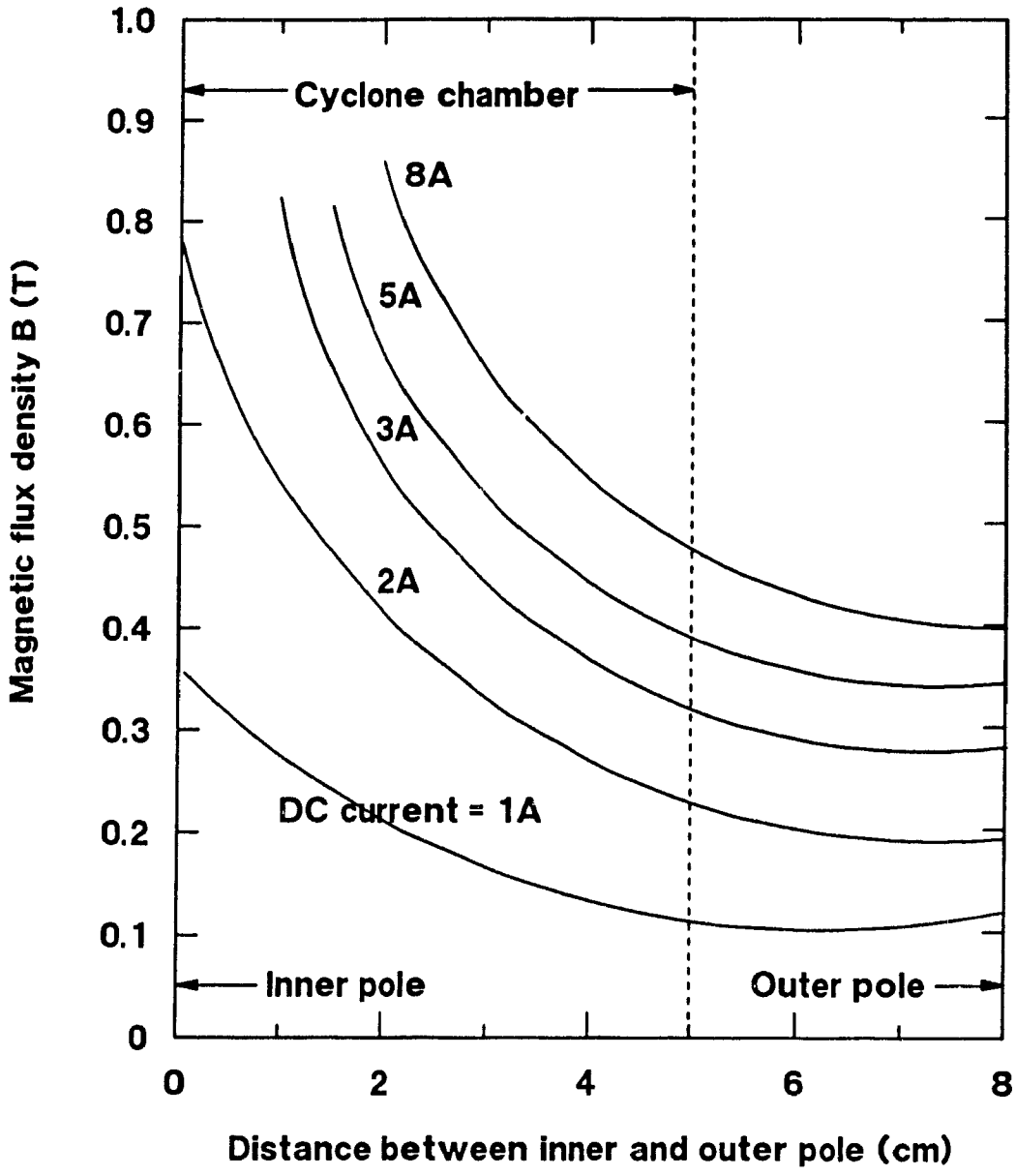

Figure 6. Magnetic field in Fricker's magnetic hydrocyclone (After Fricker [3])

angle was 54°. It had inlet, overflow, underflow and overall diameters of 35, 42, 30 and 200 mm, respectively.

1.2.2. Experiments and Results

Six samples of titanomagnetite iron sands (New Zealand) were treated in Fricker's tests. The major mineral in the samples was the titanomagnetite. The objective was to achieve the export grade of 56% iron at reasonable recovery from each sample. The results are shown in Table 1 [3].

The effectiveness of this magnetic hydrocyclone was determined by a test with an artificial feed containing 20% magnetite and 80% quartz sand between 0.1 and 1.0 mm in size. As shown in Fig.7 [3], almost all of magnetite went to the overflow with a recovery of 99% and a grade of 96% when input DC current was equal to 8A.

1.3. WATSON'S MAGNETIC HYDROCYCLONE

1.3.1. Main Design Features

Electromagnet design

Watson's design consisted of a pair of bar electromagnets, placed oppositely outside of the cyclone (Fig.3) [4].

A typical magnetic field distribution is shown in Table 2 [4] on the pole center line with two poles set 10 cm apart. The two coils were powered by a DC supply which was capable of producing a magnetic flux density B of 2.0 Tesla across the 10 cm air gap between two pole faces. From Table 2, the field gradient was at

Table 1. Summary of results with Fricker's magnetic hydrocyclone [3]

Feedstock	Feed	Product			
		single pass		two passes	
	% Fe	% Fe	% Rec.	% Fe	% Rec.
Waikato North Head					
Clay	35*	60*	55* 95* (61)	75*	
Sand	21	49	30		
Waipipi spiral tail					
January, 1982	30	47			
August, 1983	32	50	50	52	45
Taharoa	28	52	50	54	50

* Magnetics

Rec. = Recovery

The pure titanomagnetite has an iron content of about 62% .

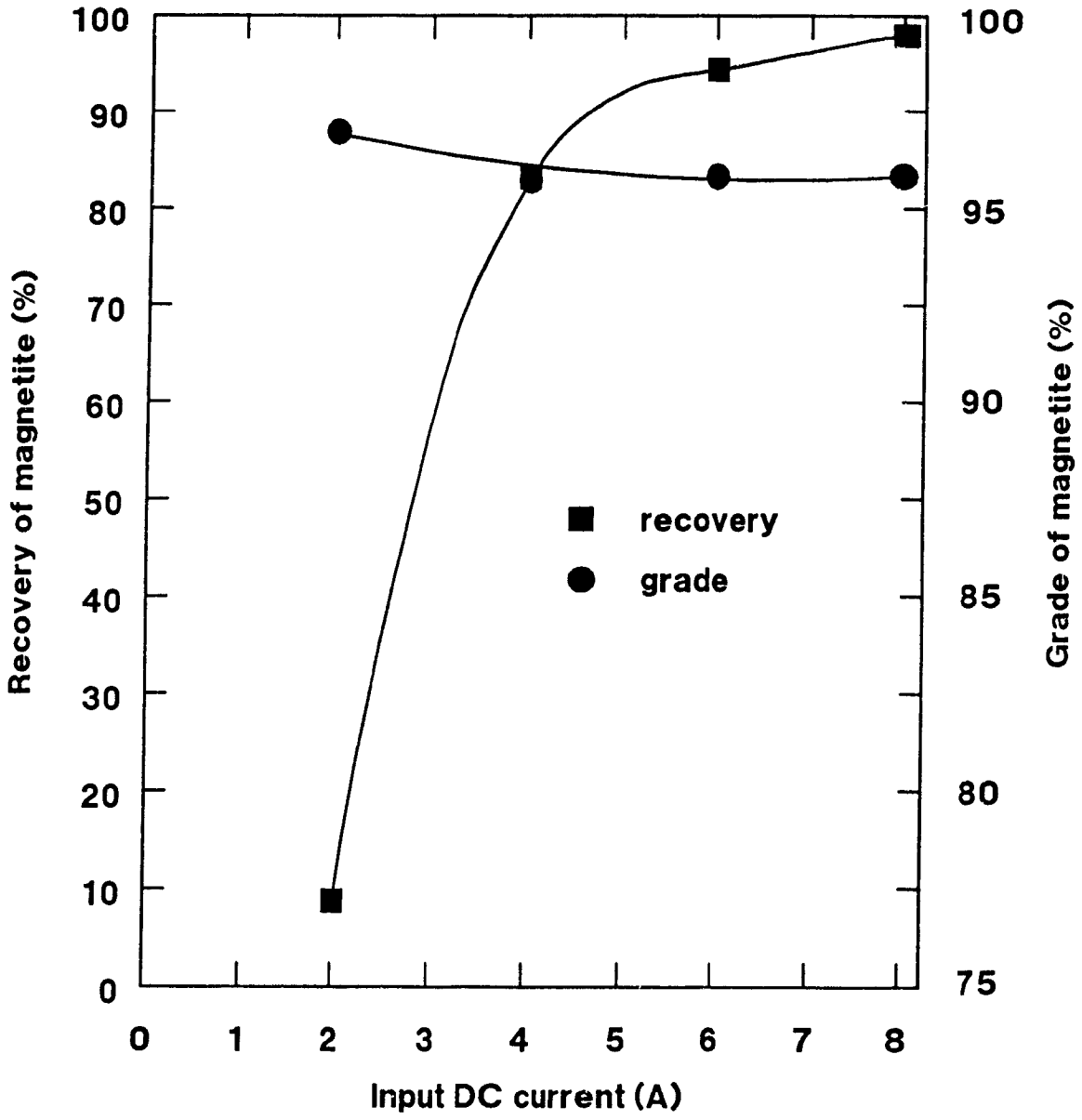

Figure 7. Effect of current on magnetite recovery of overflow in Fricker's magnetic hydrocyclone (Feed: 20% magnetite; 80% silica)

(After Fricker [3])

Table 2. Magnetic field distribution on pole center line in Watson's magnetic hydrocyclone [4]

Distance from pole face (cm)	Current (A)	0	5	10	15	20	25
		Field strength (Gauss)					
0		14	550	1070	1620	2120	2660
1.2		13	525	1030	1580	2040	2540
2.5		13	500	1000	1460	1950	2450
3.7		12	495	960	1420	1910	2340
5.0		12	490	930	1400	1880	2300

most 72 gauss/cm (0.72 Tesla/meter).

Hydrocyclone design

In Watson's tests, three magnetic hydrocyclones were used: a 10 cm diameter glass cyclone, a 7.5 cm air cyclone and a 7.5 cm diameter aluminum cyclone. The majority of experiments were carried out on the aluminum cyclone.

The aluminum cyclone had inlet, overflow and underflow of 0.5", 0.75" and 0.62", respectively. The length of the cyclone body was 8.5" and the depth of vortex finder into the cyclone body was 3.0".

1.3.2. Experiments and Results

Initial tests were carried out on the 10 cm glass magnetic hydrocyclone with a synthetic feed of titanomagnetite from New Zealand iron sands and beach sand quartz. Subsequent tests used the 7.5 cm air magnetic cyclone with a synthetic feed of dolomite / magnetite. Final tests used the 7.5 cm aluminum magnetic hydrocyclone with the feed of magnetite and the dolomite.

The typical result showed that the magnetite recovery to the underflow was about 90% with a magnetite grade of 22%, from a feed grade of 10% at a field intensity of 1000 gauss (0.1T) on the pole surface.

CHAPTER TWO

NUMERICAL ANALYSIS METHOD

Since the hydrocyclone has been studied in detail, the emphasis in this thesis is focussed on the design of the magnetic circuitry.

2.1. MATHEMATICAL FUNDAMENTALS

2.1.1. Simplification of The Three Dimensional Magnetic Field

The magnetic field in a magnetic hydrocyclone is three dimensional. In this study, this complex three dimensional problem is simplified to a two dimensional problem for two reasons.

The first reason is the symmetrical structure of the electromagnet in magnetic hydrocyclones. From Figs.2 and 3, it can be seen that two different electromagnets have a common feature: along the vertical direction, there is no variation on the shape of the magnetic poles. So we need only consider the distribution of magnetic field in the horizontal plane.

The second reason is the limitations on the speed and memory of IBM - PC/XT microcomputer. For further research, the complete distribution of the three dimensional magnetic field can be obtained with a bigger computer.

2.1.2. Laplace's Equation

In this study, the field domain of the numerical analysis is set in the chamber of the magnetic hydrocyclone. It means that the

field domain is passive, e.g. there is no "source of magnetic flux", like the magnet or coil, in the field domain.

Based on Maxwell's equations, the total points in the field domain should meet Laplace's equation [11]. In Cartesian coordinates, Laplace's equation of the magnetic scalar potential, ϕ (dimensionless), is written as

$$\nabla^2\phi = \frac{\partial^2\phi}{\partial x^2} + \frac{\partial^2\phi}{\partial y^2} = 0 \qquad (2.1)$$

In polar coordinates, setting the center of magnetic field as the origin, it becomes

$$\nabla^2\phi = \frac{\partial^2\phi}{\partial r^2} + \frac{1}{r}\frac{\partial\phi}{\partial r} + \frac{1}{r^2}\frac{\partial^2\phi}{\partial \alpha^2} = 0 \qquad (2.2)$$

where r is the radial variable and α is the angular variable.

Eq.2.1 was used in the calculation of the magnetic field of the Watson magnetic hydrocyclone. Eq.2.2 was used in the cases of the Fricker magnetic hydrocyclone and the design of the new magnetic circuitry.

In Cartesian coordinates, the relationships among ϕ, H and gradH are written as

$$\vec{H} = -\nabla\phi = -\left[\frac{\partial\phi}{\partial x}\vec{i} + \frac{\partial\phi}{\partial y}\vec{j}\right] \qquad (2.3)$$

$$\overrightarrow{\text{gradH}} = \frac{\partial H}{\partial x}\vec{i} + \frac{\partial H}{\partial y}\vec{j} \qquad (2.4)$$

and in polar coordinates:

$$\vec{H} = -\nabla\phi = -\left[\frac{\partial\phi}{\partial r}\vec{r} + \frac{1}{r}\frac{\partial\phi}{\partial \alpha}\vec{\alpha}\right] \qquad (2.5)$$

$$\overrightarrow{\text{gradH}} = \frac{\partial H}{\partial r}\vec{r} + \frac{1}{r}\frac{\partial H}{\partial \alpha}\vec{\alpha} \qquad (2.6)$$

Where equations are vector equations; $\vec{i}$ is X axial unit vector and $\vec{j}$ is Y axial unit vector in Cartesian coordinates (Fig.8(a)); $\vec{r}$ is the radial unit vector and $\vec{\alpha}$ is the angular unit vector in polar coordinates (Fig.8(b)).

2.1.3. Finite Difference Method

The finite difference method is a numerical method which can be used to obtain the solution, to any desired accuracy, of the differential equations, in the case of Eqs.2.1 and 2.2. In replacing the magnetic field equations by a set of finite difference equations which connect values of the magnetic scalar potential function, the first task is the distribution of points.

Distribution of Points in Field Domain

Any distribution of points can be used in the field, such as a triangular mesh, hexagonal mesh or an irregular mesh. However, the square mesh and the sector mesh are two of the most popular types.

Basic Equations for The Square Mesh

Point O and its neighboring points 1, 2, 3 and 4 are shown in Fig.8(a). The length h, referred to as the mesh length, is small compared with the boundary dimensions.

The difference equation is developed by expanding the magnetic scalar potential ϕ at point O in Taylor's series and deriving

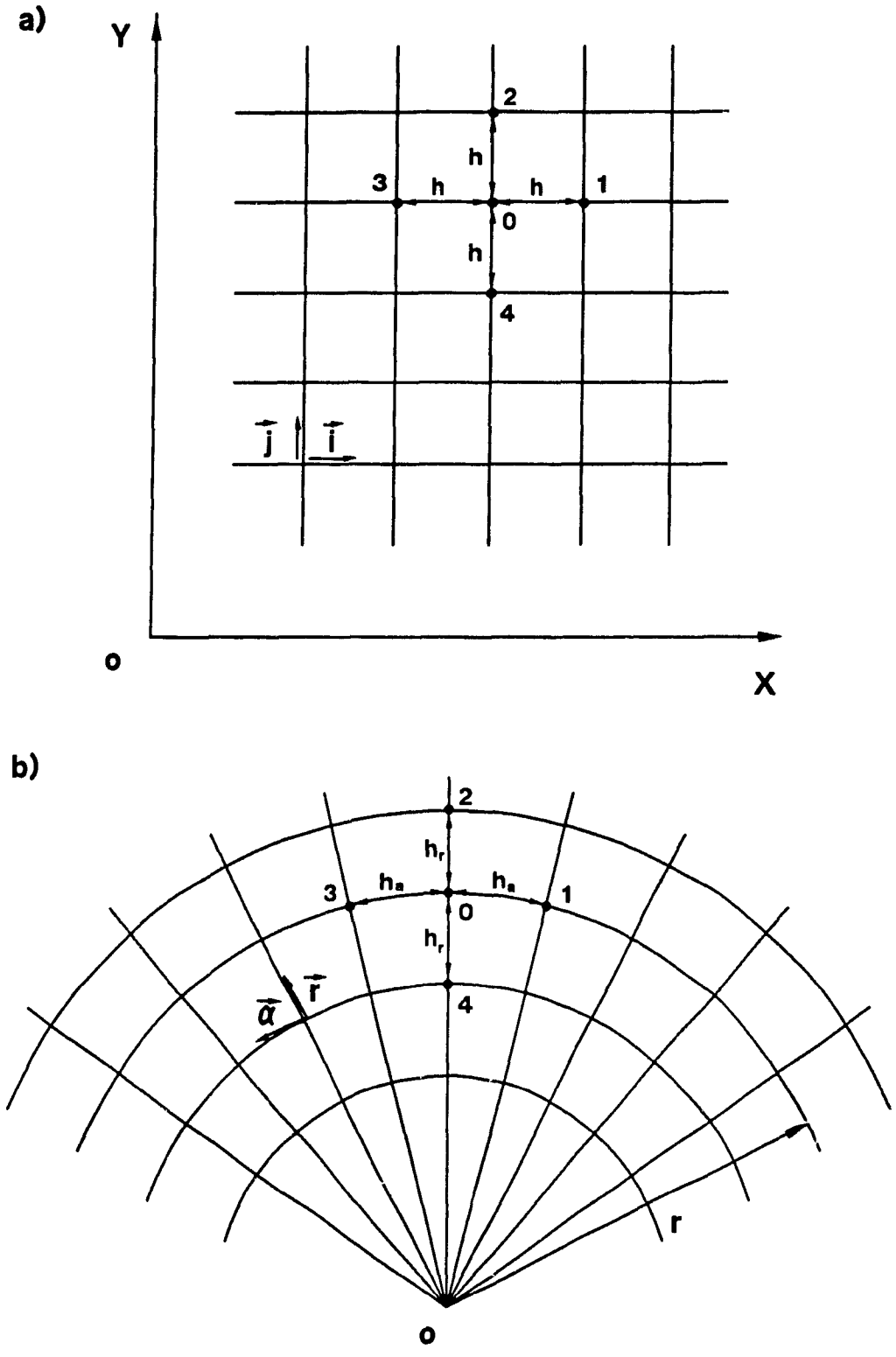

Figure 8. The field meshes in Cartesian and polar coordinates

expression for $(\partial^2\phi/\partial x^2)_o$ and $(\partial^2\phi/\partial y^2)_o$ which are substituted in Eq.2.1.

At any point x, ϕ can be expanded in terms of the ϕ_o at point 0 by the use of Taylor's series:

$$\phi = \phi_o + \left[\frac{\partial \phi}{\partial x}\right]_o (x - x_o) + \frac{1}{2!}\left[\frac{\partial^2 \phi}{\partial x^2}\right]_o (x - x_o)^2 + \frac{1}{3!}\left[\frac{\partial^3 \phi}{\partial x^3}\right]_o (x - x_o)^3 + \cdots \qquad (2.7)$$

Thus, substituting in this equation for the values $x_1 = x_o + h$ and $x_3 = x_o - h$ yields the values of ϕ at the points 1 and 3 respectively as follows

$$\phi_1 = \phi_o + h\left[\frac{\partial \phi}{\partial x}\right]_o + \frac{1}{2!}h^2\left[\frac{\partial^2 \phi}{\partial x^2}\right]_o + \frac{1}{3!}h^3\left[\frac{\partial^3 \phi}{\partial x^3}\right]_o + \cdots \qquad (2.8)$$

$$\phi_3 = \phi_o - h\left[\frac{\partial \phi}{\partial x}\right]_o + \frac{1}{2!}h^2\left[\frac{\partial^2 \phi}{\partial x^2}\right]_o - \frac{1}{3!}h^3\left[\frac{\partial^3 \phi}{\partial x^3}\right]_o + \cdots \qquad (2.9)$$

Forming the sum of Eqs.2.8 and 2.9 gives

$$\phi_1 + \phi_3 = 2\phi_o + h^2\left[\frac{\partial^2 \phi}{\partial x^2}\right]_o + \cdots \qquad (2.10)$$

Ignoring terms containing h to the power four or more, the simple expression for $(\partial^2\phi/\partial x^2)_o$ is

$$\left[\frac{\partial^2 \phi}{\partial x^2}\right]_o = \phi_1 + \phi_3 - 2\phi_o \qquad (2.11)$$

In an analogous manner, an expression for $(\partial^2\phi/\partial y^2)_o$ can be obtained, namely

$$\left[\frac{\partial^2 \phi}{\partial y^2}\right]_o = \phi_2 + \phi_4 - 2\phi_o \qquad (2.12)$$

Substituting Eqs. 2.11 and 2.12 in Eq.2.1, Laplace's equation for the point 0 not adjacent to a boundary is

$$\phi_1 + \phi_2 + \phi_3 + \phi_4 - 4\phi_o = 0 \qquad (2.13)$$

In order to solve H in Eq.2.3, $(\partial\phi/\partial x)$ and $(\partial\phi/\partial y)$ have to be obtained. Forming the difference of Eqs. 2.8 and 2.9 and ignoring the terms containing h to power three or more, the expression of $(\partial\phi/\partial x)o$ is

$$\left[\frac{\partial \phi}{\partial x}\right]_o = \frac{\phi_1 - \phi_3}{2h} \qquad (2.14)$$

In the same manner, $(\partial\phi/\partial y)o$ is written as

$$\left[\frac{\partial \phi}{\partial y}\right]_o = \frac{\phi_2 - \phi_4}{2h} \qquad (2.15)$$

The terms of $(\partial H/\partial x)o$ and $(\partial H/\partial y)o$ are obtained by a similar method

$$\left[\frac{\partial H}{\partial x}\right]_o = \frac{H_1 - H_3}{2h} \qquad (2.16)$$

$$\left[\frac{\partial H}{\partial y}\right]_o = \frac{H_2 - H_4}{2h} \qquad (2.17)$$

Basic Equations for The Sector Mesh

Fig.8(b) shows the points 1, 2, 3, 4 and point 0 in polar coordinates. Assuming the arc 3-0-1 is closed to a straight line and its length is small compared with the boundary dimensions,

Laplace's equation for the point O can be obtained with a method similar to that used in Cartesian coordinates

$$K\phi_2 + P\phi_4 + Q(\phi_1 + \phi_3) - (K + P + 2Q)\,\phi_0 = 0 \qquad (2.18)$$

Where $K = \dfrac{2r + hr}{4r \cdot hr^2}$; $P = \dfrac{2r - hr}{4r \cdot hr^2}$; $Q = \dfrac{1}{2 \cdot ha^2}$;

r = the distance from point O to the origin, m;

hr = the length of sector mesh on the radial direction, m;

ha = the length of arc 3-0 or arc 0-1, m;

The gradients of ϕ and H can also be obtained using a method similar to that used in Cartesian coordinates

$$\frac{\partial \phi}{\partial r} = \frac{\phi_2 - \phi_4}{2 \cdot hr} \; ; \qquad \frac{1}{r}\frac{\partial \phi}{\partial \alpha} = \frac{1}{r}\frac{\phi_1 - \phi_3}{2 \cdot ha} \; ;$$

$$\frac{\partial H}{\partial r} = \frac{H_2 - H_4}{2 \cdot hr} \; ; \qquad \frac{1}{r}\frac{\partial H}{\partial \alpha} = \frac{1}{r}\frac{H_1 - H_3}{2 \cdot ha} \; ;$$

2.2. COMPUTER PROGRAM

The flow - chart of the program is shown in Fig.9. The main task is to calculate the distribution of magnetic scalar potential. Then, the distributions of H and gradH are calculated.

The program can be terminated at any accuracy required by the user. In the program, the accuracy is defined by Err < 10^{-5} where Err is given by

$$Err_{i,n} = \frac{|\,\phi_{i,n} - \phi_{i,n-1}\,|}{\phi_{i,n}} \qquad (2.19)$$

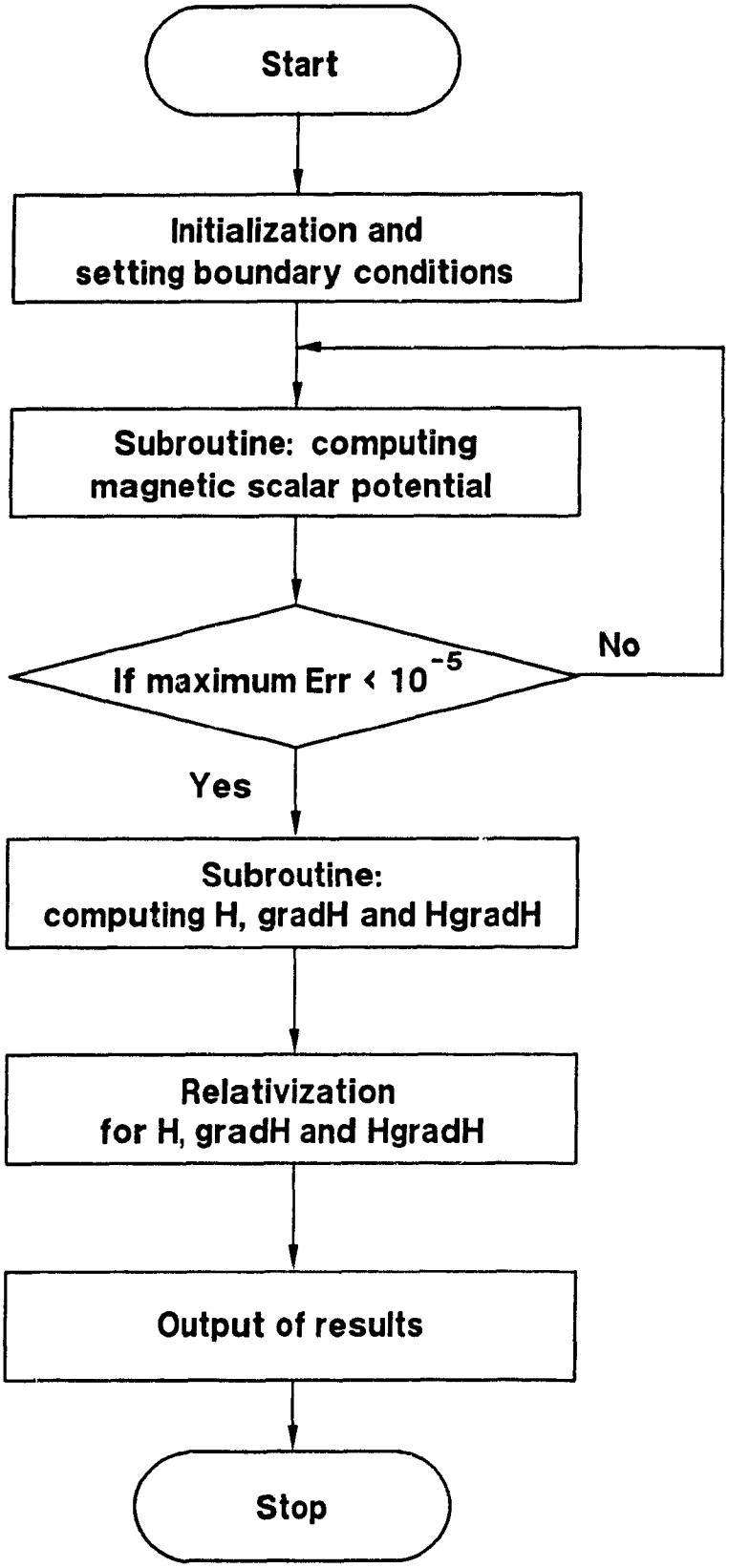

Figure 9. The flow - chart of program

Where $Err_{i,n}$ = the relative error of the n th iteration at point i, dimensionless;

$\phi_{i,n}$ = the ϕ of the n th iteration at point i, dimensionless;

$\phi_{i,n-1}$ = the ϕ of the (n - 1) th iteration at point i, dimensionless;

If a higher accuracy is required, the running time of the program is increased. In general the accuracy given by Err < 10^{-5} is sufficient for the calculation of the magnetic field [11].

In the iterative solution of Laplace's equation, the overrelaxation method which speeds up the convergence of iterations was used in conjunction with the Gauss-Seidel method. When the maximum Err was less than 10^{-5}, the number of iterations of magnetic scalar potential for each calculation was more than 450 in the case of both the Fricker and Watson magnetic hydrocyclone.

A 21 × 51 finite difference grid was used for the calculation of Watson's magnetic hydrocyclone in Cartesian coordirates; 10 × 17 and 11 × 16 grids were used respectively for Fricker's magnetic hydrocyclone and the new designs of the Watson magnetic hydrocyclone in polar coordinates. A typical run required about 40 minutes on an IBM-PC/XT microcomputer.

CHAPTER THREE

INDICES OF A MAGNETIC FIELD

The calculation of the distribution of magnetic field in a magnetic hydrocyclone results in great mass of numerical data. The objective of numerical analysis is to evaluate the magnetic field in order to improve the design of the magnetic hydrocyclone. It is useful in this regard to reduce the mass of data to a few indices for comparison of competing designs.

3.1. TWO COMPONENTS OF A FORCE FACTOR

From Fig.10, it can be seen that a force factor in polar coordinates has two components: the radial component f_r and the tangential component f_t.

The tangential component F_t is ineffective for separation in a magnetic hydrocyclone. Acting on a magnetic particle, F_t gives it a tangential force which either accelerates or decelerates the particle. However, this effect should be minimized because we want the tangential velocity of the magnetic particle to be controlled by the inlet pressure of pulp, not the magnetic field.

The radial component f_r is the effective separation component in a magnetic hydrocyclone. A positive outwards f_r is produced in Watson's magnetic hydrocyclone and a negative inwards f_r is produced in Fricker's. What should be avoided is having the component in part of the cyclone chamber inwards while it is outwards in other parts. In such a case, the magnetic force acting

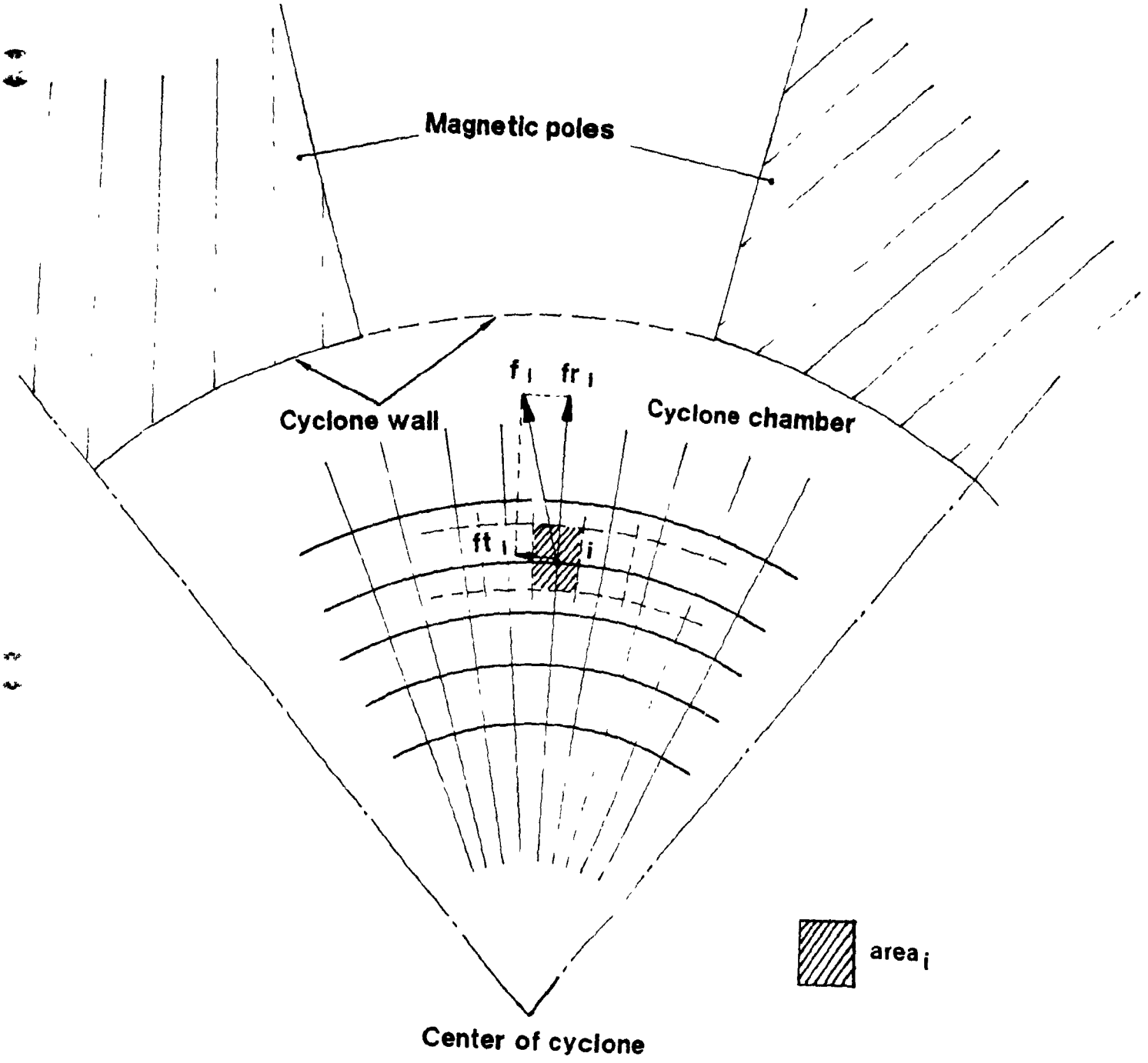

Figure 10. The effective and ineffective component of a force factor in the magnetic hydrocyclone

on the magnetic particle will be counteracted in different parts of the cyclone.

The ideal would be a magnetic field in a magnetic hydrocyclone acting totally inwards or outwards radially with no tangential component.

3.2. INDICES OF A MAGNETIC FIELD

3.2.1. Indices For Magnetic Force Factor

Fig.10 shows a section of the cyclone chamber divided into n elements. There is a magnetic force factor i in the center of the element i. It is assumed that at any point in the element i the force factor is the same as the force factor i, i.e. f_i. In polar coordinates, f_i is divided into two component: the radial component fr_i and the tangential component ft_i.

Average radial force factor. This is an areal average value of the radial component of the force factor, defined by

$$A.R.F. = \frac{1}{A} \sum_{i=1}^{n} (fr_i \cdot area_i) \qquad (3.1)$$

where

A.R.F. = the average radial force factor, T^2/m;

A = the total area of the cyclone chamber, m^2;

fr_i = the radial component of the force factor f_i, T^2/m;

$area_i$ = the area of the element i, m^2;

n = the total number of area elements, dimensionless;

It can be seen that the greater the average force factor the better the magnetic circuitry.

Average tangential force factor. This is an areal average value of the tangential component of the force factor, defined by

$$A.T.F. = \frac{1}{A} \sum_{i=1}^{n} (ft_i \cdot area_i) \qquad (3.2)$$

where

A.T.F. = the average tangential force factor, T^2/m;

ft_i = the tangential component of the force factor f_i, T^2/m;

From Fig. 10, it can be seen that the best magnetic circuitry should have a zero A.T.F..

These indices are used in the evaluation of the magnetic field. However, in the case of symmetrical magnetic circuitry, these indices are not sufficient so that a further two indices are introduced as follows.

Absolute average radial force factor. This is an areal average value of the absolute value of the radial component, defined by

$$A.A.R.F. = \frac{1}{A} \sum_{i=1}^{n} (|fr_i| \cdot area_i) \qquad (3.3)$$

Where A.A.R.F. is the absolute average radial force factor. If a magnetic field is unitary, i.e. force factors are totally inwards or outwards, A.R.F. should be equal to A.A.R.F.. Otherwise, A.R.F. should be less than A.A.R.F..

Absolute average tangential force factor. This is an areal average value of the absolute value of the tangential component, defined by

$$A.A.T.F. = \frac{1}{A} \sum_{i=1}^{n} (|ft_i| \cdot area_i) \qquad (3.4)$$

Where A.A.T.F. is the absolute average tangential force factor. If a magnetic field is a symmetrical field but not a unitary field, the A.T.F. should be zero but not A.A.T.F.. In half of the symmetrical field the tangential component of the force factor accelerates the magnetic particle but decelerates it in the other half so that the work performed by the tangential component of the force factor is totally counteracted. This will be discussed later.

3.2.2. Index For Magnetic Energy

Normally, a magnetic energy in a volume v is calculated with the equation as follows

$$E_v = \int dv \int \vec{H}\, d\vec{B} \qquad (3.5)$$

Where E_v = the magnetic energy in volume v, J;

H = the magnetic field intensity, A/m;

B = the magnetic flux density, Tesla;

v = the volume, m^3;

In air the relationship between B and H is a linear form

$$B = \mu_o H \qquad (3.6)$$

Where μ_o is the permeability of free space ($4\pi \times 10^{-7}$ T*m/A); The magnetic energy is calculated as follows

$$Ev = \frac{1}{2} \int \mu_o H^2 dv \qquad (3.7)$$

In the present case, the discretization equation has to be derived from this integral equation. By means of Fig.10 and definitions of Eq. 3.1, it is assumed that H_i is the magnetic field intensity at the center of the element i. The volume v is defined by

$$v = L \cdot \sum_{i=1}^{n} area_i \qquad (3.8)$$

Where L is the length of the cyclone chamber in meters, m; then, Eq.3.7 becomes

$$Ec = \frac{1}{2} \mu_o \cdot L \sum_{i=1}^{n} (H_i^2 \cdot area_i) \qquad (3.9)$$

Where Ec is the magnetic energy in the cyclone chamber, J; If L is assumed as 1 meter, Eq.3.9 becomes

$$E = \frac{1}{2} \mu_o \sum_{i=1}^{n} (H_i^2 \cdot area_i) \qquad (3.10)$$

Where E is the magnetic energy in the cyclone chamber with a unit length of 1 meter. E is used to evaluate the magnetic field from the energy viewpoint.

3.3. CRITERION FOR EVALUATING MAGNETIC CIRCUITRY

The ideal design of the magnetic circuitry should have five features:

A. A high average radial force factor (A.R.F.).

B. The absolute average radial force factor (A.A.R.F.) should be equal to the average radial force factor (A.R.F.).

C. The average tangential force factor (A.T.F.) should be zero.

D. The absolute average tangential force factor (A.A.T.F.) should be zero.

E. A high magnetic energy (E) in the cyclone chamber.

CHAPTER FOUR

ANALYSIS OF FRICKER AND WATSON DESIGNS OF MAGNETIC HYDROCYCLONES

Fricker's and Watson's magnetic hydrocyclones have been used for a number of experiments [3,4]. However, there is little on the relationship between the magnetic field and the separation achieved in a magnetic hydrocyclone. This relationship will be explored in this chapter.

4.1. ANALYSIS OF FRICKER'S MAGNETIC HYDROCYCLONE

Numerical analysis shows that the electromagnet of the horseshoe section in Fricker's magnetic hydrocyclone is a suitable design.

In this section, computed results of the magnetic field are based on the boundary condition of B = 1.0 Tesla on the inner pole of the electromagnet.

Both magnetic flux density B and force factor are vectors. An arrow is probably the best symbol to represent a vector: the direction of the arrow indicating the direction of the vector, the length of the arrow indicating the magnitude. However, sometimes the difference between two vectors is too large to show the smaller vector clearly. For example, if a 1 cm arrow is set to represent a force factor of 5 T^2/m, the arrow which is used for a force factor of 0.05 T^2/m will only be a point. Consequently, a combination of diagrams and tables is used to show the direction and magnitude of vectors respectively.

4.1.1. Features of Magnetic Field

Figs. 11 and 12 show diagrams of the magnetic flux density B and the force factor respectively. The distribution of their magnitude is shown in Table 3. There are two features of the magnetic field of Fricker's magnetic hydrocyclone:

(i) Concentric distribution of the magnetic field and force factor. Because of the symmetry of the magnetic circuitry, both the magnetic flux density B and force factor have the same concentric distribution. The magnitude of the vector is a single function of the distance from vector to center of the cyclone (Table 3), and;

(ii) Radial direction of the magnetic field and force factor. From Fig. 11, it can be seen that magnetic flux lines are generated from the inner pole to outer pole. The direction of all magnetic flux lines is outwards in the radial direction, or, more precisely in a direction normal to the inner pole surface. On the other hand, the direction of force factors shown in Fig. 12 is inwards in the radial direction.

From Table 3, it can be seen that when B is 1.0 T on the surface of the inner pole, it is equal to 0.5 T on the cyclone wall which is 5 cm away from inner pole. When the force factor on the inner pole is 20.2 T^2/m, it is 2.8 T^2/m (13.9% of 20.2T^2/m) on the cyclone wall.

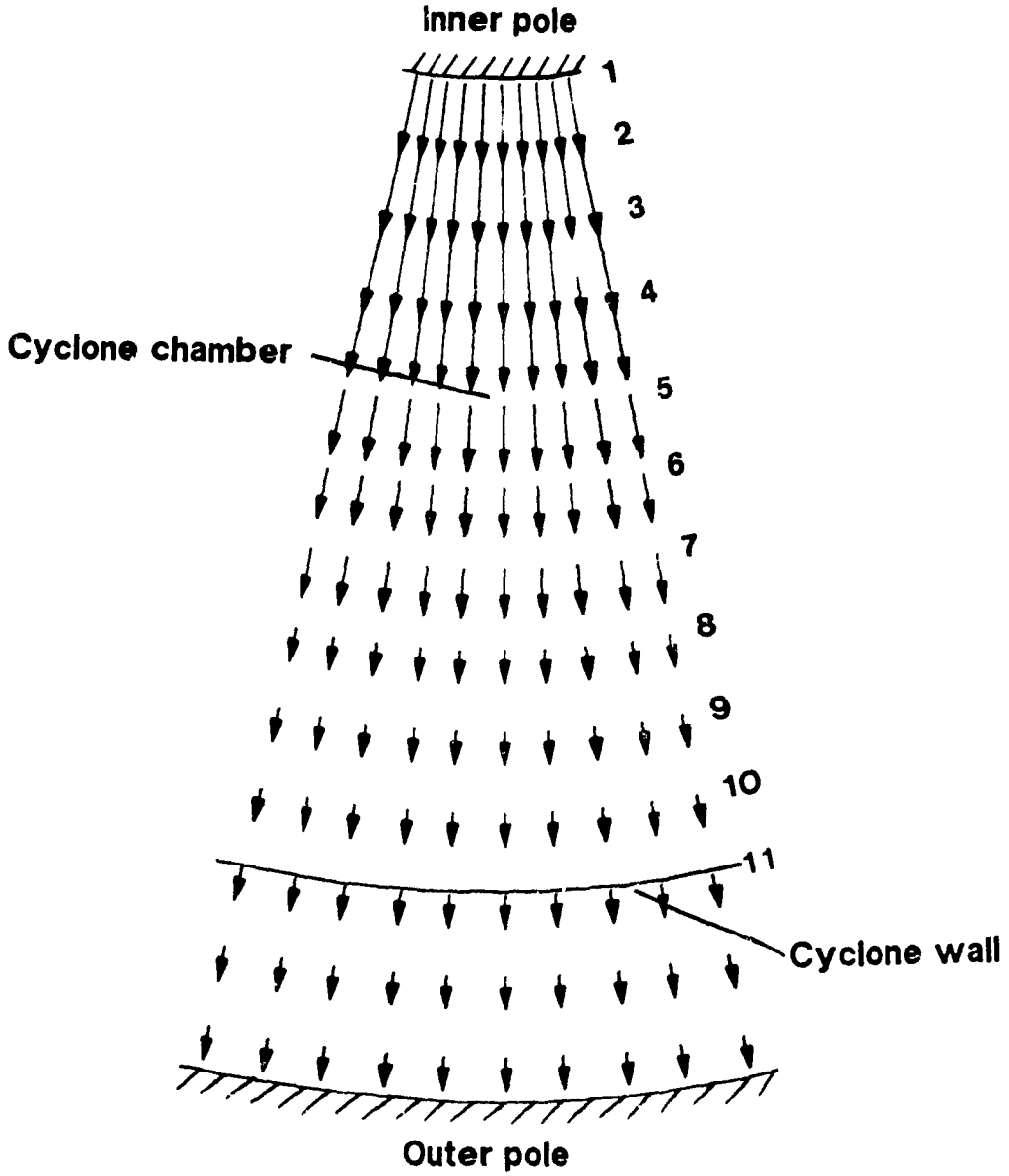

Figure 11. Magnetic flux density B between inner pole and outer pole in Fricker magnetic hydrocyclone

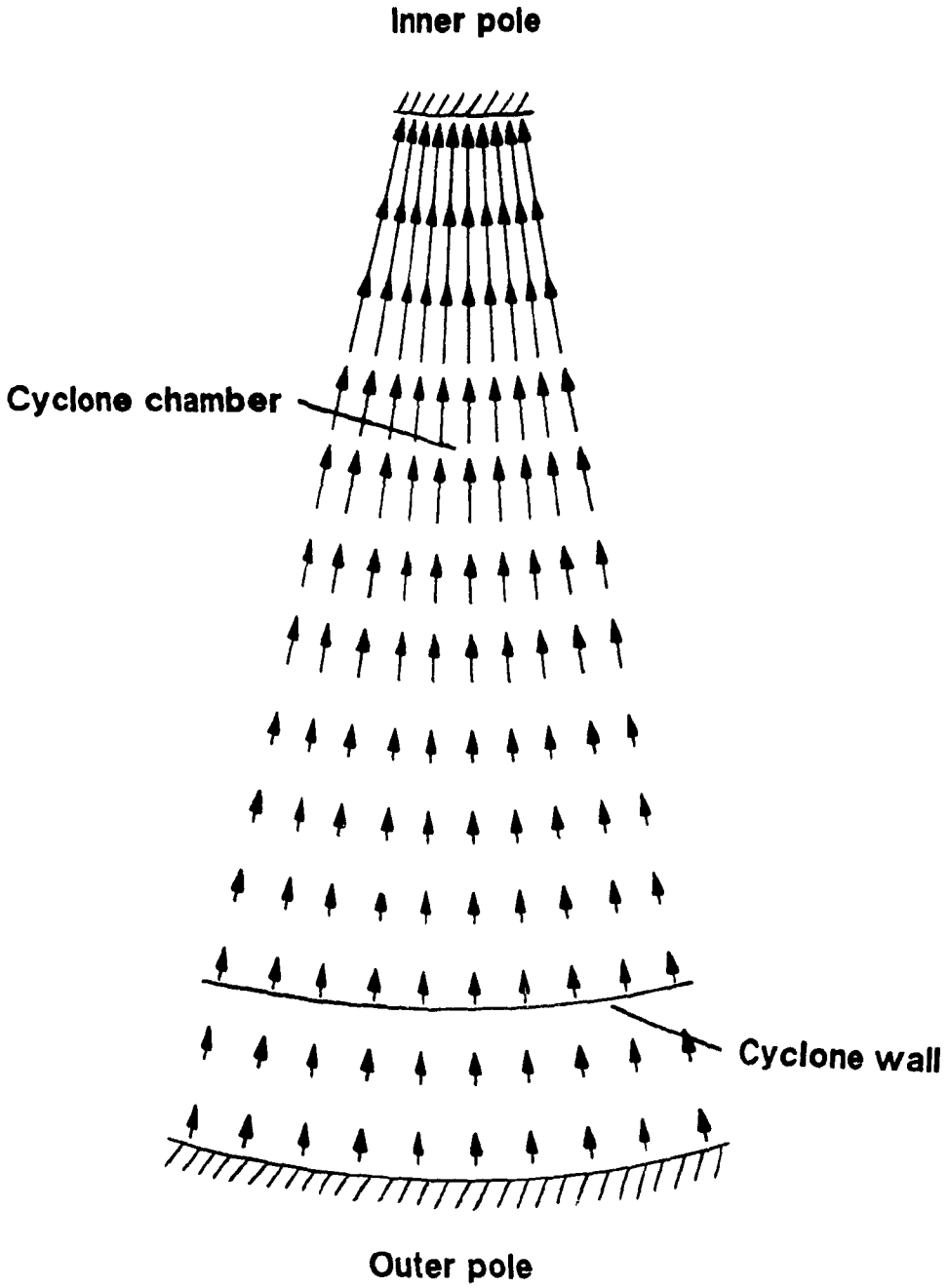

Figure 12. Force factor between inner pole and outer pole in Fricker magnetic hydrocyclone

Table 3. Computed results of B and force factor in Fricker's magnetic hydrocyclone *

(1) Distance (cm)	(2) B (T)	(3) Force factor (T^2/m)
0	1.00	20.15
0.5	0.94	15.27
1.0	0.89	13.25
1.5	0.77	10.40
2.0	0.71	8.31
2.5	0.67	6.75
3.0	0.62	5.55
3.5	0.59	4.63
4.0	0.56	3.89
4.5	0.53	3.31
5.0	0.50	2.83

* B = 1.0 Tesla on the inner pole;
(1) = distance from inner wall of cyclone, cm;
(2) = magnetic flux desity, Tesla;
(3) = magnetic force factor, T^2/m;

4.1.2. Evaluation of Magnetic Field

The indices of the magnetic field in Fricker's design are shown in the lower part of Table 4. It is obvious that this magnetic field is ideal because there is no tangential component of the force factor. In this case, A.R.F. is equal to A.A.R.F., because of the complete inwards radial direction of total force factors.

The disadvantage of Fricker's design is that there is some magnetic energy consumed in the space between cyclone wall and outer pole of the electromagnet (Fig.2). The data show the magnetic energy distributed in the cyclone chamber is 4770 J but the total magnetic energy distributed between inner and outer pole is 6481 J (Table 4). It means only 73.6% of total magnetic energy was effectively used in Fricker's magnetic hydrocyclone.

Based on Fricker's design but removing the space between cyclone wall and outer pole of the electromagnet, the computed data with various cyclone diameters are shown in the upper part of Table 4. In this case, the boundary conditions are:

(a) the ratio of the diameter of the inner pole to the outer pole of the magnet is equal to 0.5. This value is from Fricker's magnetic hydrocyclone [3];

(b) the magnetic flux density B is equal to 1.0 Tesla on the inner pole of the electromagnet.

It can be seen that when the diameter of the Fricker magnetic hydrocyclone is increased from 0.1 m to 0.5 m, the magnetic energy increases from 1.1 kJ to 28.1 kJ and the average force factor

Table 4. Computed results of force factor and magnetic energy in Fricker magnetic hydrocyclone *

(1) Diameter (m)	(2) M.E. (J)	(3) A.R.F. (T^2/m)	(4) A.A.R.F. (T^2/m)	(5) A.T.F. (T^2/m)	(6) A.A.T.F. (T^2/m)
0.1	1126	16.1951	16.1951	0	0
0.2	4502	8.0989	8.0989	0	0
0.3	10131	5.4692	5.4692	0	0
0.4	18010	4.1019	4.1019	0	0
0.5	28140	3.2390	3.2390	0	0
0.2 **	4770	8.1835	8.1835	0	0
	6481	(magnetic energy between poles)			

* B = 1.0 Tesla on the inner pole;
(1) is the diameter of cyclone, m;
(2) is the magnetic energy in cyclone chamber, J;
(3) is the average radial force factor, T^2/m;
(4) is the average of absolute value of radial force factor, T^2/m;
(5) is the average tangential force factor, T^2/m;
(6) is the average of absolute value of tangential force factor, T^2/m;

** Fricker's magnetic hydrocyclone (reference Fig.2);

decreases from 16.2 T^2/m to 3.2 T^2/m.

In fact, assuming the cyclone chamber is 1 meter long, a 0.5 m Fricker magnetic hydrocyclone needs electric energy which is greater than the magnetic energy of 28.1 kJ because of the electrical resistance of the coils.

In an electromagnet, the magnetic flux is generated by the DC current through the coils. However, the greater the current the hotter the coils. With increasing temperature, the resistance of the coils increases. Consequently increasing power is required as temperature increases. The circuit will limit the magnitude of the increase of the magnetic flux density on the inner pole. As a consequence, for the same capacity, a bank of parallel small magnetic hydrocyclones is better than one large magnetic hydrocyclone.

4.1.3. Comparison Between Computed and Measured Data of Magnetic Field

Fig. 13 shows the comparison between the computed and measured flux density in Fricker's magnetic hydrocyclone. In order to compare, the vertical axis is set as the relative magnetic field strength. For example, setting the relative value at 100% on the inner pole, the relative value will be 50% on the outer wall of the cyclone in the computed data. The computed data are from Table 3, and the measured data are from the curve of DC current = 2A in Fig.7 [3].

The magnetic circuitry of Fricker's magnetic hydrocyclone is a

half - open circuitry. From Fig.2, it can be seen that the magnetic circuitry is opened at the lower end. Fricker measured the magnetic flux density across the section of the open end, and the results are shown in Fig.7 [3]. Because of the divergence of the magnetic flux at the open end, B at this section should be weaker than B at the mid and upper sections.

The computed data are based on an ideal two dimensional magnetic field which is the simplification of the real three dimensional field. Thus the computed result is the upper boundary of the magnetic field. Consequently, the curve of the measured data is lower than that of the computed data. The true curve of B at the mid section will be somewhere between the curves of the computed data and measured data in Fig.13.

The best section for analysis is the mid section in the Fricker magnetic hydrocyclone. The distribution of the magnetic field in the mid section will be solved in the three dimensional numerical analysis conducted later.

4.1.4. Relationships Between A.R.F., Magnetic Energy and Cyclone Diameter

Based on the computed data shown in the upper part of Table 4, two regressions have been performed under the condition of B = 1.0 Tesla on the inner pole of the magnet.

Regression of average radial force factor. The A.R.F. is a hyperbolic function of the cyclone diameter, defined by

$$A.R.F. = 1.622 \cdot \frac{1}{D} \qquad (4.1)$$

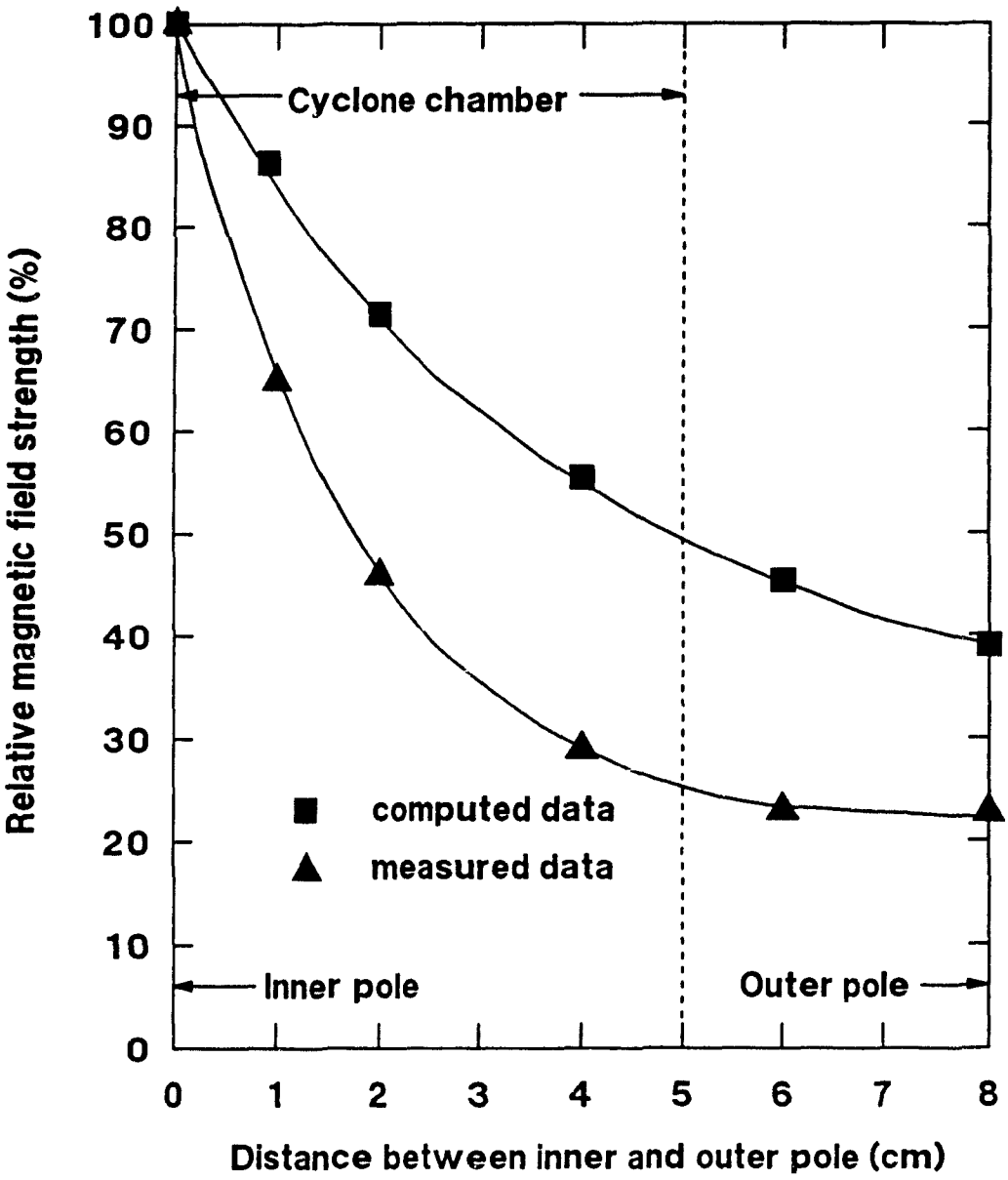

Figure 13. Comparison of computed and measured data of magnetic field in Fricker's magnetic hydrocyclone

where A.R.F. is the average radial force factor, T^2/m; D is the cyclone diameter, m. From Table 5, it can be seen that the maximum relative error of the regression is about 1.14 %.

Regression of magnetic energy. The magnetic energy is a function of the square of the cyclone diameter, defined by

$$E = 1.126 \times 10^5 \cdot D^2 \qquad (4.2)$$

Where E is the magnetic energy in cyclone chamber, J; Table 5 shows that the maximum relative error of the regression is about 0.035 %.

4.1.5. Forces on a Magnetite Particle

In the Fricker magnetic hydrocyclone, the magnetic force is inwards. Defining the inwards direction as positive, the combined force on a magnetic particle F_J is

$$F_J = F_m + F_d - F_c \qquad (4.3)$$

From this equation, it can be seen that forces are divided into two groups: one group has F_m and F_d and another group has F_c. When the two groups are in balance, $dso_{c,m}$ is defined.

Fig.14 shows forces and force ratios vs. a size range of magnetite particles. In the upper part, three forces are drawn using Eqs.1.1, 1.2 and 1.3. The cyclone diameter is 0.2 m. Vt and Vr are 0.95 m/s and 0.011 m/s respectively [1,13]. Other conditions are:

$r = 0.075$ m; $\mu = 0.001$ kg/m·s;

$\rho_s = 5200$ kg/m^3; $\rho_l = 1000$ kg/m^3;

Table 5. The relative error of the regressions in Fricker magnetic hydrocyclone *

(1) Dia. (m)	(2) M.E. (J)	(3) Reg.M.E. (J)	(4) |Err| (%)	(5) A.R.F. (T^2/m)	(6) Reg.A.R.F. (T^2/m)	(7) |Err| (%)
0.1	1126	1125.6	0.035	16.1951	16.2208	0.169
0.2	4502	4502.4	0.010	8.0989	8.1104	0.142
0.3	10131	10130.5	0.005	5.4692	5.4069	1.139
0.4	18010	18009.8	0.001	4.1019	4.0552	1.139
0.5	28140	28140.3	0.001	3.2390	3.2442	0.159

* B = 1.0 Tesla on the inner pole;

(1) is the diameter of cyclone, m;

(2) is the magnetic energy in cyclone chamber, J;

(3) is the regressive value of magnetic energy in cyclone chamber, J;

(4) is the absolute value of relative error between (2) and (3), defined by:

$$(4) = \frac{|\ (3) - (2)\ |}{(2)} \cdot 100\%$$

(5) is the average radial force factor, T^2/m;

(6) is the regressive value of average radial force factor, T^2/m;

(7) is the absolute value of relative error between (5) and (6), defined by:

$$(7) = \frac{|\ (6) - (5)\ |}{(5)} \cdot 100\%$$

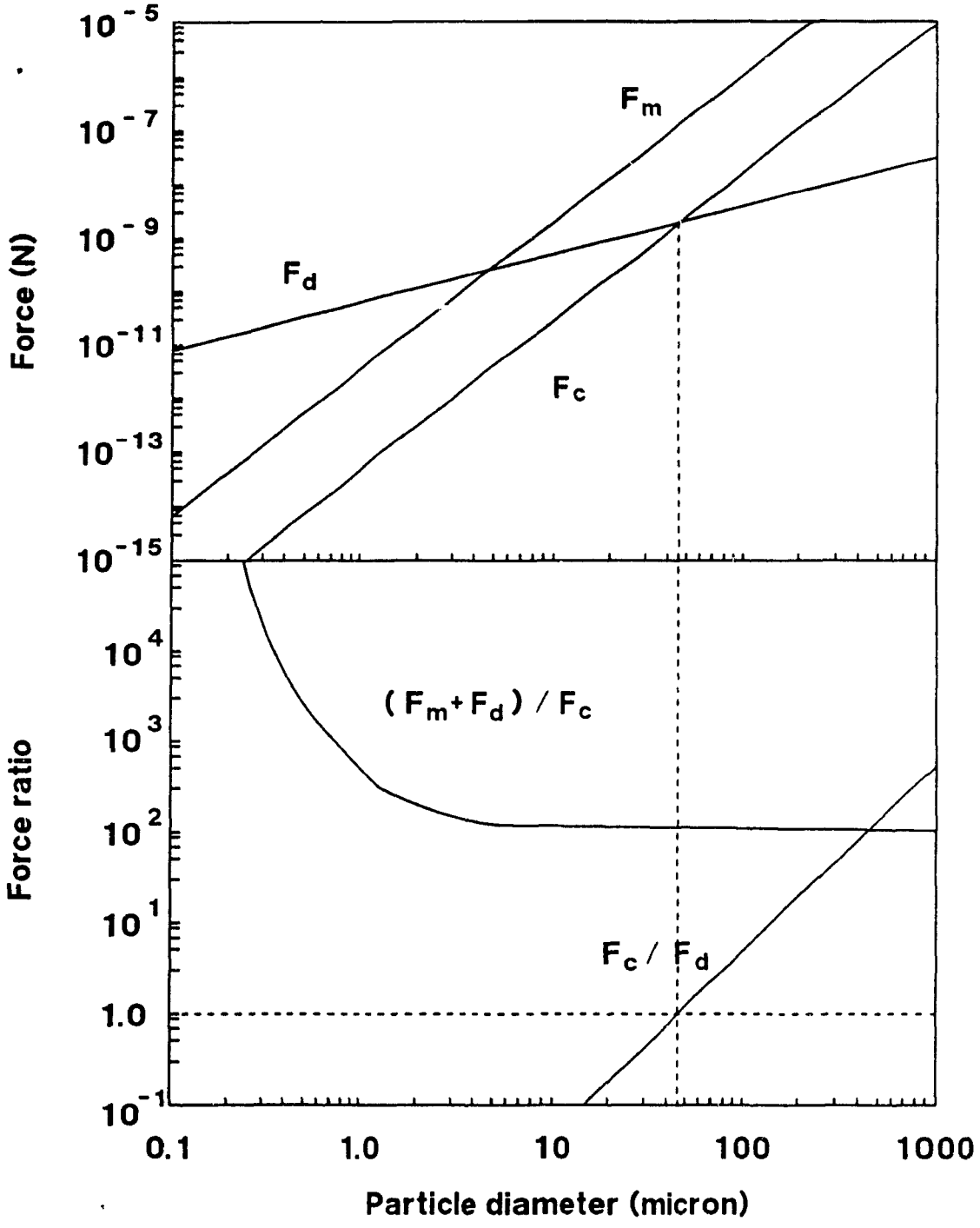

Figure 14. Forces and force ratios as functions of magnetite particle size in Fricker magnetic hydrocyclone

κ = 2.375; H•gradH = 8.18 T^2/m (Table 4);

It can be seen that the line Fd intersects the line Fc at a particle size of about 47 μm. This represents the cut size of magnetite particle without a magnetic force. The ratio of Fc to Fd is equal to 1 at this point.

In the lower part of Fig. 14, it can be seen that the sum of Fm and Fd is always greater than Fc because Fm is always greater than Fc. From Eqs. 1.1 and 1.3, we get

$$Fc = \left[\frac{\pi}{6} \frac{\rho_s - \rho_l}{r} v_t^2 \right] \cdot d^3 \qquad (4.4)$$

$$Fm = \left[\frac{\pi}{6} \mu_o \kappa H \, gradH \right] \cdot d^3 \qquad (4.5)$$

set $C1 = \left[\frac{\pi}{6} \frac{\rho_s - \rho_l}{r} v_t^2 \right]$; $C2 = \left[\frac{\pi}{6} \mu_o \kappa H \, gradH \right]$;

Then, the equations become

$$Fc = C1 \cdot d^3 \qquad (4.6)$$

$$Fm = C2 \cdot d^3 \qquad (4.7)$$

Taking the logarithm of both equations, they become

$$Ln(Fc) = Ln(C1) + 3 \cdot Ln(d) \qquad (4.8)$$

$$Ln(Fm) = Ln(C2) + 3 \cdot Ln(d) \qquad (4.9)$$

Because they have the same slope, line Fm dose not intersect line Fc in Fig. 14. The curve of (Fm + Fd) / Fc also shows that it becomes a constant at about 100 when the particle size goes to the infinite value.

The calculated result does not yield a finite $d_{50c,m}$ in the

Fricker magnetic hydrocyclone. However, experience indicates a quite large cut size exists (see "discussion"). It is difficult to consider the total effect of complex flow patterns on a particle in a magnetic hydrocyclone (Fig.4). Consequently problems are simplified in the section 1.1.3. Only two forces F_c and F_d are used to describe the effect of flow patterns on the two dimensional section. The inability to solve $d_{50c,m}$ mathematically is because the modeling equations used for the calculation are over - simplified.

Although this model could be improved, it still gives us useful information. According to the results, the Fricker magnetic hydrocyclone has a quite large $d_{50c,m}$ and almost all magnetite particles will be attracted to the overflow.

4.1.6. Discussion

With an artificial feed of pure magnetite and quartz, Fricker obtained experimental results. In the case of the coarse feed between 0.1 and 1.0 mm which contained 20% magnetite and 80% silica (Fig.6), the magnetite recovery to the overflow was almost 100% (with a grade of 96%) for a DC current greater than 6 A. In the case of test aimed at the recovery of fine magnetite media from the dilute medium circuit, an artificial (1:1) mixture of fine magnetite and sand was separated at 55 kPa and 6 A at 2.5 wt% pulp density (Fig.15). The magnetite recovery to the overflow was greater than 96% (with a grade of over 86%) within the particle size range of 30 - 250 μm. Another test gave the magnetite

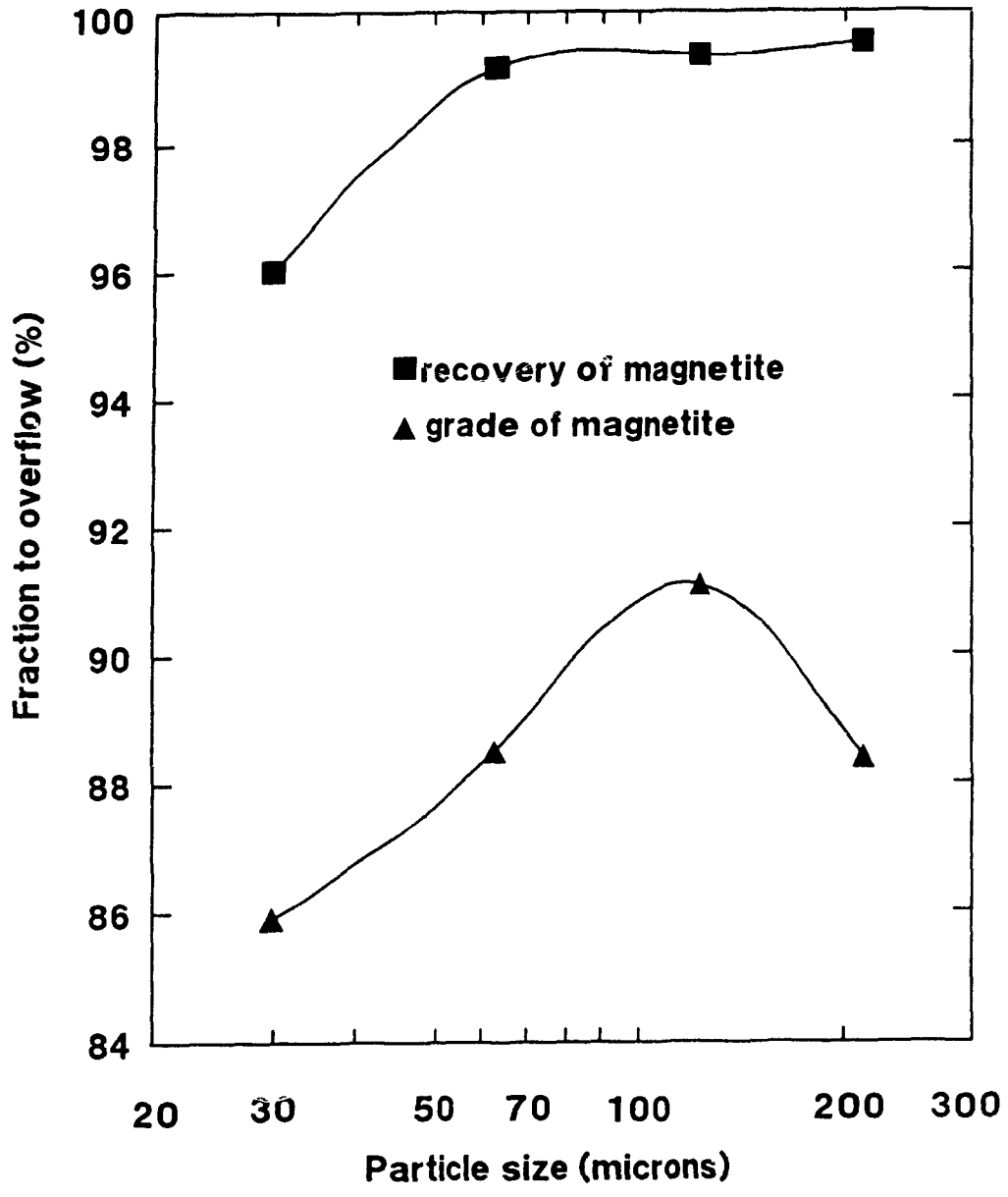

Figure 15. Recovery of magnetic media by particle size from simulated dilute medium slurry (magnetite : silica = 1:1; current = 6A) (pressure, 55kPa; pulp density, 2.5wt%)

(After Fricker [3])

recovery greater than 95% down to 5 μm with a finer artificial feed [3]. From Fig. 14, it can be seen that the finer the magnetite particle the greater the value of $(F_m + F_d) / F_c$. This corresponds with the high recovery to the overflow of the fine magnetite particles in Fricker's tests.

An important feature of the Fricker magnetic hydrocyclone is the cleaning effect which gives a high grade in the overflow.

The cleaning effect is the effect of the slurry which breaks the magnetic flocs and decreases the entrapment of the non - magnetic particles. In magnetic separators, magnetic flocculation occurs at a low magnetic field and causes entrapment [10]. A high slurry velocity can be used to break flocs and increase the grade of concentrate [1,14]. However, the slurry velocity must not be too high because of the decreased recovery. In a magnetic hydrocyclone, the tangential velocity of the slurry can be kept within the range of 0.5 - 5 m/s which is greater than the slurry velocity of other magnetic separators So a magnetic hydrocyclone has a stronger cleaning effect than other magnetic separators.

In the case of the magnetic hydrocyclone, the high magnetic field can be used to increase the recovery with less decrease of the grade. Fig. 16 shows that because of the cleaning effect the grade to the overflow decreased only about 1.5% while the recovery to the overflow increased from 15% to 55% with a DC current range of 4 - 12 A.

Although the Fricker magnetic hydrocyclone has a strong cleaning effect, Fig. 17 suggests that there was magnetic

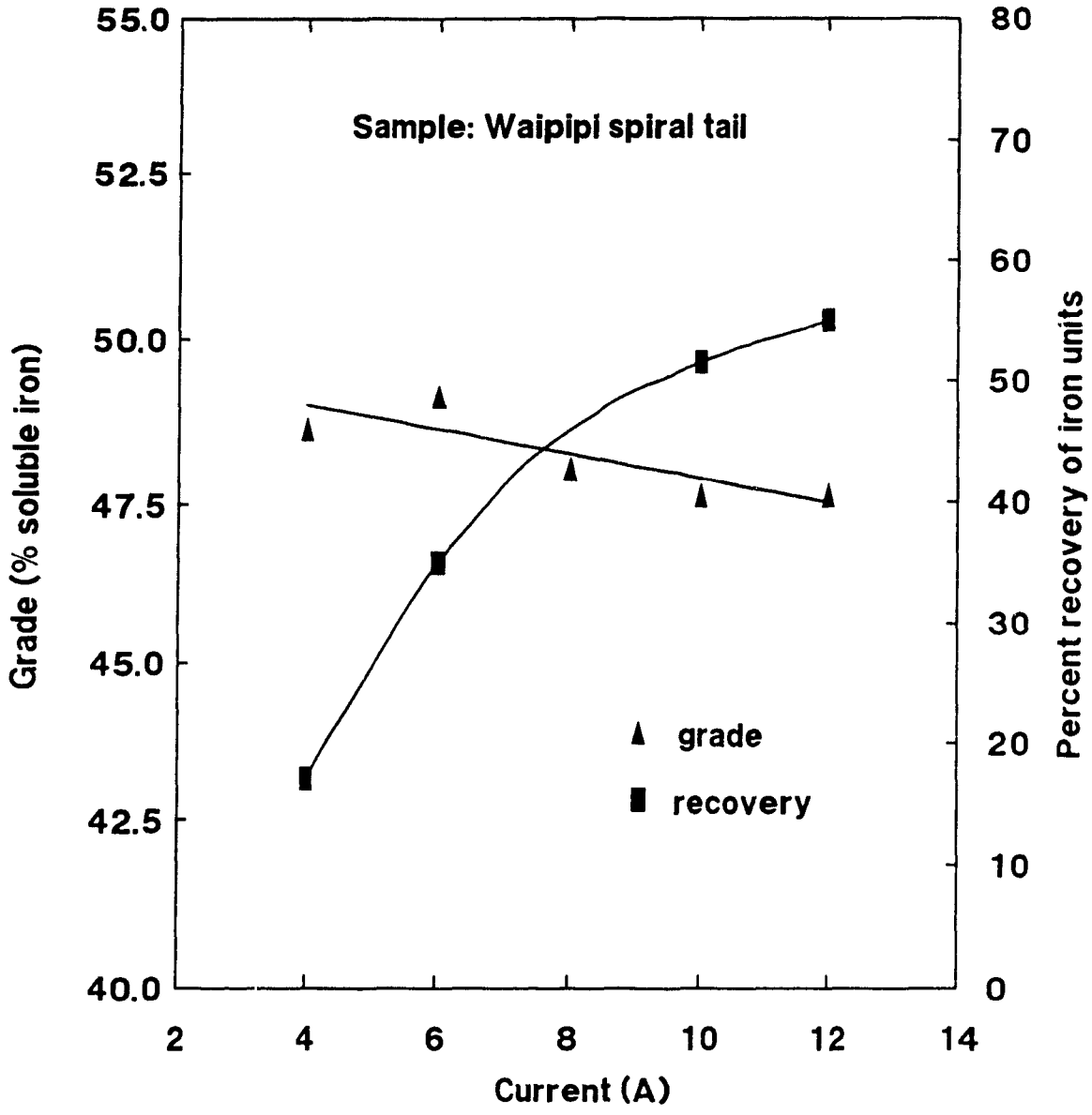

Figure 16. Effect of current on grade and recovery (pressure, 65kPa) (After Fricker [3])

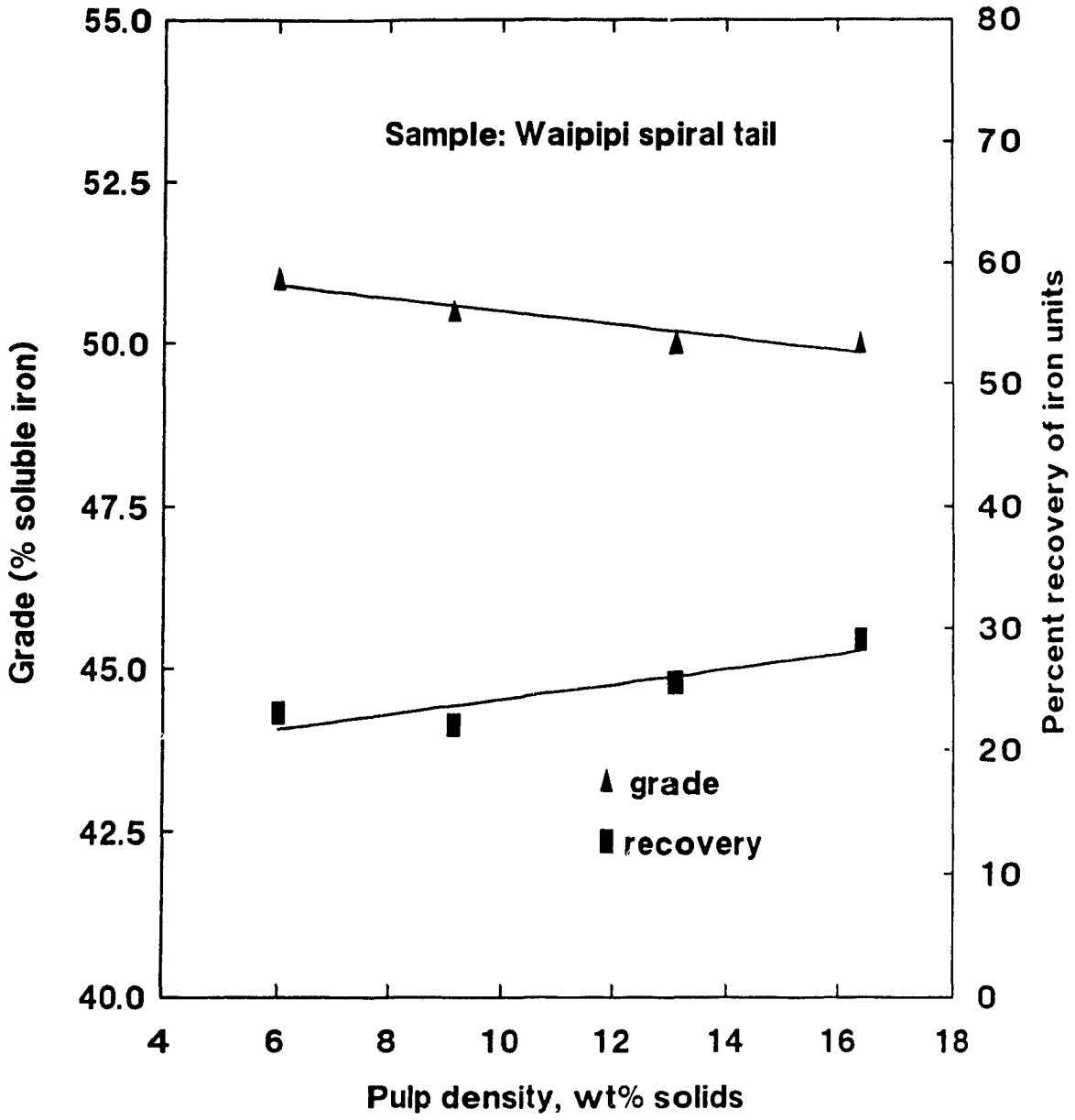

Figure 17. Effect of pulp density on grade and recovery (current, 6A; pressure, 69kPa)

(After Fricker [3])

flocculation occurring. It may account for the recovery increase with increasing pulp density while the associated increase in entrapment possibility decreased the grade.

In order to minimize magnetic flocculation, a demagnetizing coil should be used. This will be discussed in the following section.

4.2. ANALYSIS OF WATSON'S MAGNETIC HYDROCYCLONE

Watson sought an outward distribution of the magnetic force factor and designed a pair of bar electromagnets for his magnetic hydrocyclone However, both numerical analysis and Watson's test results show that the efficiency of the magnetic circuitry is not as good as Fricker's

4.2.1. Features of Magnetic Field

Fig. 18 shows the magnetic flux density B between two poles. It is easy to make a mistake as to the direction of the flux ensity B compared to the direction of the magnetic force. The direction and magnitude of the force factor are shown in Fig. 19 and Table 6 respectively. There are two features of the magnetic field in Watson's magnetic hydrocyclone:

(i) Non - uniformity of the direction of the force factor. The magnetic field between two poles can be divided into four parts. Force factors in each part are forward to the corner of the magnetic pole in that part, except the force factors on column 1

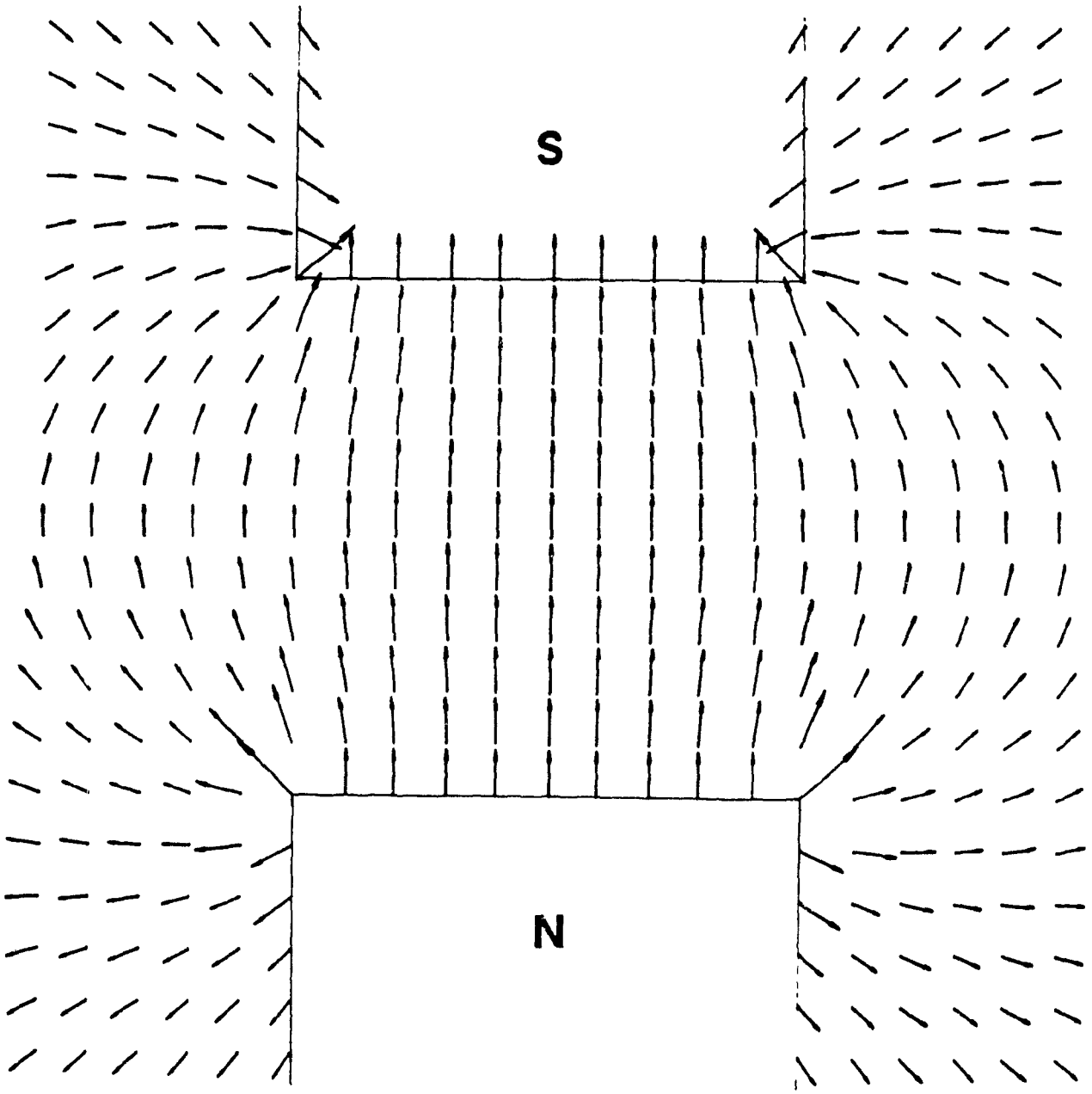

Figure 18. Magnetic flux density B between two poles in Watson magnetic hydrocyclone

and row I (Fig.19). In Watson's design, the hydrocyclone was set in the space between the two poles. It can be seen that in the cyclone chamber the directions of force factors counteract in some areas.

(ii) Magnetic energy consumed outside of the cyclone chamber.

Watson's magnetic hydrocyclone has an open magnetic circuitry (Fig.3). As shown in Fig. 19 and Table 6, assuming the magnitude of the force factor on the corner of the pole is 100%, force factors distributed in the cyclone chamber are lower than 3%. However, outside of the cyclone chamber, there are a number of areas with force factors higher than 3% This means that areas with stronger magnetic force are outside of the cyclone chamber and magnetic energy is wasted.

4.2.2. Evaluation of Magnetic Field

The indices of magnetic field in the cyclone chamber are shown in Table 7. Comparing the first row with data from a 0.1 m Fricker magnetic hydrocyclone (first row of Table 4), it can be seen that the indices for Watson's magnetic hydrocyclone are lower. For example, the A.R.F. in the cyclone chamber is 0.166 T^2/m, much lower than the 16.2 T^2/m of the 0.1 m Fricker magnetic hydrocyclone.

Comparing columns (3) with (4) in Table 7, it is seen that some outwards force factors are counteracted by the inwards force factors; this is evidenced by the A.R.F. (0.1662 T^2/m) being much less than the A.A.R.F. (0.5492 T^2/m).

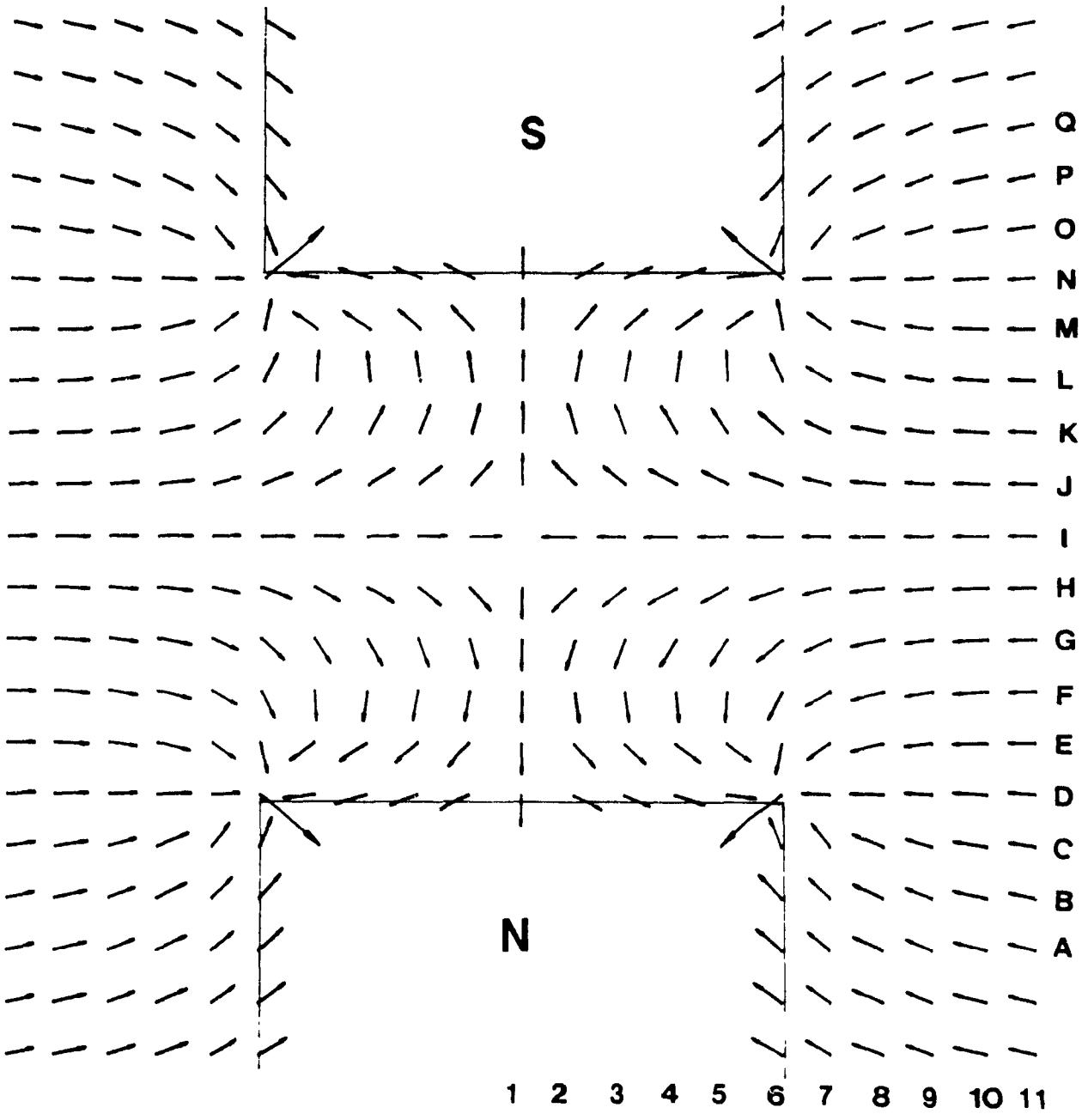

Figure 19. Force factor between two poles in Watson magnetic hydrocyclone

Table 6. The distribution of force factors in Watson magnetic hydrocyclone *

	A	B	C	D	E	F	G	H	I	J	K	L	M	N	O	P	Q
1				0 3	0.4	0.7	0.6	0.4	0 0	0.4	0.6	0.7	0 4	0.3			
2				0.7	0 7	0.8	0 7	0.5	0.4	0.5	0.7	0.8	0.7	0.7			
3		N		1.6	1.4	1 3	1.1	1.0	0.9	1.0	1.1	1 3	1.4	1 6		S	
4				3 7	3 0	2.3	1.9	1.6	1 5	1 6	1.9	2 3	3 0	3 7			
5				25.0	7 5	4.5	3.2	2 5	2.3	2.5	3.2	4 5	7 5	25 0			
6	4.8	8.7	29.8	100.0	30 6	10.5	4.8	3 3	2.9	3.3	4.8	10 5	30.6	100 0	29.8	8.7	4.8
7	3.6	5 9	12 2	33 7	14 6	6 8	4 3	3 3	3 0	3.3	4.3	6 8	14 6	33.7	12 2	5 9	3.6
8	2.5	3 7	5.8	10 8	6 2	4.3	3.2	2 7	2 6	2 7	3.2	4 3	6 2	10.8	5 8	3.7	2.5
9	1.7	2.2	3 0	4 0	3 2	2.6	2 2	2.0	1 9	2 0	2.2	2 6	3.2	4 0	3.0	2.2	1.7
10	1.1	1 4	1 7	1 9	1 8	1 6	1.5	1.4	1.3	1.4	1.5	1.6	1 8	1.9	1.7	1.4	1.1
11	0.7	0.8	1.0	1 0	1 0	1.0	0.9	0.9	0.9	0 9	0.9	1.0	1 0	1 0	1.0	0 8	0.7
12	0.5	0.5	0.6	0 6	0 6	0 6	0.6	0.6	0.6	0.6	0.6	0.6	0 6	0 6	0 6	0.5	0.5
13	0.3	0.3	0.4	0 4	0 4	0 4	0 4	0 4	0.4	0 4	0.4	0 4	0 4	0 4	0.4	0.3	0.3
14	0.2	0.2	0 2	0 2	0 2	0 2	0.2	0 2	0 2	0 2	0.2	0.2	0 2	0.2	0.2	0.2	0.2

* Distance from N pole to S pole is 10 cm;
Width of magnetic pole = 10 cm;

Table 7. Computed results of force factor and magnetic energy in Watson's magnetic hydrocyclone *

(1) B (T)	(2) M.E. (J)	(3) A.R.F (T^2/m)	(4) A.A.R.F. (T^2/m)	(5) A.T.F. (T^2/m)	(6) A.A.T.F. (T^2/m)
1.0	785	0.1662	0.5492	0.15E-05	0.4512
0.056**	10.3	0.0022	0.0072	0.19E-07	0.0059

* Distance between N and S pole is 0.1 m;
Diameter of cyclone is 0.1 m;
(1) is the magnetic flux density on the corner of the pole, Tesla;
(2) is the magnetic energy in cyclone chamber, J;
(3) is the average radial force factor, T^2/m;
(4) is the average of absolute value of radial force factor, T^2/m;
(5) is the average tangential force factor, T^2/m;
(6) is the average of absolute value of tangential force factor, T^2/m;

** B is 0.056T on the central line of poles at 2 cm away from the pole surface;

The magnetic field in the cyclone chamber is a symmetrical field so that the tangential component of force factors can be totally counteracted. (It means that the A.T.F., column (5), should be zero; however, it is not zero because of the numerical errors associated with the iteration. Compared with the magnitude of the A.A.T.F., column (6), this error can be ignored.)

The A.A.T.F., column (6), is 0.4512 T^2/m. Comparing it with the A.R.F. of 0.1662 T^2/m, column (3), it can be seen that much of the magnetic energy is consumed in doing no useful work.

In order to compare the result of the numerical analysis with Watson's tests, a group of computed data is shown in the second row of Table 7. The boundary condition is B = 0.056T on the central line of poles at 2 cm from the pole surface [4].

4.2.3. Forces on a Magnetite Particle

In Watson's magnetic hydrocyclone, the average effect of the radial component of the force factor is outwards and the average effect of the tangential component is zero. Assuming the outwards direction is positive, the combined force on a magnetic particle F_j can be written as

$$F_j = F_m + F_c - F_d \qquad (4.10)$$

When the sum of F_m and F_c is equal to F_d, $d_{50c,m}$ will be found.

Fig.20 shows three forces on a magnetite particle and their ratios in Watson's magnetic hydrocyclone. Three forces are calculated with Eqs.1.1, 1.2 and 1.3. In this case, V_t and V_r are 1.06 m/s and 0.012 m/s respectively. The cyclone diameter is 0.1m.

Other conditions are:

$r = 0.022$ m; $\mu = 0.001$ kg/m·s;

$\rho_s = 5200$ kg/m^3; $\rho_l = 1000$ kg/m^3;

$\kappa = 2.375$; $H \cdot \text{grad}H = 0.1662$ T^2/m (Table 7);

Fig.20 shows the cut size of the magnetite is about 32 μm without a magnetic force. When B is 1 Tesla on the corner of the pole, i.e. the average force factor is 0.1662 T^2/m in the cyclone chamber, $ds_{0c,m}$ of the magnetite particle is about 20 μm.

4.2.4. Discussion

In Watson's tests, performance curves of both magnetite and dolomite were measured [4]. Fig.21 shows the performance curves of the magnetite and dolomite without a magnetic field. The individual magnetite and dolomite curves revealed ds_{0c} values of 32 and 34 μm [4]. Fig.22 shows the performance curves when B was 0.056 Tesla on the central line at 2 cm from the pole surface. In this case, $ds_{0c,m}$ of the magnetite was reduced below 10 μm. On the other hand, $ds_{0c,m}$ of the dolomite became 26.3 μm, which was 8.1 μm lower than that produced without the magnetic force [4].

The result of the numerical analysis does not support Watson's measurements. The second row of Table 7 shows that the A.R.F. in the cyclone chamber is 0.0022 T^2/m. If this value is put into Eq.4.10 and setting F_j to zero, $ds_{0c,m}$ will be 31.4 μm which is only 0.6 μm lower than that produced without a magnetic force.

The difference may be due to magnetic flocculation. Because of the limitations in laboratory testing, the minerals were

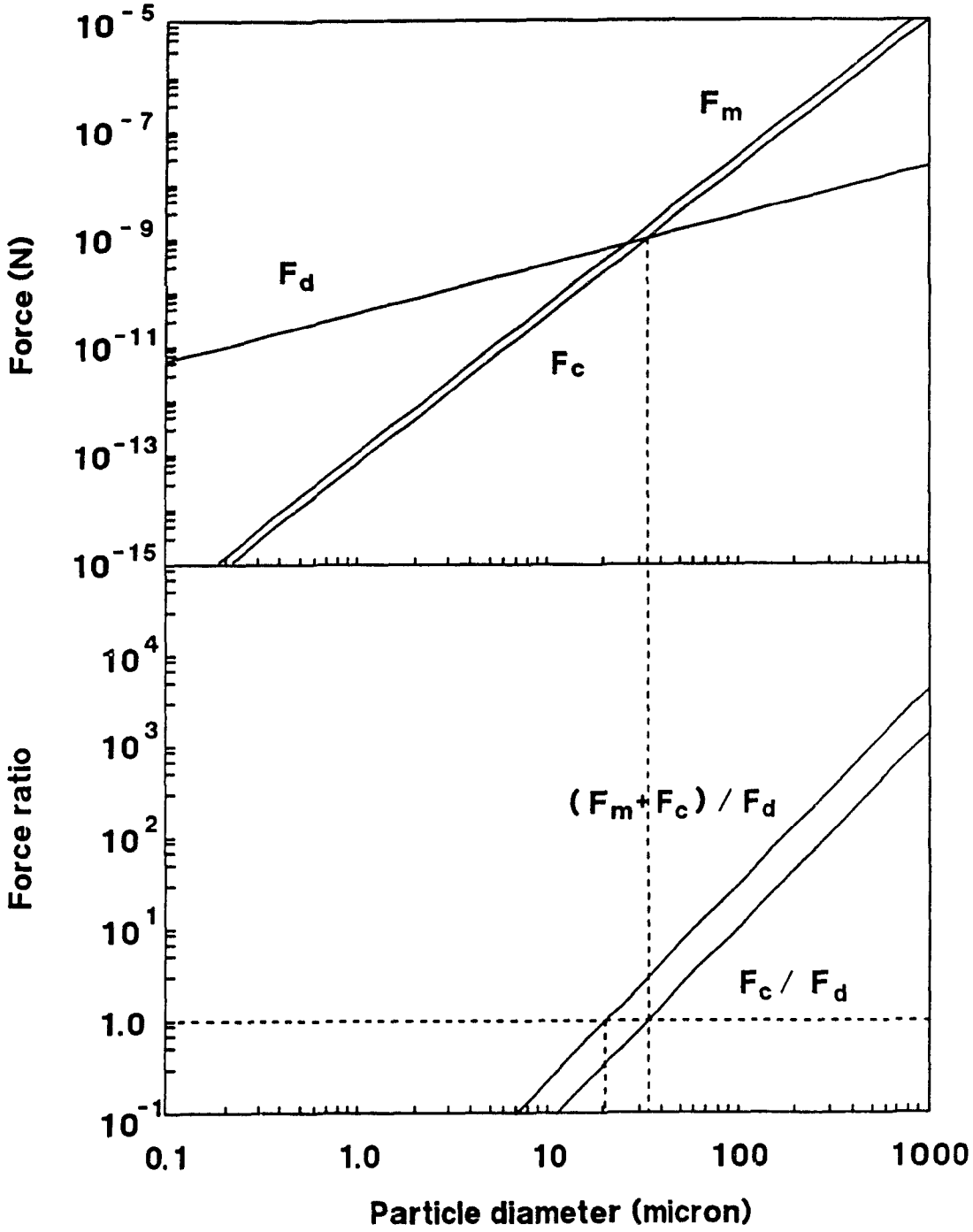

Figure 20. Forces and force ratios as functions of magnetite particle size in Watson magnetic hydrocyclone (B = 1.0 T on the corner of poles)

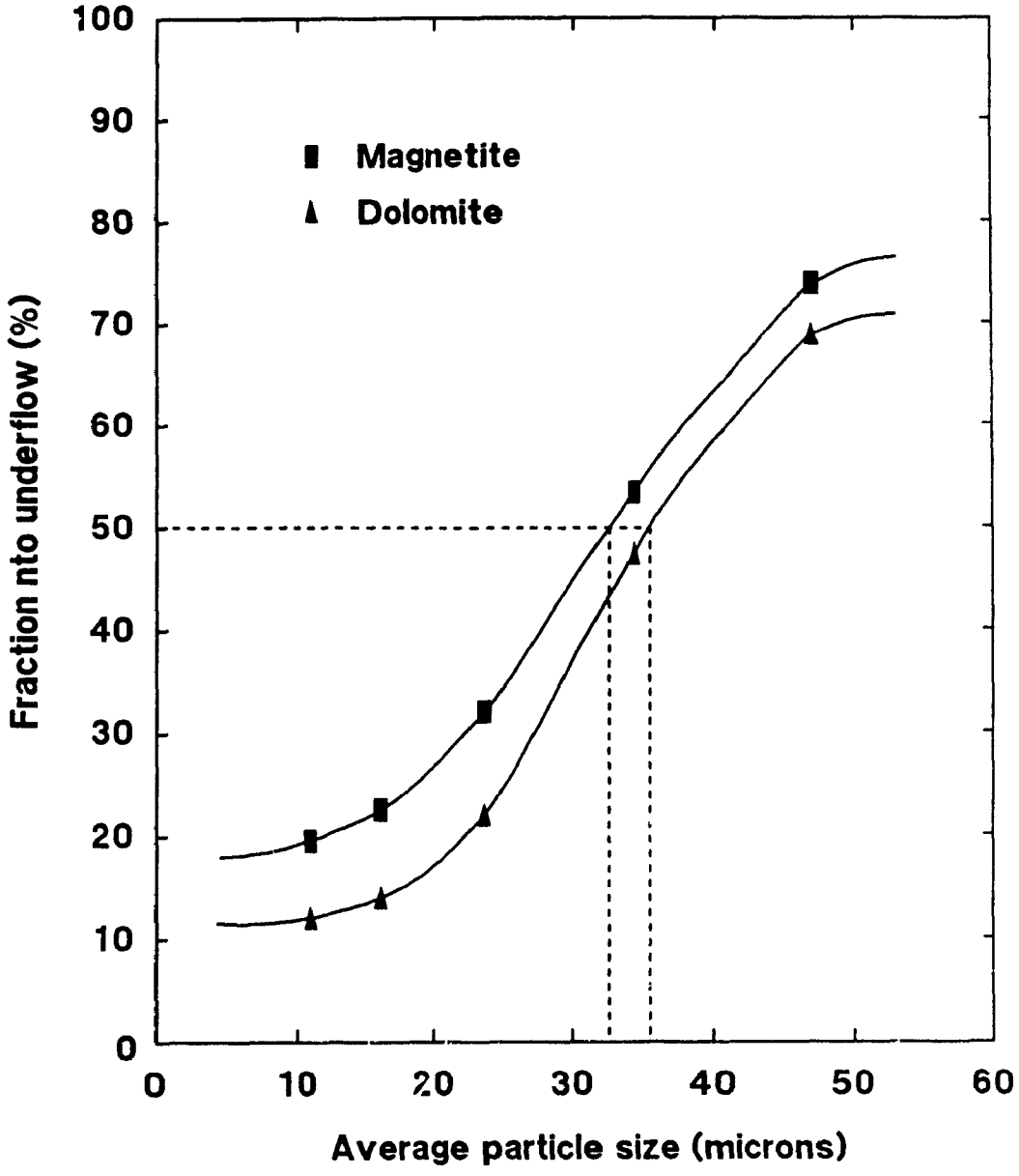

Figure 21. Performance curves of magnetite and dolomite without magnetic field

(After Watson [4])

circulated in the test rig. If there is no demagnetizing coil in the circuit, the magnetic hydrocyclone will become a magnetizer, the particles will become larger and the separating force more effective. In Watson's paper, the diagram of the test circuit showed that a demagnetizing coil was not used for the tests [4]. In Fig.22, it can be seen that $d_{50c,m}$ of the dolomite was also decreased when the magnetic force existed, suggesting dolomite particles were entrapped in the flocs of magnetite.

Magnetic flocculation of magnetite occurs at low magnetic fields [10]. Further evidence of the magnetic flocculation is shown in Fig.23. The decrease in grade at high field suggests the entrapment of dolomite. Watson noted floc formation and attributed their effect on flow patterns to the lowering in recovery [4].

Although the cleaning effect exits in magnetic hydrocyclones, it is not able to overcome magnetic flocculation. A demagnetizing coil should be used in the test circuit.

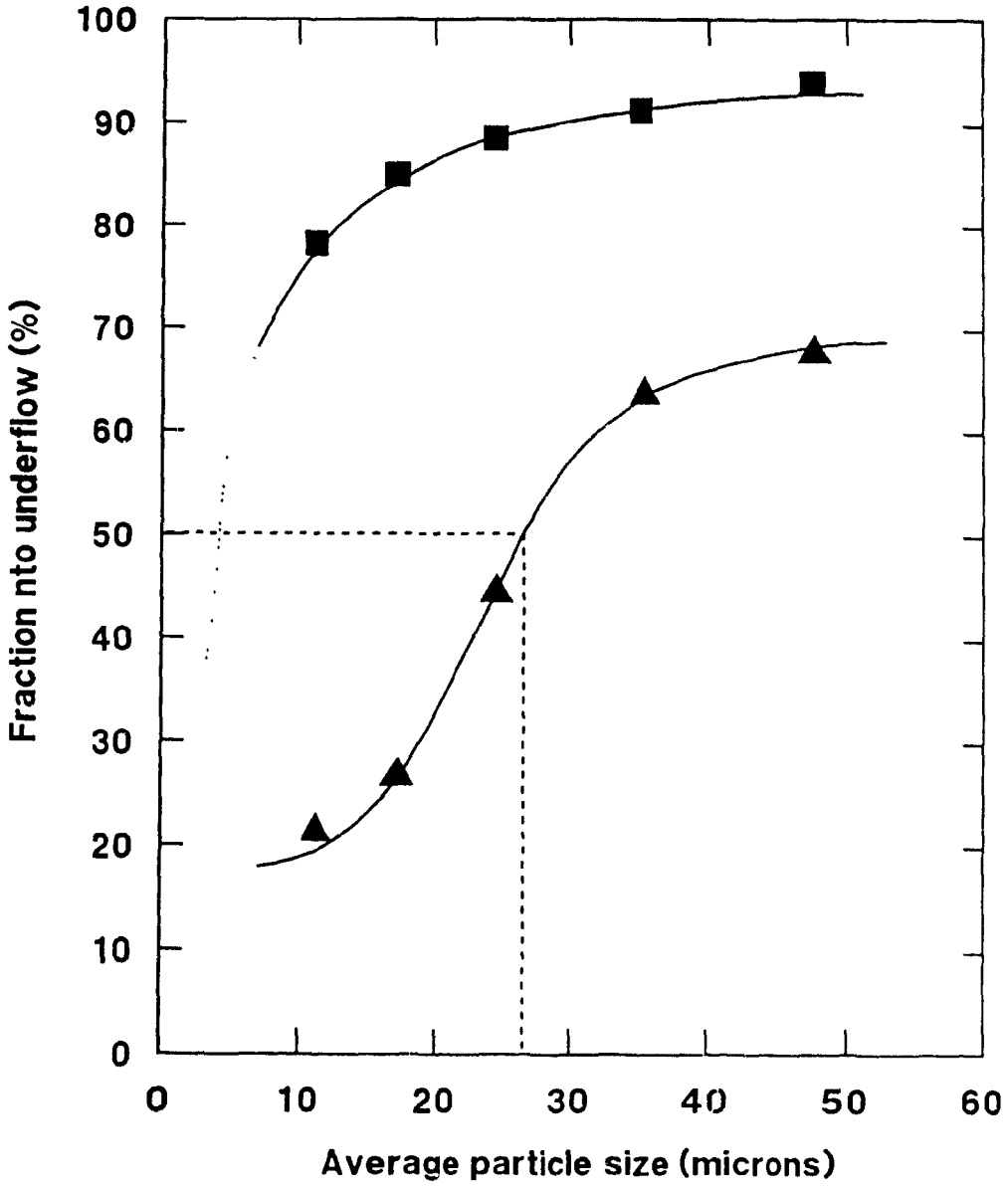

Figure 22. Performance curves of magnetite and dolomite with magnetic field

(After Watson [4])

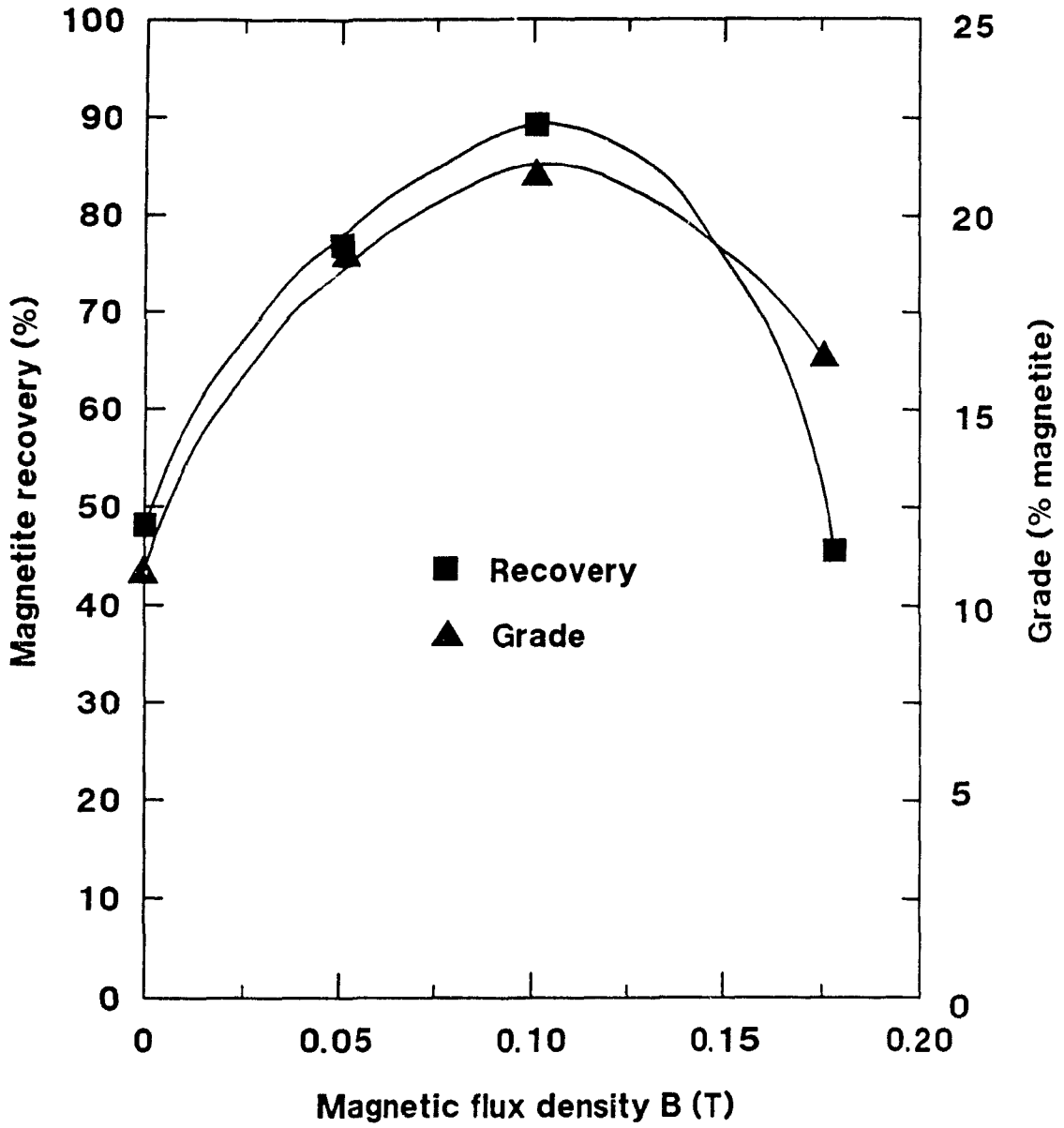

Figure 23. Grade and recovery curves for separation with varying magnetic flux density (pressure, 6 psi; pulp density 19.4 wt%) (magnetite : dolomite = 1:9)

(After Watson [4])

CHAPTER FIVE

THE NEW DESIGN OF WATSON MAGNETIC HYDROCYCLONE

In Chapter 4, both Fricker's and Watson's magnetic hydrocyclones were analysed. The data from the numerical analysis show that the efficiency of Watson's magnetic circuitry was lower than that of Fricker's. Watson's design needs improving. In this chapter, new designs are explored.

5.1. A NEW DESIGN USING FOUR MAGNETIC POLES

A new design employing four magnetic poles has been studied by numerical analysis The top view of the new design is shown in Fig.24. It has two parts: coils and toothed poles. The structure of the magnetic poles differs from Watson's. It can be seen that each two opposite poles have the same magnetic polarity, i.e. N pole vs. N pole and S pole vs. S pole.

5.1.1. Design Variations

In this 4 pole design, there are three design parameters: the width and height of the magnetic pole, and the diameter of the cyclone.

In this study, only two parameters are varied: the width of the pole and the diameter of the cyclone. The height of the magnetic pole is fixed to equal the radius of the cyclone. For example, when the cyclone diameter is 0.1 m, the magnetic pole is 0.05 m high.

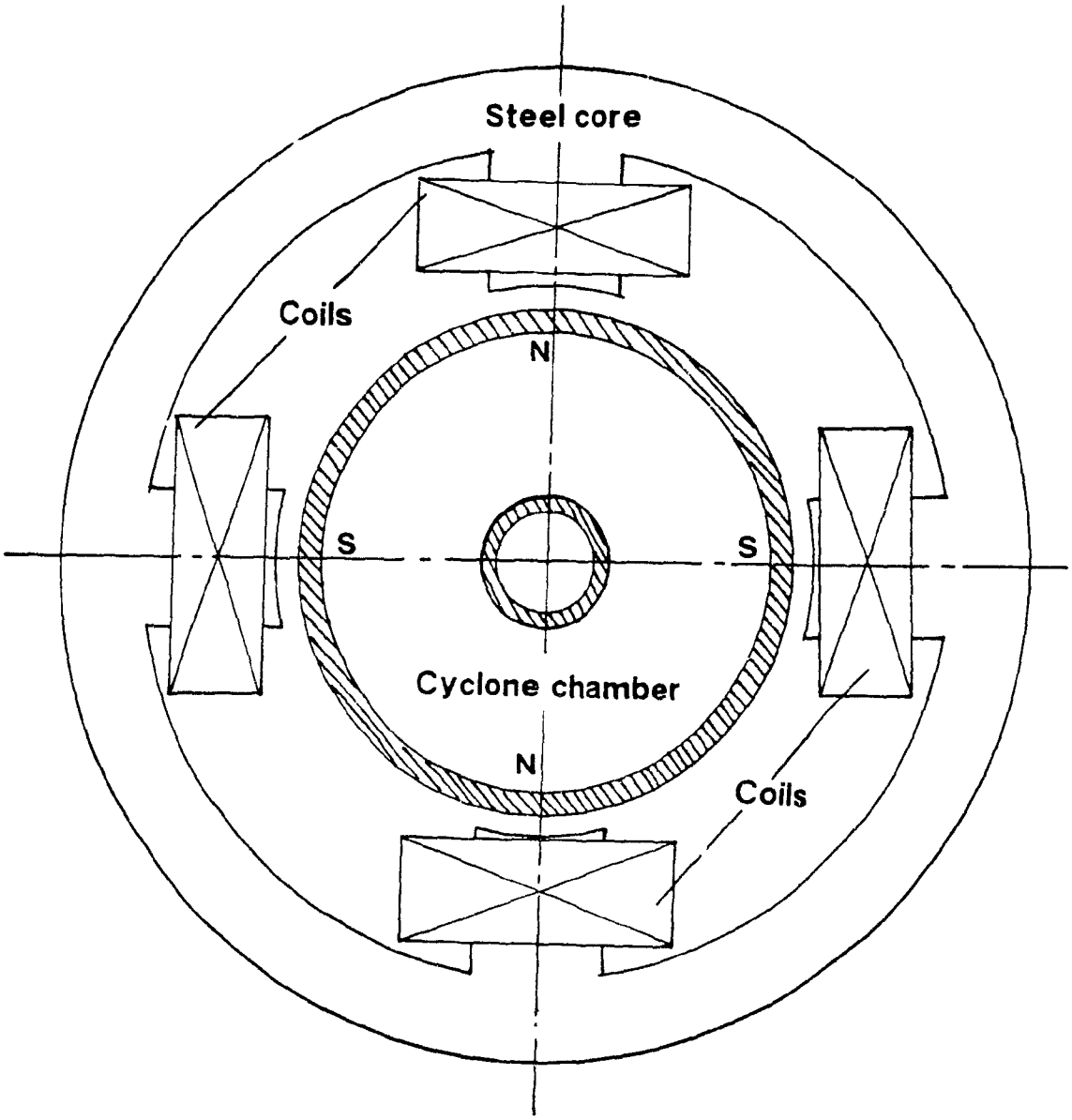

Figure 24. Top view of a new design for Watson magnetic hydrocyclone

The ratio of the width of poles to the circumference of the cyclone is used to scale the width of the pole. For example, when the ratio is 0.4 and the cyclone diameter is 0.1 m (i.e. the circumference is 0.314 m), the width of a magnetic pole is equal to 0.0314 m.

5.1.2. Features of Magnetic Field

Because the 4 pole design has a symmetrical magnetic circuitry, the total area of the magnetic field can be divided into four parts for study. Each part represents one quarter of the cyclone chamber.

Fig.25 shows the magnetic flux density B between N pole and S pole when the width ratio is 0.53 and the cyclone diameter is 0.1m. It can be seen that the magnetic flux lines are curved in the cyclone chamber The magnetic flux density B is equal to zero at the center of the cyclone chamber From the center of the cyclone chamber to the pole surface, the flux density B increases.

The direction and magnitude of the force factor are shown in Fig.26 and Table 8 respectively. There are two features of the force factor in this design:

(i) Direction of force factors.

From Fig.26, it can be seen that force factors are outward in most of the area of the cyclone chamber. Only in the small area bounded by force factors H5, H6, I5 and I6, is the radial component of force factors inward. Consequently the direction of the average radial force factor is outwards.

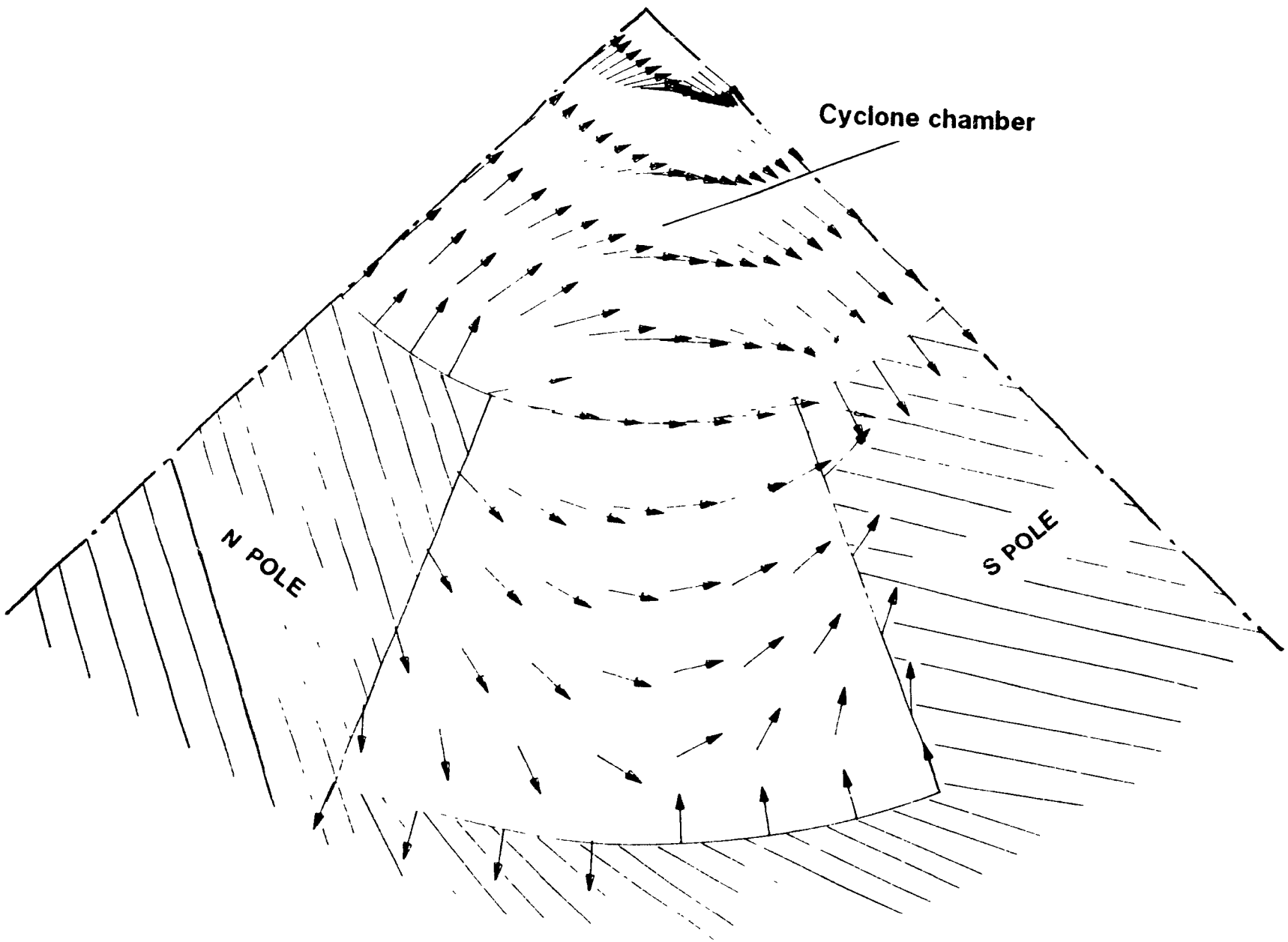

Figure 25. Magnetic flux density B between N and S pole
(1/4 of total area)

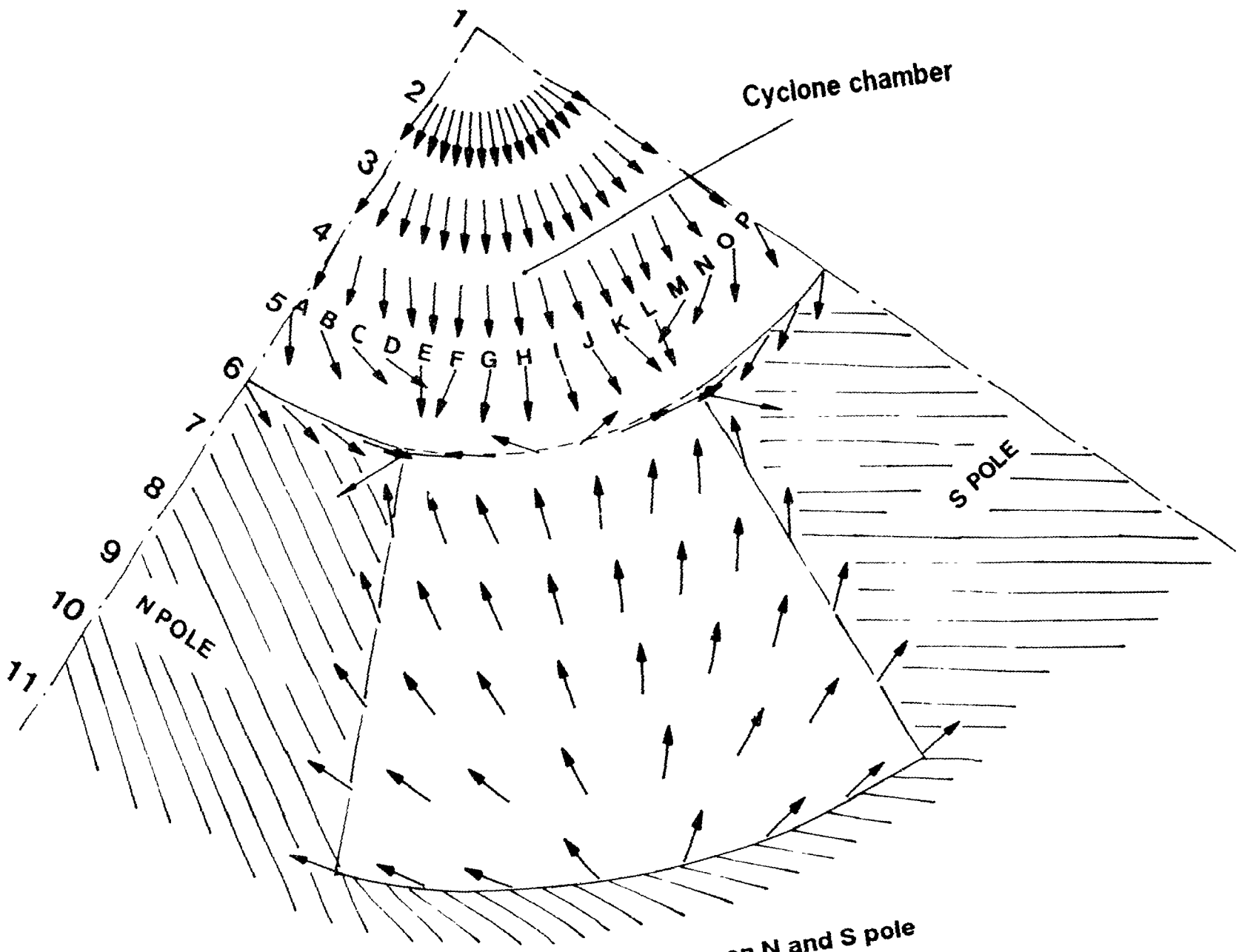

Figure 26. Force factors between N and S pole
(1/4 of total area)

Table 8. The distribution of force factors in the new design *

	A	B	C	D	E	F	G	H	I	J	K	L	M	N	O	P
1	0.0	0.0	0.0	0.0	0.0	0.0	0.0	0.0	0.0	0.0	0.0	0.0	0.0	0.0	0.0	0.0
2	1.7	1.7	1.7	1.7	1.8	1.8	1.8	1.8	1.8	1.8	1.8	1.8	1.7	1.7	1.7	1.7
3	3.1	3.1	3.3	3.5	3.7	3.7	3.7	3.7	3.7	3.7	3.7	3.7	3.5	3.3	3.1	3.1
4	3.1	3.3	4.2	5.4	7.6	6.5	6.1	5.9	5.9	6.1	6.5	7.6	5.4	4.2	3.3	3.1
5	1.7	2.6	5.5	11.5	25.7	14.9	8.9	6.6	6.6	8.9	14.9	25.7	11.5	5.5	2.6	1.7
6	1.1	2.1	5.0	38.2	100.0	41.8	17.1	5.1	5.1	17.1	41.8	100.0	38.2	5.0	2.1	1.1
7					25.2	15.4	10.2	7.9	7.9	10.2	15.4	25.2				
8					7.8	6.6	5.4	4.7	4.7	5.4	6.6	7.8				
9		N			4.2	3.5	2.7	2.2	2.2	2.7	3.5	4.2		S		
10					3.0	2.1	1.3	0.7	0.7	1.3	2.1	3.0				
11					2.6	1.7	0.9	0.2	0.2	0.9	1.7	2.6				

* 4 poles;

B = 1.0 Tesla on poles;

Diameter of cyclone chamber = 0.1 m;

Width of poles / circumference of cyclone = 0.53;

(ii) The magnetic energy consumed between poles.

In this structure, the toothed poles are necessary for forming the magnetic field having radially outwards force factors. From Fig.25, it can be seen that there is magnetic field distributed in the space between the poles, i.e some of the magnetic energy is consumed between the magnetic poles.

5.1.3. Comparison with Fricker's and Watson's (2-pole) Magnetic Hydrocyclones

Table 9 shows the comparison between the 4 pole design, Fricker's, and Watson's original 2 pole magnetic hydrocyclone. Their diameters are set at 0.1 meter. The boundary conditions are: a) B is 1.0 Tesla on the inner pole of Fricker's magnetic hydrocyclone; b) B is 1.0 Tesla on the corner of poles in either Watson's 2 pole magnetic hydrocyclone or the 4 pole design.

It can be seen that the best magnetic circuitry is Fricker's. Fricker's magnetic hydrocyclone has the highest average radial force factor (A R F.) and there is no tangential component of the force factor in the cyclone chamber (thus A T F. and A A T F. are zero). From the viewpoint of the magnetic energy, Fricker's is also the best. These advantages result from the magnetic circuitry which has the symmetrical cylindrical poles.

Comparing the 2 and new 4 pole Watson magnetic hydrocyclone designs, the new 4 pole design is a significant improvement. From Table 9, it can be seen that A.R.F. of the 4 pole design is 4.93 T^2/m which is much higher than the $0.1662^2/m$ of the 2 pole design.

Table 9. Comparision of three magnetic hydrocyclones

		Fricker's	Watson's 2-pole	Watson's 4-pole
Diameter	m	0.1	0.1	0.1
B (max)	Tesla	1.0*	1.0**	1.0**
F.F.(max)	T^2/m	43.4	50.3	68.8
A.R.F.	T^2/m	16.20	0.1662	4.93
A.A.R.F.	T^2/m	16.20	0.5492	5.23
A.T.F.	T^2/m	0	1.5×10^{-6}	4.7×10^{-5}
A.A.T.F.	T^2/m	0	0.4512	6.85
E(c)	J	1126	785	672

* B (max) is 1 Tesla on the surface of the inner pole;

** B (max) is 1 Tesla on the corner of poles;

Diameter is the cyclone diameter, m;

B (max) is the maximum flux density in the field, T;

F.F.(max) is the maximum force factor in the cyclone chamber, T^2/m;

A.R.F. is the average radial force factor, T^2/m;

A.A.R.F is the average of absolute value of radial force factor, T^2/m;

A.T.F. is the average tangential force factor, T^2/m;

A.A.T F. is the average of absolute value of tangential force factor, T^2/m;

E(c) is the magnetic energy in the cyclone chamber, J;

Also the difference between A.A.R.F. and A.R.F. in the 4 pole design is 0.3 T^2/m (about 6% of A.A.R.F.). This means that only a small part of the outwards force factors is being counteracted. However, in the 2 pole design, the difference between A.A.R.F. and A.R.F. is equal to about 70% of A.A.R.F., i.e. a great deal of the outwards force factor is counteracted.

From Fig.26, it can be seen that the directions of force factors A5 - P5 and A6 - P6 are toward the corner of the poles; It is these force factors that yield the large tangential component. Table 9 shows A.A.T.F. of the 4 pole design is equal to 6.85 T^2/m.

5.1.4. Gradient of Magnetic Field

Compared with the 4 pole design, in the cyclone chamber the magnetic energy of the 2 pole magnetic hydrocyclone is 785 J, which is larger than the 672 J of the 4 pole design. The boundary condition in both cases is that B = 1.0 Tesla on the corner of the poles. However, the average radial and tangential force factors of the 2 pole design is less than that of the 4 pole design. The reason is that the gradient of the magnetic field in the 2 pole design is lower.

From Fig.18, it can be seen that the magnetic field between two poles, i.e. the magnetic field in the cyclone chamber, is almost a uniform magnetic field. The gradient of the magnetic flux density B is, therefore, quite low. For example, at the center of the chamber B is 0.463 Tesla but the gradient of B is zero and consequently the force factor is zero.

In the case of Watson's original magnetic hydrocyclone, part of the energy is used to generate this uniform magnetic field in the cyclone chamber while another part is distributed outside of the cyclone. This type of magnetic circuitry, i.e. two opposite poles (N pole vs. S pole), should be avoided.

5.1.5. Effect of Design Variables

(i) Effect of the width of poles

Table 10 (a) shows the effect of the width of poles on the force factor. It can be seen that with increasing pole width, A.R.F. varies slightly and reaches a maximum value when the width ratio is 0.67.

On the other hand, columns (5) and (3) show that both A.A.T.F. and A.A.R.F. attain the minimum values with the width ratio of 0.8. It means that the wider the poles the less the wastage of the magnetic energy.

As discussed above, the width of poles should be as wide as possible in the 4 pole design. If electromagnets are contemplated, the space between magnetic poles will be occupied by the coil so that the width of poles is limited. In the case of a permanent magnet, the width of poles does not have this limitation.

In Table 11 (a), it can be seen that the fraction of the energy in the chamber R(e) varies slightly with increasing width ratio. When the width ratio is set at 0.53, R(e) is equal to 0.6524 no matter the cyclone diameter (Table 11 (b)). It means that the distribution of the magnetic energy in the total volume

Table 10. Indices of force factor in 4 pole design

(B = 1.0 Tesla on the corner of poles)

(a) various width of poles *

(1) Ratio	(2) A.R.F. (T^2/m)	(3) A.A.R.F. (T^2/m)	(4) A.T.F. (T^2/m)	(5) A.A.T.F. (T^2/m)
0.2667	4.6745	5.2605	8.58E-05	7.6804
0.4	4.8282	5.379	9.35E-05	7.309
0.5333	4.9281	5.2314	4.76E-05	6.8524
0.6667	4.9711	4.9711	3.58E-05	5.9327
0.8	4.8155	4.8192	1.68E-05	3.9163

* Diameter of cyclone = 0.1 m;

(1) is the ratio of total width of poles to circumference;

(b) various diameter of cyclone **

(1) Diameter (m)	(2) A.R.F. (T^2/m)	(3) A.A.R.F. (T^2/m)	(4) A.T.F. (T^2/m)	(5) A.A.T.F. (T^2/m)
0.1	4.9281	5.2314	4.76E-05	6.8524
0.15	3.2854	3.4876	3.17E-05	4.5682
0.2	2.464	2.6157	2.38E-05	3.4262
0.25	1.9712	2.0926	1.90E-05	2.7409
0.35	1.408	1.4947	1.36E-05	1.9578
0.5	0.9856	1.0463	9.52E-06	1.3705

** Width of poles / circumference = 0 53;

(1) is the diameter of cyclone, m;

(2) is the average radial force factor, T^2/m;

(3) is the average of absolute value of radial force factor, T^2/m;

(4) is the average tangential force factor, T^2/m;

(5) is the average of absolute value of tangential force factor, T^2/m;

Table 11. Indices of magnetic energy in 4 pole design

(B = 1.0 Tesla on the corner of poles)

(a) various width of poles *

Ratio	E(c) (J)	E(t) (J)	R(e)
0.2667	626.1	1042.8	0.6004
0.4	680.3	1077.2	0.6315
0.5333	672.3	1030.5	0.6524
0.6667	593.4	900.7	0.6588
0.8	428	669.8	0.6390

* Diameter of cyclone = 0.1 m;

Ratio = width of poles / circumference;

(b) various diameter of cyclone **

Diameter (m)	E(c) (J)	E(t) (J)	R(e)
0.1	672.3	1030.5	0.6524
0.15	1512.6	2318.6	0.6524
0.2	2689.1	4122.0	0.6524
0.25	4201.7	6400.7	0.6524
0.35	8235.3	12623.7	0.6524
0.5	16806.8	25762.7	0.6524

** Width of poles / circumference = 0.53;

Diameter = the diameter of cyclone, m;

E(c) = the magnetic energy in cyclone chamber, J;

E(t) = the magnetic energy in total volume, J;

R(e) = E(c) / E(t);

is only a function of the pole width.

(ii) Effect of the cyclone diameter

From Table 10 (b), it can be seen that A.R.F. decreases sharply with increasing cyclone diameter. When the cyclone diameter is 0.5 m, A.R.F. equals 0.99 T^2/m which is only 20% of 4.93 T^2/m with a cyclone diameter of 0.1 m.

Table 11 (b) shows that the magnetic energy both in the chamber and in the total volume increases sharply with increasing cyclone diameter.

Comparing with Table 4, the magnetic energy in the total volume of the 4 pole design is slightly less than the magnetic energy in the chamber of Fricker's magnetic hydrocyclone at the same diameter.

5.1.6. Forces on a magnetite particle and d50c, m

Because the radial component of the force factor is outwards in the 4 pole design, the combined force on a magnetite particle can be written as:

$$F_j = F_m + F_c - F_d \qquad (5.1)$$

The definition of the forces is same as that in Eq.4.10 for Watson's 2 pole magnetic hydrocyclone.

Fig.27 shows the three forces on a magnetite particle and force ratios in the 4 pole design. Three forces are calculated with Eqs.1.1, 1.2 and 1.3. The force factor equals 4.82 T^2/m, which is A.R.F. of the 4 pole design with a width ratio of 0.8

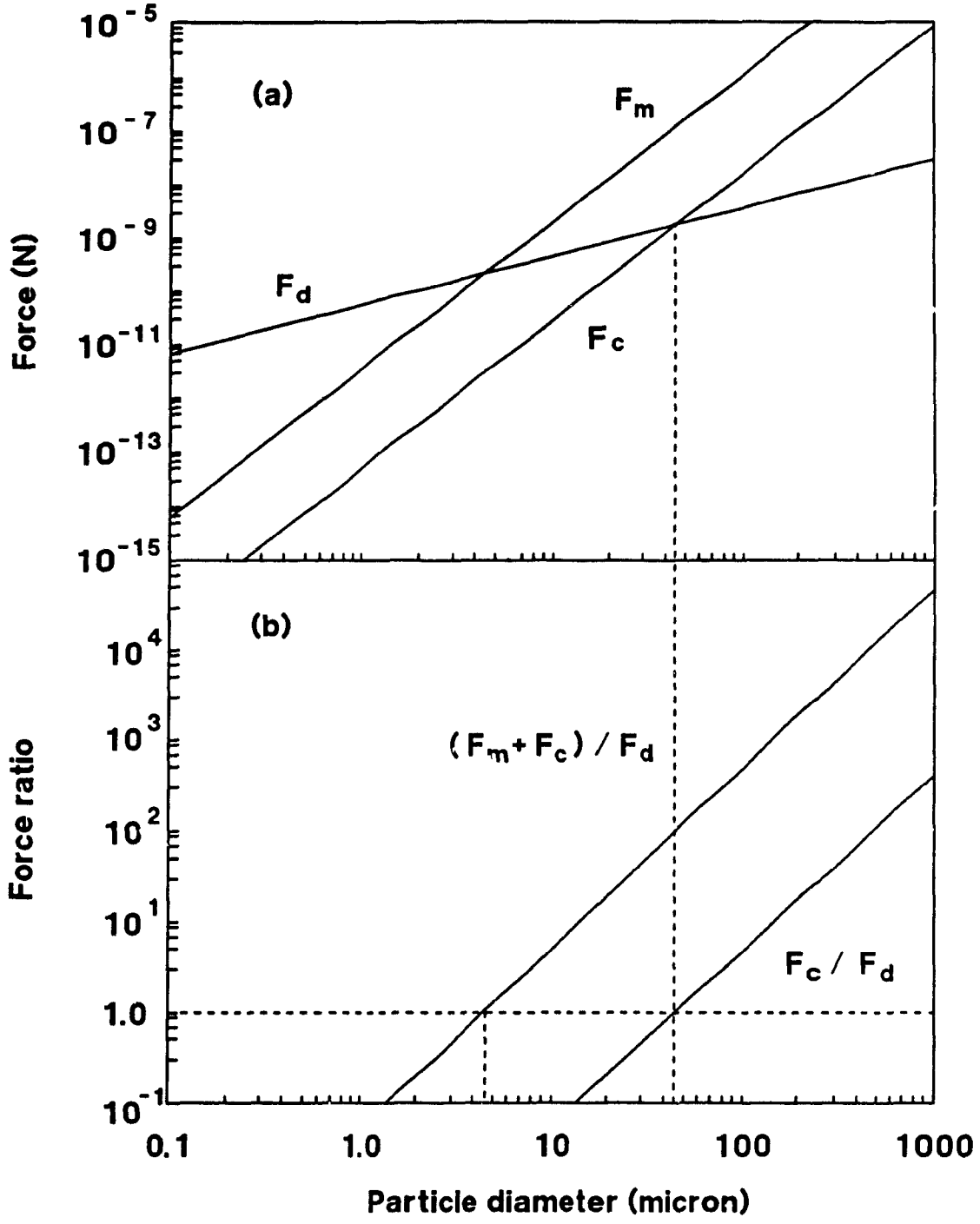

Figure 27. Forces and force ratios as functions of magnetite particle size in 4 pole design

(Table 10.(a)). Other conditions are the same as those of the 2 pole magnetic hydrocyclone. They are:

cyclone diameter = 0.1 m; κ = 2.375;

V_t= 1.06 m/s; V_r= 0.012 m/s;

r = 0.022 m; μ = 0.001 kg/m·s;

ρ_s= 5200 kg/m^3; ρ_l= 1000 kg/m^3;

Fig.27 shows the cut size of the magnetite is 32 μm without a magnetic force. When the force factor is 4.82 T^2/m in the cyclone chamber, $d_{50c,m}$ of the magnetite is 4.8 μm. This value should be compared with the 20.2 μm of Watson's 2 pole magnetic hydrocyclone.

Table 12 shows the effect of the cyclone diameter on $d_{50c,m}$ of the magnetite. It can be seen that although A.R.F decreases from 4.92 to 0.99 T^2/m, a five fold decrease, with increasing cyclone diameter from 0.1 to 0.5m, $d_{50c,m}$ of the magnetite increases only from 4.8 to 10.6 μm, i.e. two fold increase.

5.2. DESIGNS OF MULTIPOLE MAGNETIC CIRCUITRY

An obvious extension of the 4 pole design is to go to a multipole magnetic circuitry. However, the magnetic field of the multipole magnetic circuitry is much more complex than that of 4 pole design.

Table 12. Effect of cyclone diameter on cut size in 4 pole design *

Diameter (m)	A.R.F. (T^2/m)	$ds0_{c,m}$ (μm)
0.1	4.92	4.8
0.15	3.29	5.8
0.2	2.46	6.7
0.25	1.97	7.5
0.35	1.41	8.9
0.5	0.99	10.6

* Width of poles / circumference = 0.53;
B = 1.0 Tesla on the corner of poles;
Diameter = the diameter of cyclone, m;
A.R.F. = the average radial force factor, T^2/m;
$ds0_{c,m}$ = the cut size of magnetite, μm;

5.2.1. Magnetic flux patterns

Fig.28 (a) shows the magnetic flux patterns in Watson's 2 pole magnetic hydrocyclone. Results of both numerical analysis and Watson's tests have shown the low efficiency of this magnetic circuitry. Fig.28 (b) shows the magnetic flux patterns in the 4 pole design. Numerical analysis has shown the greater efficiency of this magnetic circuitry. The general design feature of adjoining opposite poles is preferable in going to a multipole design.

In a multipole design, there are some restrictions:

(i) Any structure with an odd number of magnetic poles is not available. For example, a magnetic circuitry of five magnetic poles must have an asymmetric field no matter how the poles are arranged.

(ii) Any structure which uses opposite poles should be avoided (cf the 2 pole design). Fig.29 shows the magnetic flux patterns in a design of six magnetic poles. In Fig.29, the curved arrows show the magnetic flux patterns which are similar to those in the 4 pole design. However, the straight darker arrows show the patterns which are similar to those of the 2 pole magnetic hydrocyclone. In this case, the efficiency of the flux patterns N_1-S_1, N_1-S_3, N_2-S_1, N_2-S_2, N_3-S_2 and N_3-S_3 is reduced by the flux patterns N_1-S_2, N_3-S_1 and N_2-S_3. So this 6 pole design is not recommended. Some others, such as the magnetic circuitries of 10, 14 and 18 poles, are not recommended for the same reason.

The remaining possible magnetic circuitries, such as

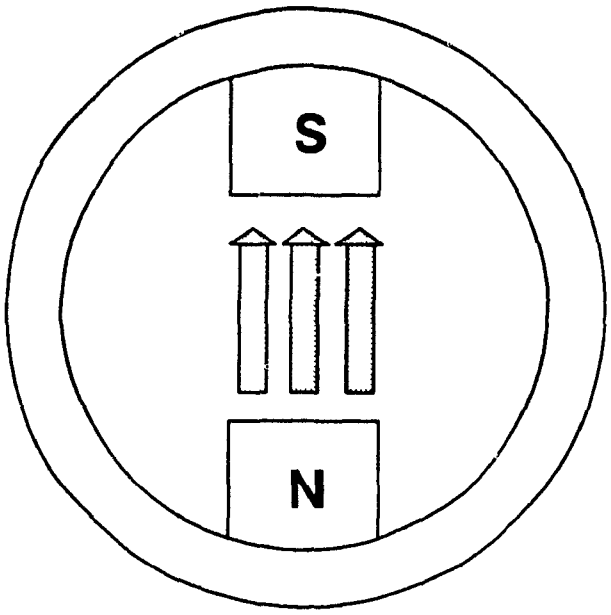

(a) 2 poles

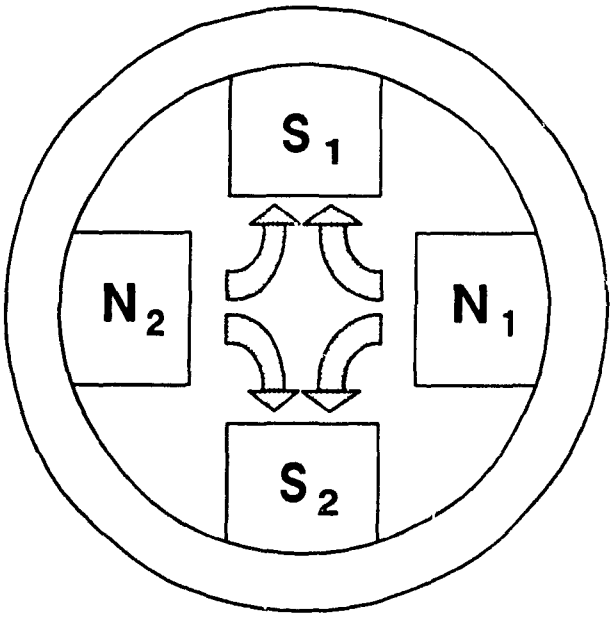

(b) 4 poles

Figure 28. Magnetic flux patterns of two magnetic circuitries

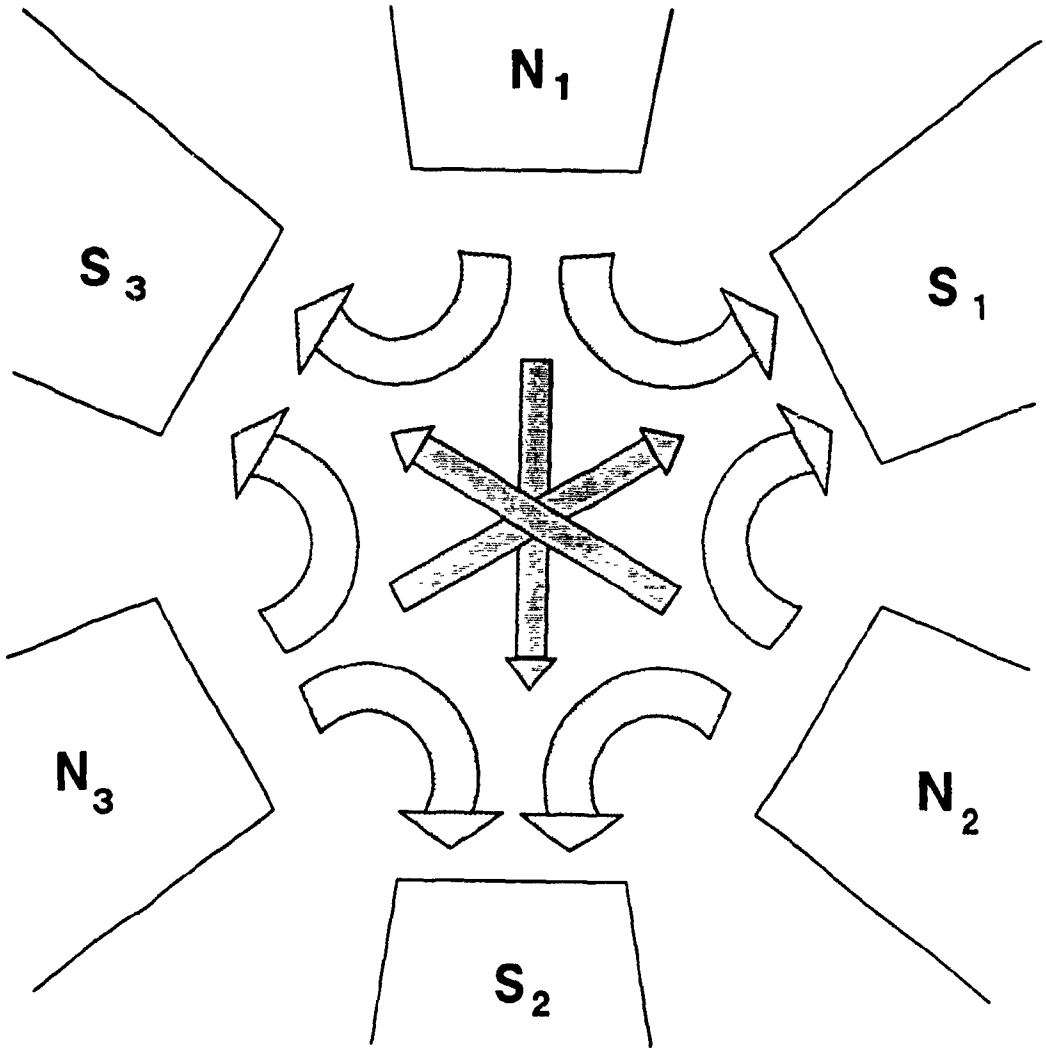

Figure 29. Magnetic flux patterns of the 6 pole magnetic circuitry

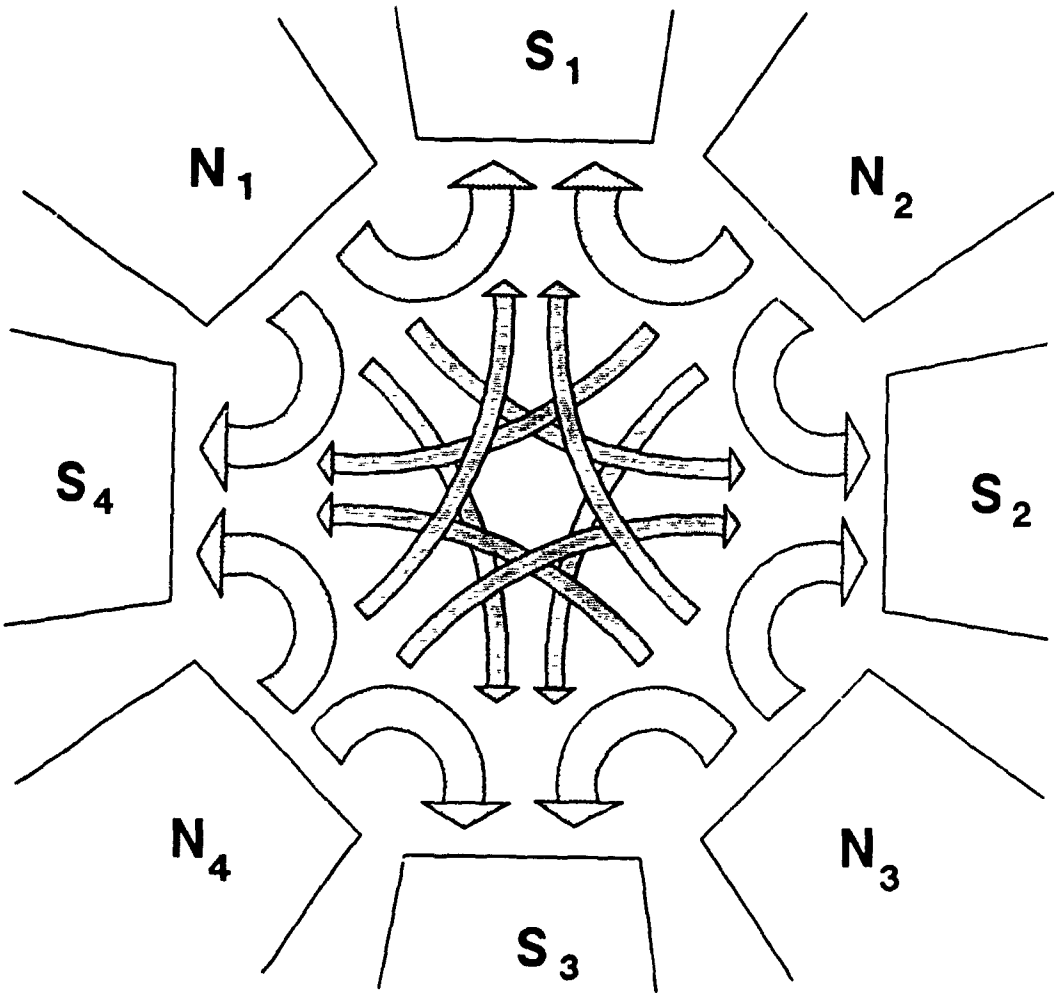

Figure 30. Magnetic flux patterns of the 8 pole magnetic circuitry

structures of 8, 12, and 16 magnetic poles, are recommended. Fig.30 shows the flux patterns of an 8 pole magnetic circuit. The magnetic flux patterns are divided into two groups. The first group includes the flux patterns N_1-S_1, N_1-S_4, N_2-S_1, N_2-S_2, N_3-S_2, N_3-S_3, N_4-S_3 and N_4-S_4. The magnetic field generated by these flux patterns can be calculated with the method used in the 4 pole design.

The second group includes the flux patterns N_1-S_2, N_1-S_3, N_2-S_4, N_2-S_3, N_3-S_1, N_3-S_4, N_4-S_2 and N_4-S_1. The features of the magnetic field generated by these patterns are at present unknown. An assumption is that this magnetic field is sufficiently weaker than that generated by the flux patterns in the first group so that it can be ignored.

In this study, only the magnetic field generated by flux patterns of the first group is evaluated.

5.2.2. Features of Magnetic Field

The numerical analysis has been performed for the designs of 8, 12 and 16 magnetic poles. The distributions of the magnetic field density B and the force factors are similar to those of the 4 pole design. From Table 13, it can be seen that the three magnetic fields are symmetrical fields because the A.T.F.'s are almost zero. A feature of the three fields, which the 4 pole design does not have, is that there is no inwards force factor in the cyclone chamber because all A.A.R.F. are equal to A.R.F. (Table 13).

Table 13. Indices of force factor in 8, 12 and 16 pole designs with various width of poles *

(a) 8 Poles

(1) Ratio	(2) A.R.F. (T^2/m)	(3) A.A.R.F. (T^2/m)	(4) A.T.F. (T^2/m)	(5) A.A.T.F. (T^2/m)
0.2667	6.9792	6.9792	1.73E-04	11.8344
0.4	7.3134	7.3134	1.18E-04	10.6557
0.5333	7.2576	7.2576	1.00E-05	9.2044
0.6667	6.7819	6.7819	5.87E-05	7.0748
0.8	5.8339	5.8339	1.90E-05	4.0594

(b) 12 poles

(1) Ratio	(2) A.R.F. (T^2/m)	(3) A.A.R.F. (T^2/m)	(4) A.T.F. (T^2/m)	(5) A.A.T.F. (T^2/m)
0.2667	8.4207	8.4207	2.42E-04	14.5496
0.4	8.6101	8.6101	2.14E-04	12.5096
0.5333	8.2812	8.2812	1.20E-04	10.1267
0.6667	7.4364	7.4364	4.70E-05	7.2701
0.8	6.1432	6.1432	1.24E-05	3.976

Table 13. Indices of force factor in 8, 12 and 16 pole designs with various width of poles * (cont'd)

(c) 16 poles

(1) Ratio	(2) A.R.F. (T^2/m)	(3) A.A.R.F. (T^2/m)	(4) A.T.F. (T^2/m)	(5) A.A.T.F. (T^2/m)
0.2667	9.4069	9.4069	3.20E-04	16.1682
0.4	9.3504	9.3504	1.83E-04	13.4621
0.5333	8.7648	8.7648	1.24E-04	10.4968
0.6667	7.6931	7.6931	7.53E-05	7.2726
0.8	6.2564	6.2564	1.04E-05	3.9432

* Diameter of hydrocyclone = 0.1 m;
B = 1.0 Tesla on poles;
(1) is the ratio of width of poles to circumference;
(2) is the average radial force factor, T^2/m;
(3) is the average of absolute value of radial force factor, T^2/m;
(4) is the average tangential force factor, T^2/m;
(5) is the average of absolute value of tangential force factor, T^2/m;

5.2.3. Effects of Design Variables

(i) Effect of the width of the pole

Table 13 shows the effect of the pole width on the force factor in designs of 8, 12 and 16 poles.

In order to compare the three designs with the 4 pole design, A.R.F. and A.T.F. of the four circuitries are shown in Figs.31 and 32 respectively. In the 4 pole design, the maximum value (4.97 T^2/m) of A.R.F. is attained with a width ratio of 0.67. In the 16 pole design, the maximum A.R.F. (9.4 T^2/m) occurs with a width ratio of 0.27. The optimum value of the pole width becomes smaller with increasing number of magnetic poles.

Fig.32 shows that A.T.F. increases sharply as the width ratio decreases. The maximum A.T.F. is 16.2 T^2/m (172% of A.R.F.) with the width ratio of 0.27 in the 16 pole design.

With the view to seek a maximum A.R.F., the choice is the 16 pole design with the width ratio of 0.27 although it has a large A.T.F..

Table 14 shows the effect of the pole width on the magnetic energy in designs of 8, 12 and 16 poles. From Figs.33 and 34, it can be seen that in 4 and 8 pole designs the maximum values of magnetic energy both in the cyclone chamber and total volume occurs with the width ratio of 0.4. However, in 12 and 16 pole designs, the maximum values are at a width ratio of 0.27. The 16 pole design with a width ratio of 0.27 has the greatest magnetic energy in the cyclone chamber (724J) and in the total volume (1293J).

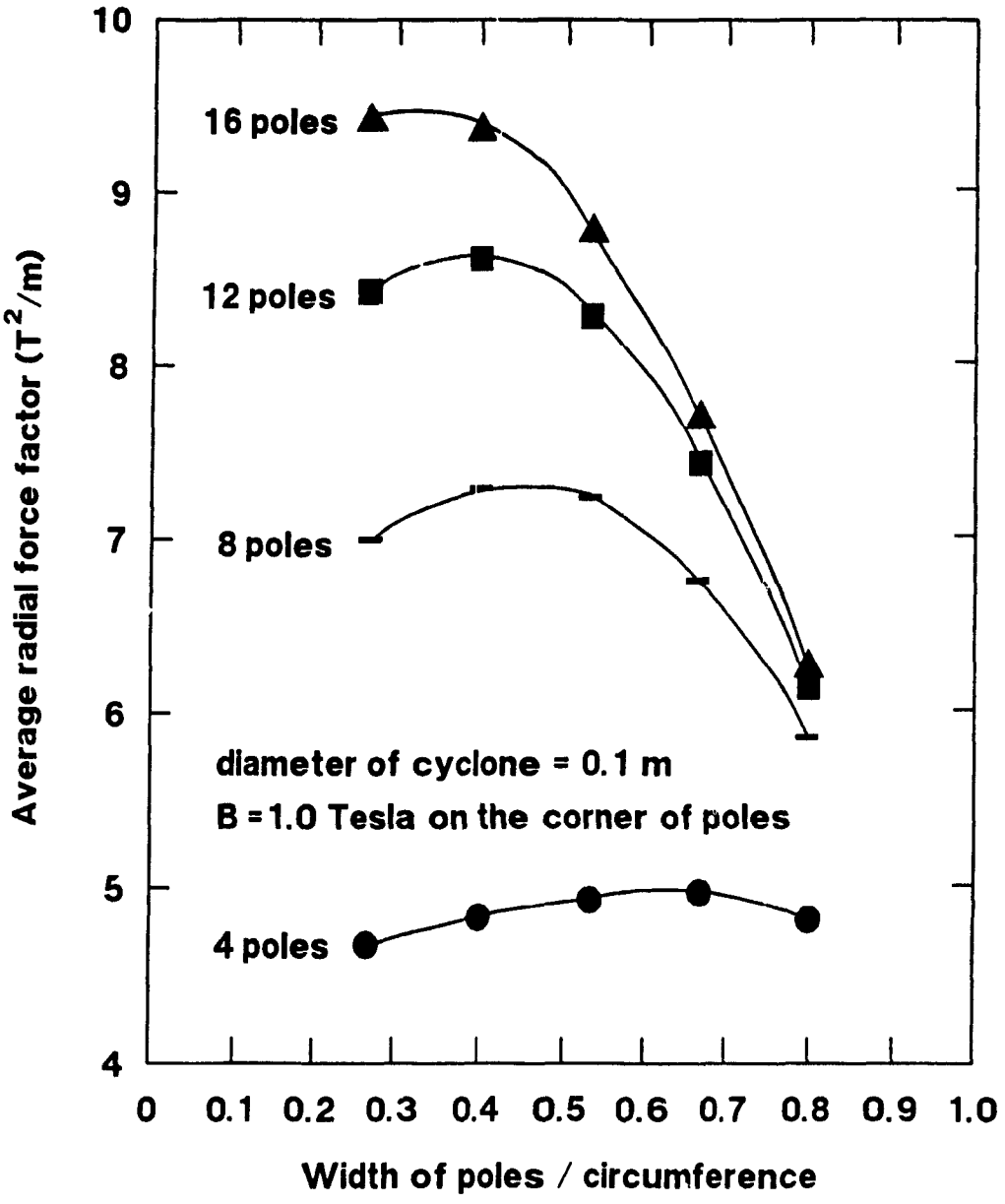

Figure 31. Average radial force factor in cyclone chamber as a function of width ratio in new designs

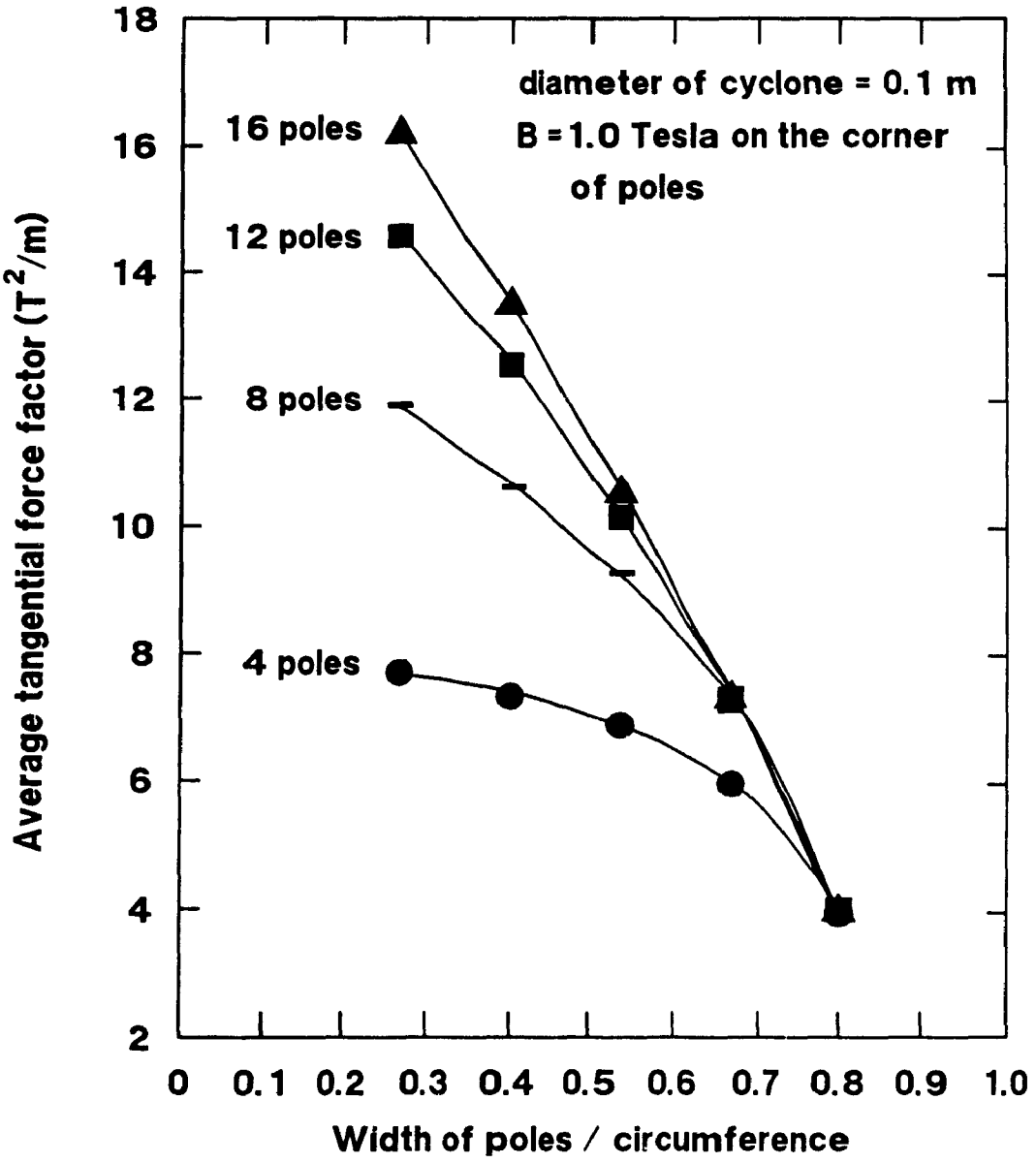

Figure 32. Average tangential force factor in cyclone chamber as a function of width ratio in new designs

Table 14. Indices of magnetic energy in 8, 12 and 16 pole designs with various width of poles *

(a) The magnetic energy in cyclone chamber

Ratio	8 poles (J)	12 poles (J)	16 poles (J)
0.2667	652.7	687.2	723.5
0.4	673.2	679.5	690.4
0.5333	634.5	618	609.8
0.6667	531.8	501.7	484.6
0.8	365	338.8	325.3

(b) The magnetic energy in total volume

Ratio	8 poles (J)	12 poles (J)	16 poles (J)
0.2667	1087.4	1190.4	1293.2
0.4	1095.8	1161.1	1222.5
0.5333	1026.5	1055.7	1080.9
0.6667	872.1	869.6	869.3
0.8	624.1	607	598

(c) E (c) / E (t)

Ratio	8 poles	12 poles	16 poles
0.2667	0.6002	0.5773	0.5595
0.4	0.6143	0.5852	0.5647
0.5333	0.6181	0.5854	0.5642
0.6667	0.6098	0.5769	0.5575
0.8	0.5848	0.5582	0.5440

* Diameter of hydrocyclone = 0.1 m;
B = 1.0 Tesla on the corner of poles;
Ratio = width of poles / circumference;
E (c) = magnetic energy in the chamber, J;
E (t) = magnetic energy in total volume, J;

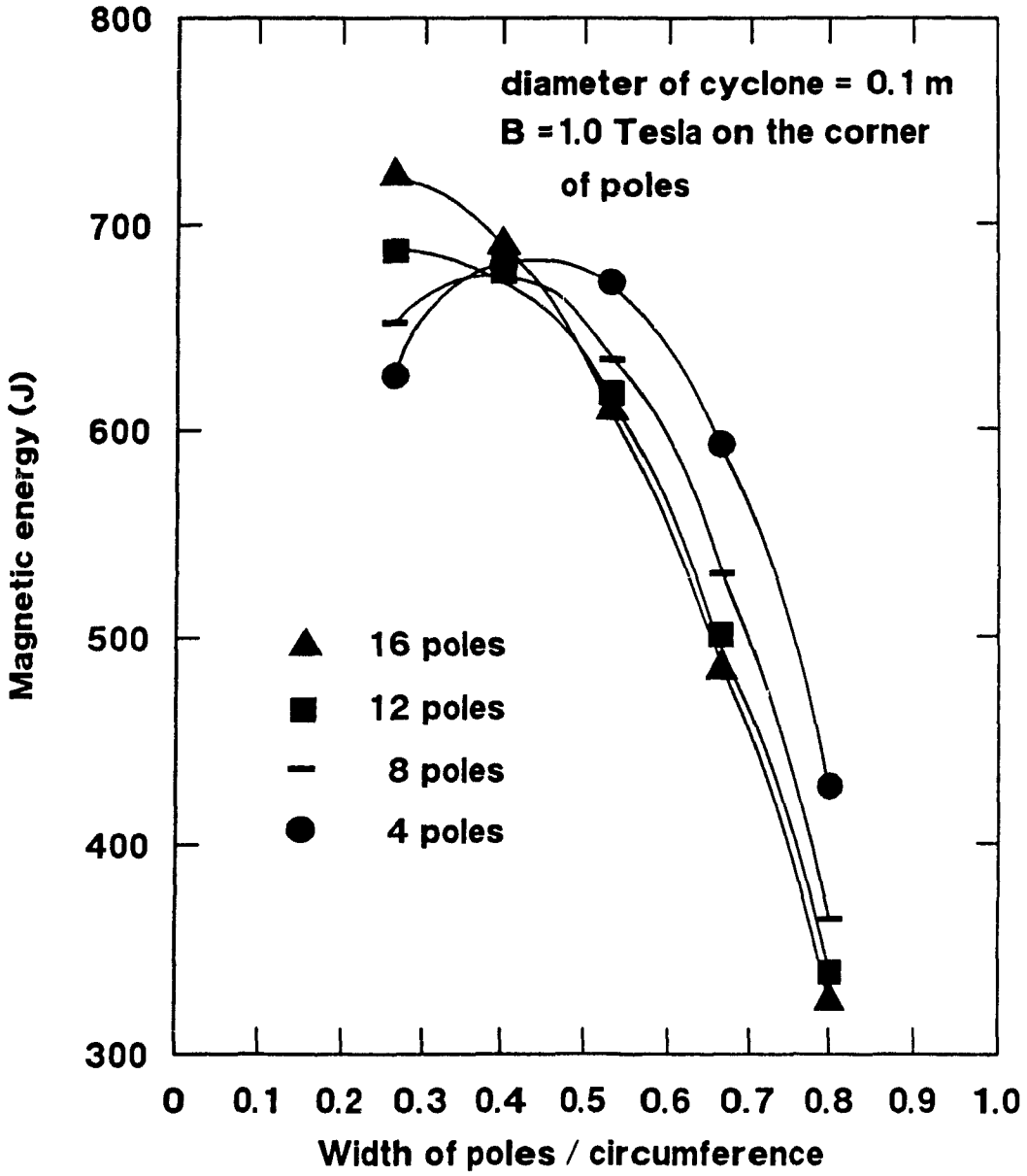

Figure 33. Magnetic energy in cyclone chamber as a function of width ratio in new designs

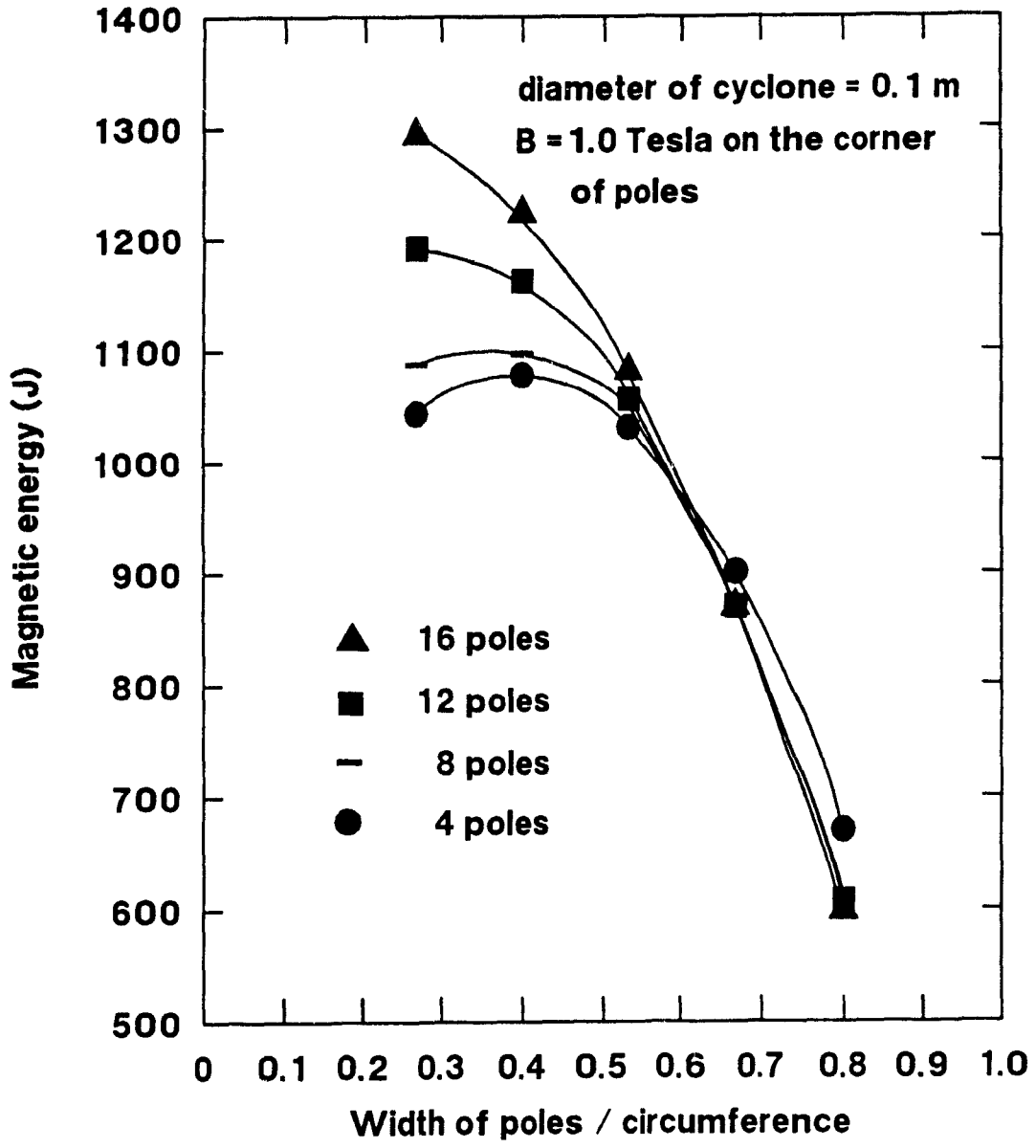

Figure 34. Magnetic energy in total volume as a function of width ratio in new designs

In Table 14 (c), it can be seen that the ratio of E(c) to E(t) varies slightly: the 16 pole design with a width ratio of 0.8 shows the minimum value 0.544.

(ii) Effect of the cyclone diameter

Table 15 shows the effect of the cyclone diameter on the force factor in designs of 8, 12 and 16 poles. In Figs.35 and 36, it can be seen that both A.R.T and A.T.F. decrease sharply upon increasing cyclone diameter. In Fig.35, at a cyclone diameter of 0.5 m, the difference among the curves is less than the difference at a cyclone diameter of 0.1 m. It means that the advantage of the 16 pole design is more apparent at a cyclone diameter of 0.1 m than at a diameter of 0.5 m.

Table 16 shows the effect of the cyclone diameter on the magnetic energy in the designs of 8, 12 and 16 poles. From Figs.37 and 38, it can be seen that there is no obvious difference among the curves. As a result all designs have almost the same power consumption at the same cyclone diameter.

As discussed above, the optimum choice for the multipole magnetic circuitry remains the 16 pole design with the width ratio of 0.27.

5.2.4. Relationship between $d_{50c,m}$ and cyclone diameter

Table 17 shows the effect of the cyclone diameter on $d_{50c,m}$ of magnetite in the 16 pole design. The conditions are the same as those in Table 12.

Table 15. Indices of force factor in 8, 12 and 16 pole designs with various diameter of cyclone #

(a) 8 Poles

(1) Diameter (m)	(2) A.R.F. (T^2/m)	(3) A.A.R.F. (T^2/m)	(4) A.T.F. (T^2/m)	(5) A.A.T.F. (T^2/m)
0.1	7.2576	7.2576	1.01E-04	9.2044
0.15	4.8384	4.8384	6.70E-05	6.1363
0.2	3.6288	3.6288	5.02E-05	4.6022
0.25	2.903	2.903	4.02E-05	3.6818
0.35	2.0736	2.0736	2.87E-05	2.6298
0.5	1.4515	1.4515	2.01E-05	1.8409

(b) 12 Poles

(1) Diameter (m)	(2) A.R.F. (T^2/m)	(3) A.A.R.F. (T^2/m)	(4) A.T.F. (T^2/m)	(5) A.A.T.F. (T^2/m)
0.1	8.2812	8.2812	1.20E-04	10.1267
0.15	5.5208	5.5208	8.02E-05	6.7511
0.2	4.1406	4.1406	6.01E-05	5.0633
0.25	3.3125	3.3125	4.81E-05	4.0507
0.35	2.3661	2.3661	3.44E-05	2.8933
0.5	1.6562	1.6562	2.41E-05	2.0253

Table 15. Indices of force factor in 8, 12 and 16 pole designs with various diameter of cyclone * (cont'd)

(c) 16 Poles

(1) Diameter (m)	(2) A.R.F. (T^2/m)	(3) A.A.R.F. (T^2/m)	(4) A.T.F. (T^2/m)	(5) A.A.T.F. (T^2/m)
0.1	8.7648	8.7648	1.24E-04	10.4968
0.15	5.8432	5.8432	8.29E-05	6.9979
0.2	4.3824	4.3824	6.22E-05	5.2484
0.25	3.5059	3.5059	4.97E-05	4.1987
0.35	2.5042	2.5042	3.55F-05	2.9991
0.5	1.753	1.753	2.49E-05	2.0994

* Width of poles / circumference = 0.53;
B = 1.0 Tesla on the corner of poles;
(1) is the diameter of cyclone, m;
(2) is the average radial force factor, T^2/m;
(3) is the average of absolute value of radial force factor, T^2/m;
(4) is the average tangential force factor, T^2/m;
(5) is the average cf absolute value of tangential force factor, T^2/m;

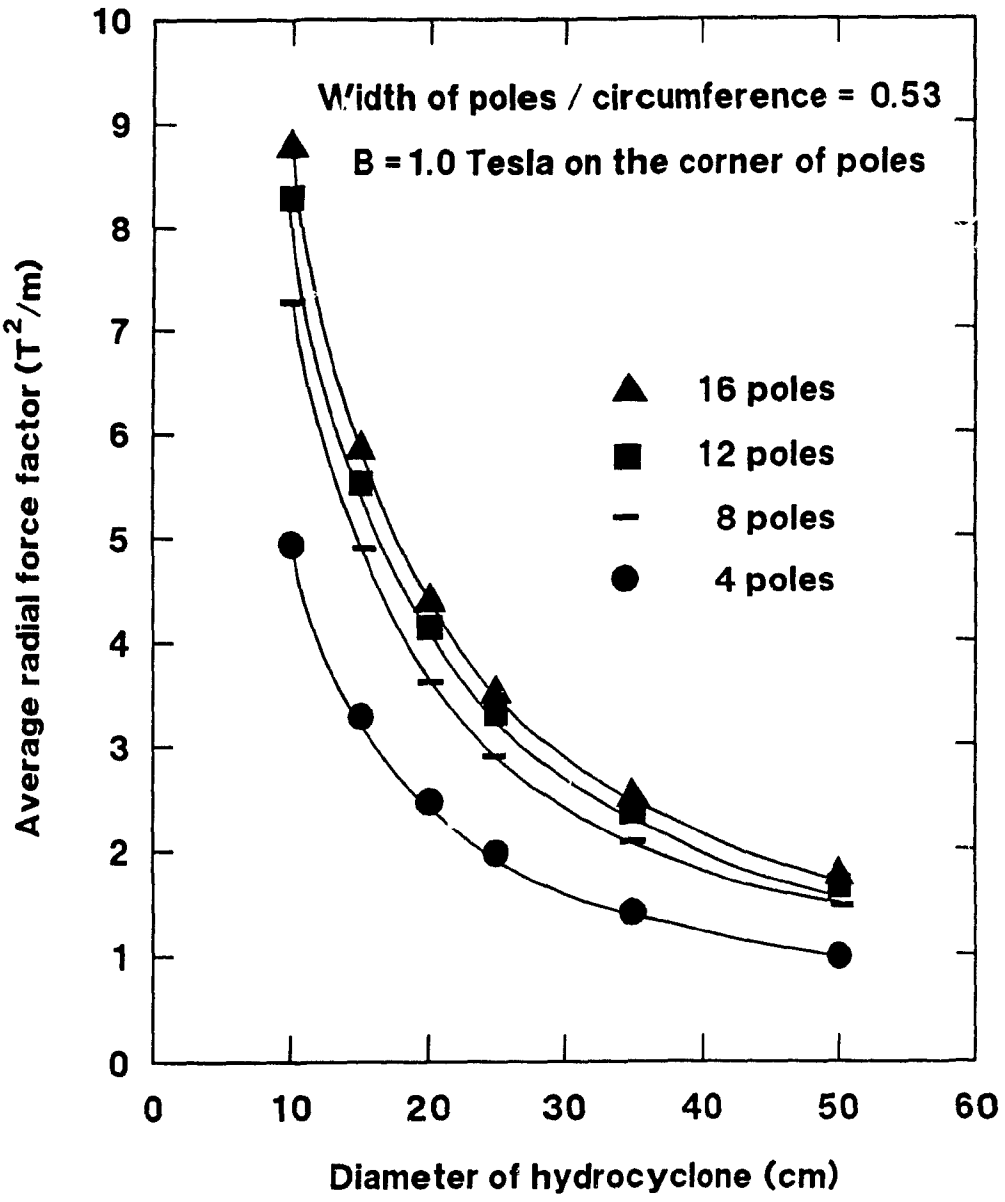

Figure 35. Average radial force factor in cyclone chamber as a function of cyclone diameter in new designs

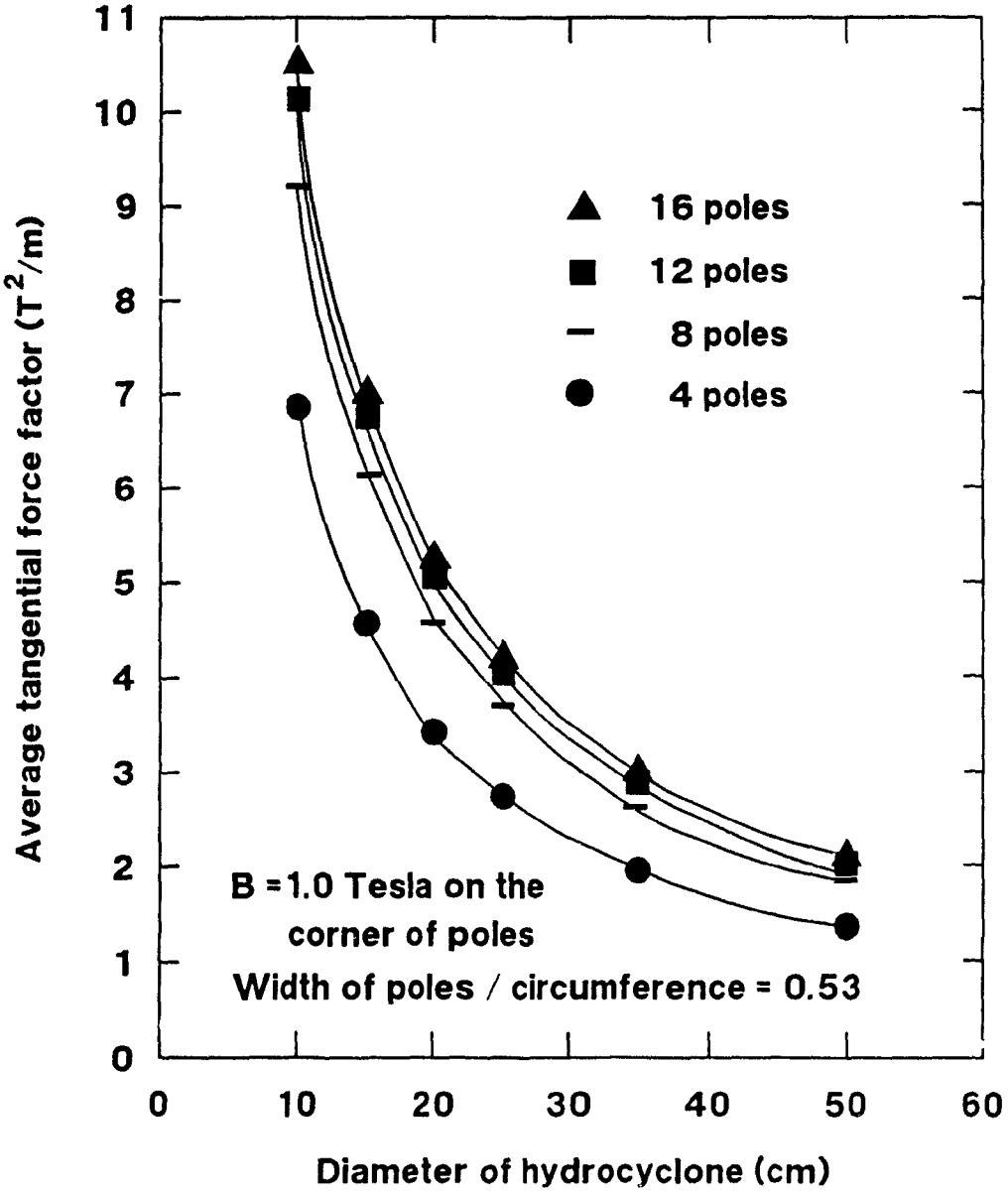

Figure 36. Average tangential force factor in cyclone chamber as a function of cyclone diameter in new designs

Table 16. Indices of magnetic energy in 8, 12 and 16 pole designs with various diameter of cyclone *

(a) The magnetic energy in cyclone chamber

Diameter (m)	8 poles (J)	12 poles (J)	16 poles (J)
0.1	634.5	618	609.8
0.15	1427.6	1390.4	1372.1
0.2	2537.9	2471.8	2439.3
0.25	3965.4	3862.2	3811.4
0.35	7772.2	7570	7470.3
0.5	15861.7	15448.8	15245.6

(b) The magnetic energy in total volume

Diameter (m)	8 poles (J)	12 poles (J)	16 poles (J)
0.1	1026.5	1055.7	1080.9
0.15	2309.6	2375.3	2432
0.2	4106	4222.7	4323.6
0.25	6415.6	6598	6755.6
0.35	12574.6	12932	13241.1
0.5	25662.5	26391.9	27022.6

(c) E (c) / E (t)

Dia.(m)	8 poles	12 poles	16 poles
0.1	0.6181	0.5854	0.5642
0.15	0.6181	0.5854	0.5642
0.2	0.6181	0.5854	0.5642
0.25	0.6181	0.5854	0.5642
0.35	0.6181	0.5854	0.5642
0.5	0.6181	0.5854	0.5642

* Width of poles / circumference = 0.53;
B = 1.0 Tesla on the corner of poles;
Dia. = the diameter of cyclone, m;
E (c) = magnetic energy in the chamber, J;
E (t) = magnetic energy in total volume, J;

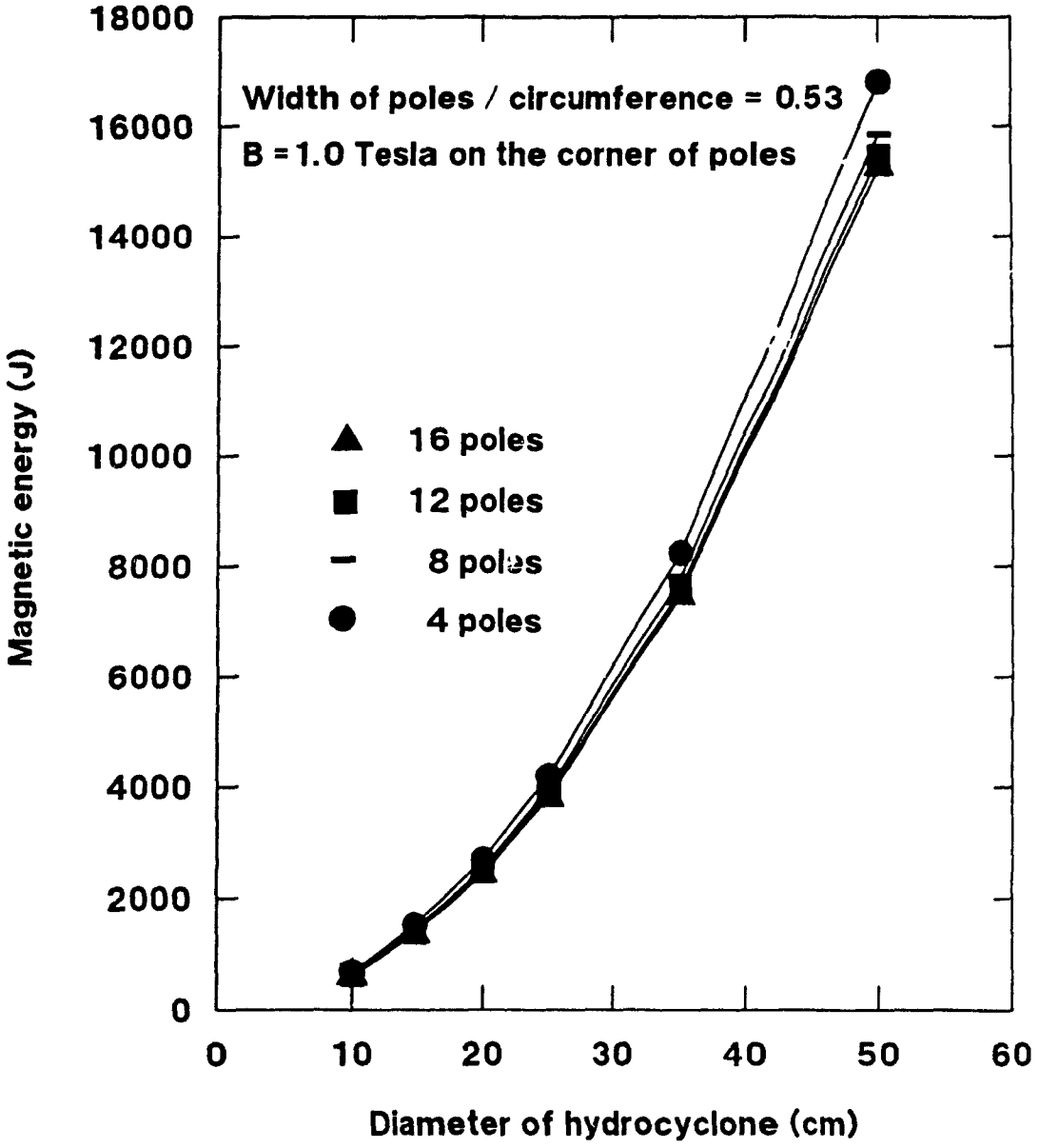

Figure 37. Magnetic energy in cyclone chamber as a function of cyclone diameter in new designs

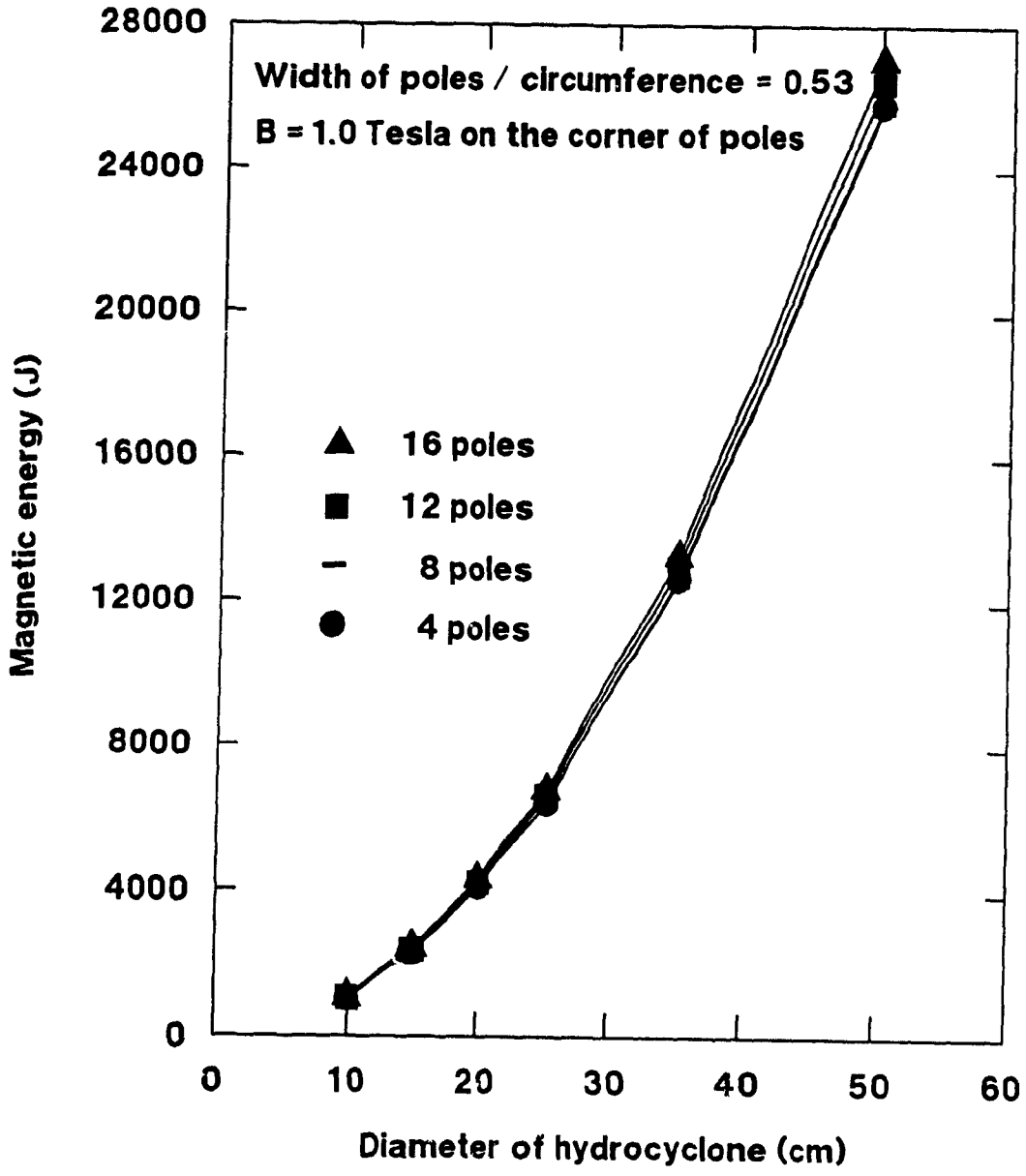

Figure 38. Magnetic energy in total volume as a function of cyclone diameter in new designs

When the cyclone diameter equals 0.5 m, A.R.F is 1.75 T^2/m, which is about a five fold decrease compared with a cyclone diameter at 0.1 m; however, $d_{50c,m}$ of magnetite is only about two times as large (7.8 μm vs. 3.6μm).

Comparing the $d_{50c,m}$ of magnetite at a cyclone diameter of 0.5m with that of the 4 pole design (Table 12), the decrease from 10.2 to 7.8 μm in cut size of the magnetite may be attractive for the industrial user. The performance of the new design will be evaluated by the simulation in the following chapter.

Table 17. Effect of cyclone diameter on cut size in 16 pole design*

Diameter (m)	A.R.F. (T^2/m)	$d_{50c,m}$ (μm)
0.1	8.76	3.6
0.15	5.84	4.4
0.2	4.38	5.1
0.25	3.51	5.7
0.35	2.50	6.7
0.5	1.75	8.0

* Width of poles / circumference = 0.53;
B = 1.0 Tesla on the corner of poles;
Diameter = the diameter of cyclone, m;
A.R.F. = the average radial force factor, T^2/m;
$d_{50c,m}$ = the cut size of magnetite, μm;

CHAPTER SIX

MATHEMATICAL SIMULATION OF MAGNETITE RECOVERY

Dense medium separation has been widely used in coal preparation. In the coarse coal treatment by the dense-media process, after the dense-media cyclone, sieve-bend screens, vibrating screens and drum magnetic separators are used to separate and recover the media from the coal and refuse products [7]. This media recovery flowsheet is complex. It is desirable to simplify the circuit. Attempts to do so by using magnetic separation alone have generally been unsuccessful, because of entrainment of coal which has lead, for example, to trying high gradient devices operated at high slurry velocity [6].

The possibility exists to use magnetic hydrocyclones to simplify the media recovery circuit. Either alone, or in particular combinations of Fricker and Watson type magnetic hydrocyclones may permit the efficient media recovery with a smaller difference in particle size between media and coal or waste eliminating need to use screens as part of the recovery process. The possibility then exists of using heavy media on finer coal particles. These possibilities are explored here by mathematical simulation.

In this simulation, the Fricker magnetic hydrocyclone and the new 16 pole design with the width ratio of 0.27 are used as models.

6.1. FUNDAMENTALS OF SIMULATION

6.1.1. Corrected Performance Curves of Magnetic Hydrocyclones

By means of Plitt's equation [8], the separation performance of the magnetic hydrocyclone can be represented as follows

$$C_i = 1 - e^{-0.693\ x_i^m} \tag{6.1}$$

$$x_i = \frac{d_i}{d_{50c,m}} \tag{6.2}$$

where

$d_{50c,m}$ = the corrected cut size, μm;

d_i = the characteristic size of particle size class i, μm;

m = the sharpness of separation coefficient, dimensionless;

C_i = the function to the underflow of class i, dimensionless;

According to Eq.6.1, the corrected performance curves of Fricker's magnetic hydrocyclone and the new 16 pole design are shown in Figs. 39 and 40 respectively. In this case, m is set at 2.5 [1,2]. The specific gravities of the coal and shale are 1.32 and 2.5 respectively [7].

6.1.2. Mathematical Model of Simulation

Some mathematical models of the hydrocyclone have been constructed [2,5,8]. However, they can not be used for magnetic hydrocyclones because of the introduction of the magnetic force. The mathematical model for the simulation is based only on the corrected performance curves shown in Figs. 39 and 40.

There are two components in the feed: mineral A (magnetite)

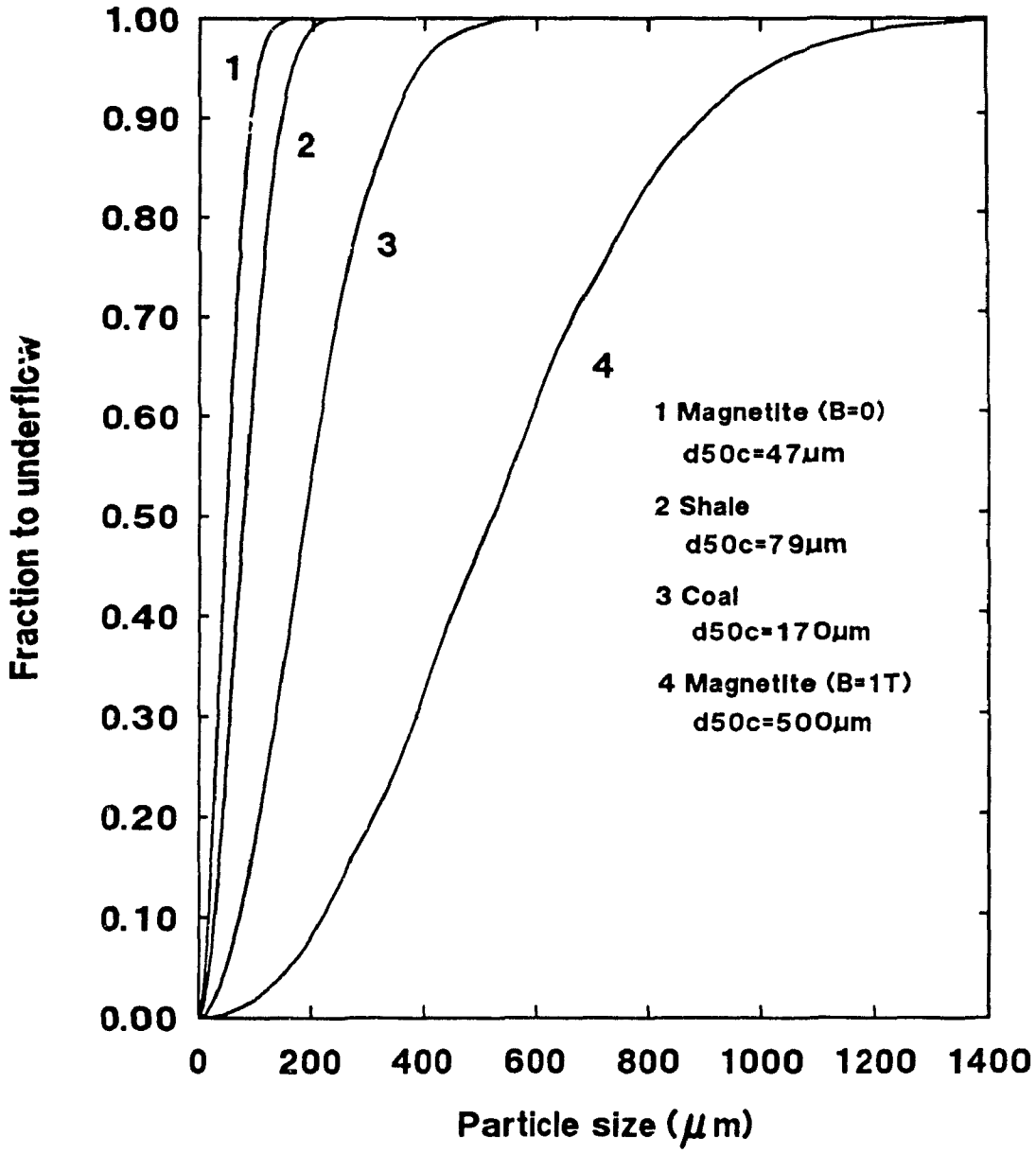

Figure 39. Corrected performance curves in the Fricker magnetic hydrocyclone

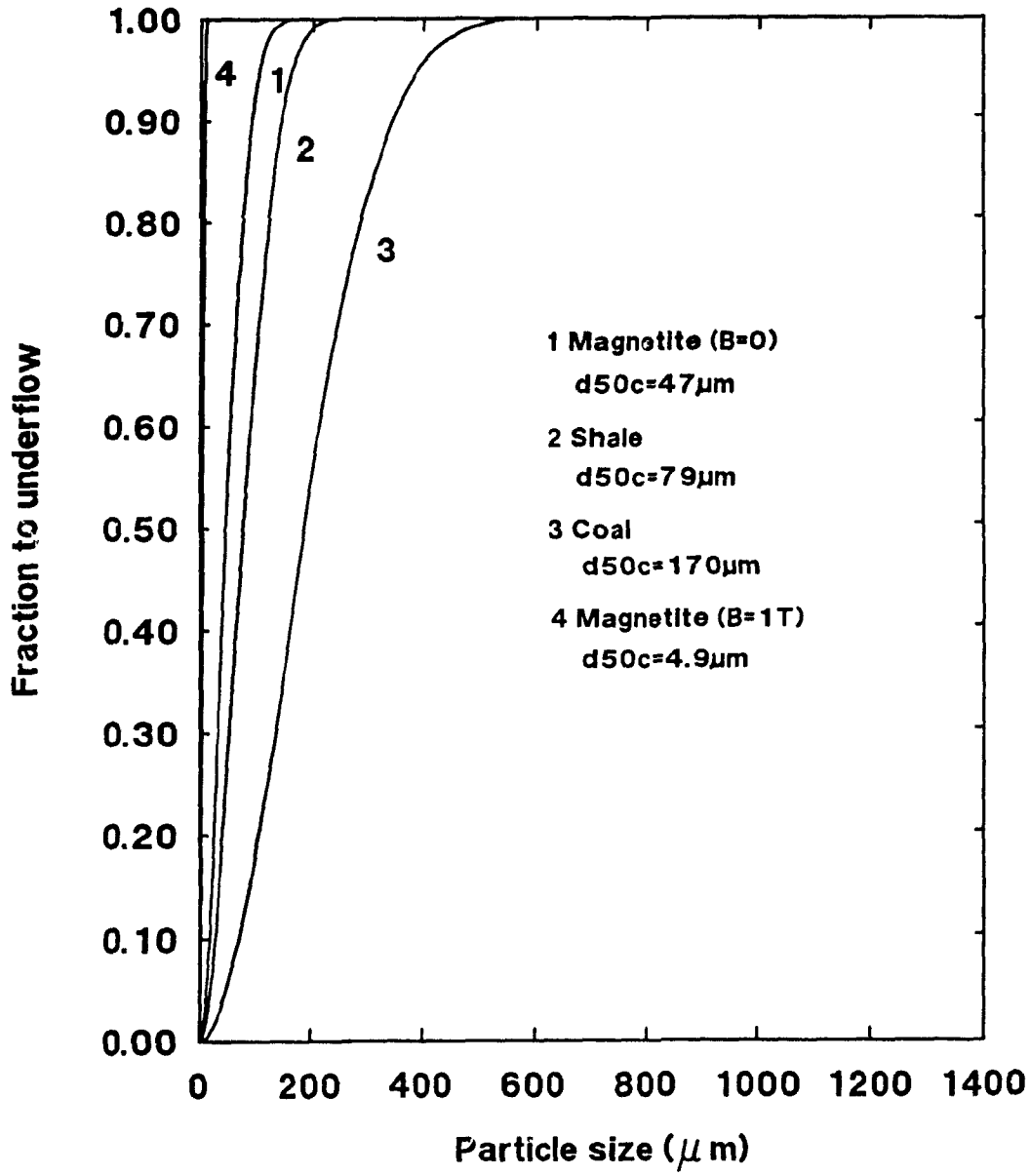

Figure 40. Corrected performance curves in the 16 pole design of the Watson magnetic hydrocyclone

and mineral B (coal or shale). The size range of the feed is divided into one hundred size classes.

In the feed, the fraction of the mineral A is F_A. In the size class i of the feed, the fraction of the mineral A is fA_i. The relationship between F_A and fA_i is defined as

$$F_A = \sum_{i=1}^{100} fA_i \qquad (6.3)$$

With the same meaning as Eq.6.3, the relationship between F_B and fB_i is defined as

$$F_B = \sum_{i=1}^{100} fB_i \qquad (6.4)$$

In the simulation, an assumption is that there is no bypass effect on the mineral A (magnetite) because of the magnetic force. But the mineral B (coal or shale) still has the bypass effect. In the underflow, the component of the mineral A, U_A is defined as

$$U_A = \sum_{i=1}^{100} fA_i \cdot Ci_A \qquad (6.5)$$

and the component of the mineral B, U_B is defined as

$$U_B = \sum_{i=1}^{100} fB_i \cdot \left[Rf + (1- Rf)\, Ci_B \right] \qquad (6.6)$$

where Ci_A and Ci_B are the fractions reporting to the underflow of class i of the mineral A and B respectively, which are defined by Eq.6.1; Rf (set at 0.2) is the recovery of the feed water to the underflow (see Appendix B).

In the underflow, five characteristics are defined as

$$G_{UA} = \frac{U_A}{U_A + U_B}; \qquad G_{UB} = \frac{U_B}{U_A + U_B};$$

$$R_{UA} = \frac{U_A}{F_A}; \qquad R_{UB} = \frac{U_B}{F_B};$$

$$Y_U = U_A + U_B;$$

where the R_{UA} and G_{UA} are the recovery and grade of the mineral A respectively; the R_{UB} and G_{UB} are the recovery and grade of the mineral B respectively; the Y_U is the yield of the underflow.

The fractions of the mineral A and B reporting to the overflow are defined as

$$O_A = 1 - U_A; \qquad O_B = 1 - U_B;$$

Other characteristics of the overflow are defined as

$$G_{OA} = \frac{O_A}{O_A + O_B}; \qquad G_{OB} = \frac{O_B}{O_A + O_B};$$

$$R_{OA} = \frac{O_A}{F_A}; \qquad R_{OB} = \frac{O_B}{F_B};$$

$$Y_O = O_A + O_B;$$

where the R_{OA} and G_{OA} are the recovery and grade of the mineral A respectively; the R_{OB} and G_{OB} are the recovery and grade of the mineral B respectively; the Y_O is the yield of the overflow.

6.2. CONDITIONS OF SIMULATION

In this simulation, two types of magnetic hydrocyclones are used. The conditions are:

(i) The Fricker magnetic hydrocyclone.

the diameter of the cyclone = 0.2 m;

the magnetic flux density B on the inner pole = 1.0 Tesla;

$d_{50c,m}$ of the shale = 79 μm;

$d_{50c,m}$ of the coal = 170 μm;

$d_{50c,m}$ of the magnetite = 500 μm;

(ii) The 16 pole design of the Watson magnetic hydrocyclone.

the diameter of the cyclone = 0.2 m;

the ratio of the width of poles to the circumference of the cyclone = 0.27;

the magnetic flux density B on the corner of poles = 1.0 Tesla;

$d_{50c,m}$ of the shale = 79 μm;

$d_{50c,m}$ of the coal = 170 μm;

$d_{50c,m}$ of the magnetite = 4.86 μm;

6.3. SIMULATION OF MEDIA (MAGNETITE) RECOVERY USING MAGNETIC HYDROCYCLONES AS SEPARATORS IN COAL WASHING PLANT

6.3.1. A Single Stage Fricker Magnetic Hydrocyclone

A single Fricker magnetic hydrocyclone is used to recover the heavy media (fine magnetite) in the simulation.

In a coal washing plant, heavy media particles (magnetite) are mixed with the coal as the feed to the dense-media cyclone [7]. The size distribution of the coal is shown in Table 18. The relationship between the cumulative mass fraction (Y, %) and the coal size (X, mm) can be described as

$$Y = 5.37 + 41.22 \cdot Ln(X) \qquad (6.7)$$

The ash mineral, shale, has the same size distribution as the

Table 18 Size distribution of coal in the feed of dense-medium cyclone [7]

size range (mm)	ave. size (mm)	fraction (%)	cum. fraction (%)
12.5 - 9.5	11.0	5.3	100.0
9.5 - 6.3	7.9	25.1	94.7
6.3 - 2.36	4.33	47.3	69.6
2.36 - 1.18	1.77	18.9	22.3
1.18 - 0.6	0.89	3.4	3.4
Total		100.0	

coal.

As the dense medium, the magnetite particles (about 65% -325 mesh (-0.045μm)) are finer than the coal [7]. The assumption is that the size distribution of the magnetite follows the Gaudin - Schuhmann equation [1]

$$Y' = 100 \cdot \left[\frac{d}{d^*}\right]^{0.5} \qquad (6.12)$$

where Y' = the cumulative mass fraction of magnetite finer than d, %;

d* = the maximum magnetite particle size, μm;

d = the magnetite particle size, μm;

In this case, d* is 107 μm and the 50% passing size of the magnetite particles equals 27μm.

In the coal washing plant, the dense-media cyclone gives two products: the washed coal (coal and magnetite) and the waste (shale and magnetite). Assuming the size distribution of two products are the same as that of the feed to the dense-media cyclone, the result of the simulation is shown in Fig.41.

It can be seen that magnetite reports to the overflow with a recovery of 99.6% and grade of about 100% from either washed coal or waste. A Fricker magnetic hydrocyclone may be able to replace the present screen - drum magnetic separator media recovery system.

There is a feature in the magnetic hydrocyclone media recovery system: the magnetic field (> 0.5 Tesla) in the cyclone chamber is greater than that (about 0.1 Tesla) of the drum magnetic separator. Consequently a demagnetizing stage must be used to

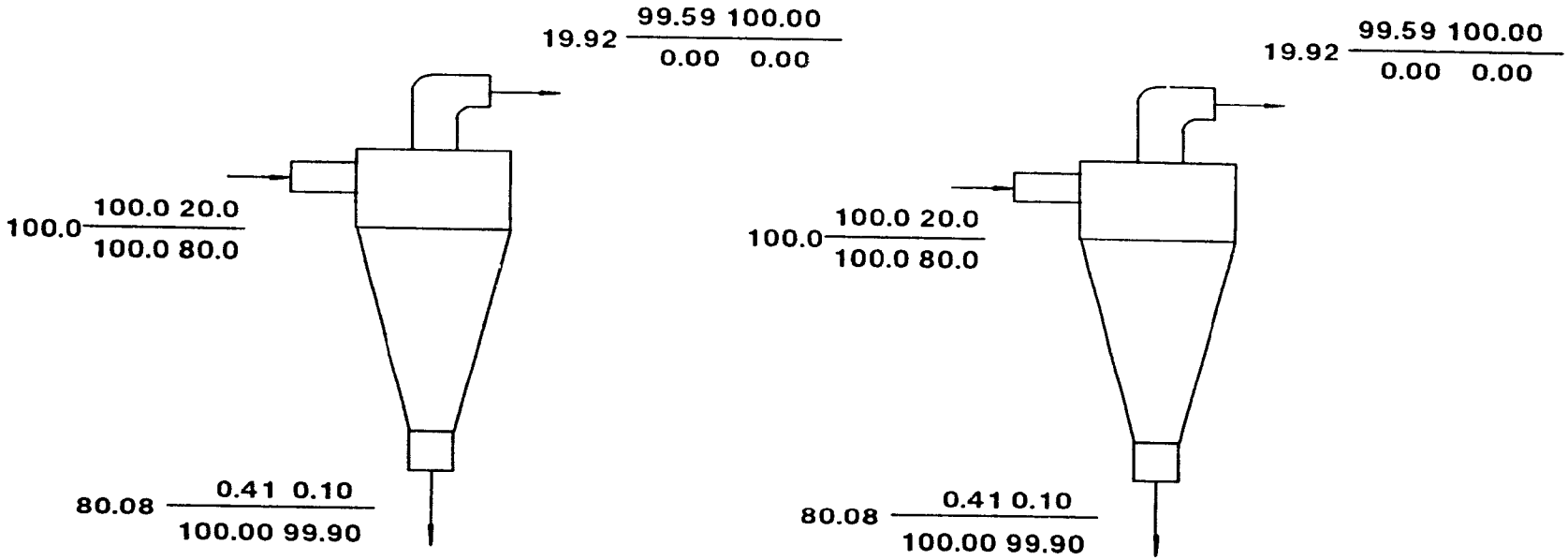

(a) magnetite-coal

(b) magnetite-shale

$$D \frac{E\ F}{G\ H}$$

D - mass recovery of the product,%

E - recovery of magnetite,%

F - grade of magnetite,%

G - recovery of coal or shale,%

H - grade of coal or shale,%

Figure 41. Simulation of a Fricker magnetic hydrocyclone for recovering heavy media (magnetite) in coal washing plant

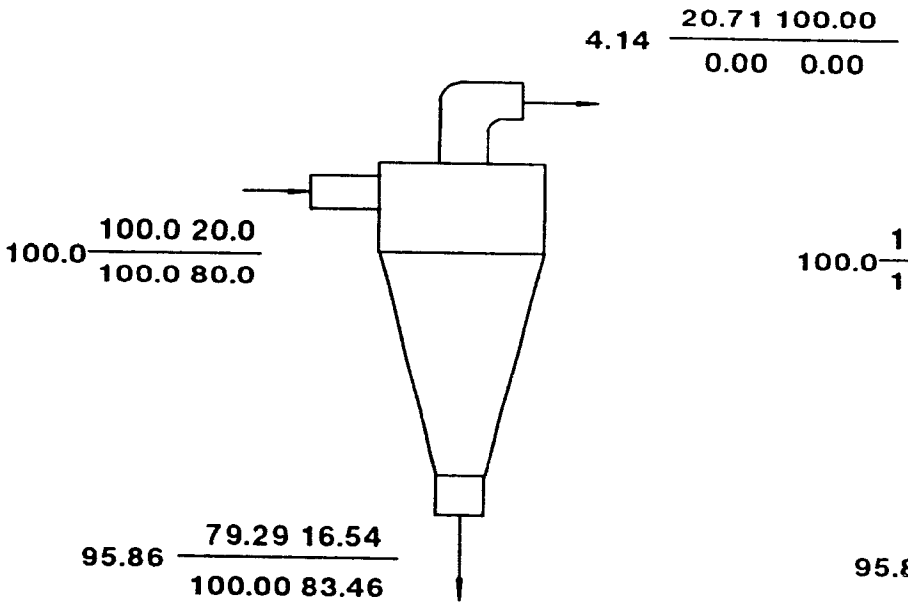

(a) magnetite-coal

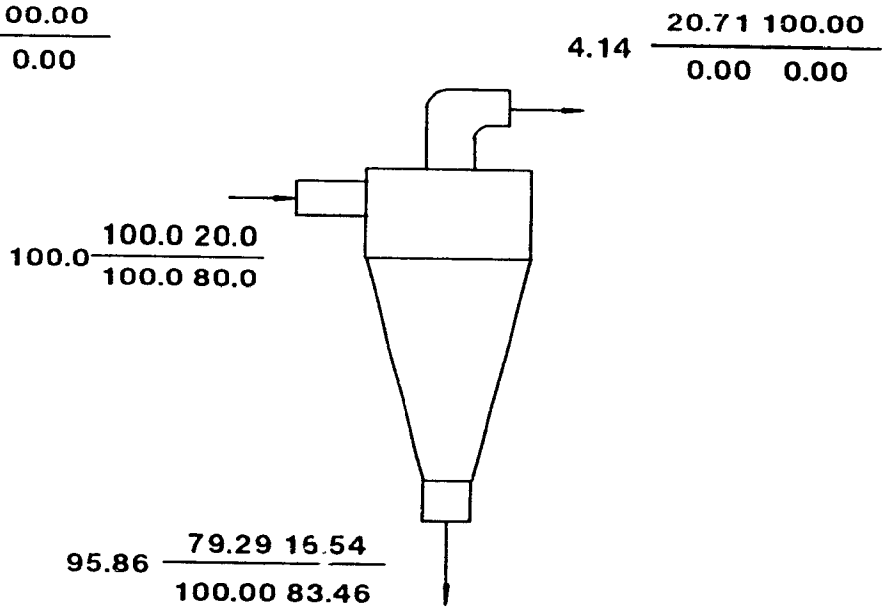

(b) magnetite-shale

$D \frac{E\ F}{G\ H}$

D - mass recovery of the product,%

E - recovery of magnetite,%

F - grade of magnetite,%

G - recovery of coal or shale,%

H - grade of coal or shale,%

Figure 42. Simulation of the 16 pole design of Watson magnetic hydrocyclone for heavy media (magnetite) in coal washing plant

avoid magnetic flocculation in the recycle of dense media.

6.3.2. A Single Stage 16 pole Watson Magnetic Hydrocyclone

In the Watson magnetic hydrocyclone, fine magnetite particles are attracted to the underflow by a strong magnetic force and the coarse coal (or shale) particles report to the underflow as well. Fig. 42 shows that the magnetite is mixed with the coal (or shale) in the underflow. Although the magnetite can be obtained with a grade of about 100% in the overflow, its recovery (20.7%) is much lower than that (99.6%) of the Fricker's magnetic hydrocyclone. It can be seen that a single stage 16 pole Watson magnetic hydrocyclone is not suited to recover dense media in coal washing plants.

6.3.3. Simulation of Combination of Magnetic Hydrocyclones For Fine particles

In order to test the hypothesis that magnetic hydrocyclones could permit a smaller difference in media (magnetite) and coal/waste (shale) particle size to be efficiently separated, a simulation has been conducted with a 50% passing size of media of 37μm and of coal/waste of 75μm both of which follow the Gaudin - Schuhmann distribution (Eq. 6.12).

From Figs. 43 and 44, it can be seen that a single stage of either the Fricker magnetic hydrocyclone or the 16 pole design of the Watson magnetic hydrocyclone is not able to yield a good result. However, when both magnetic hydrocyclones are used in a

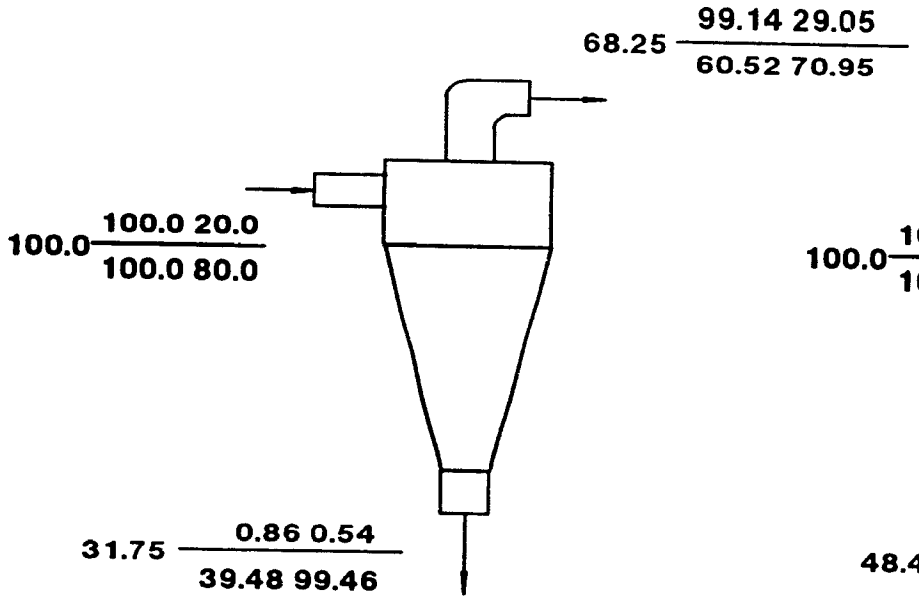

(a) Fricker

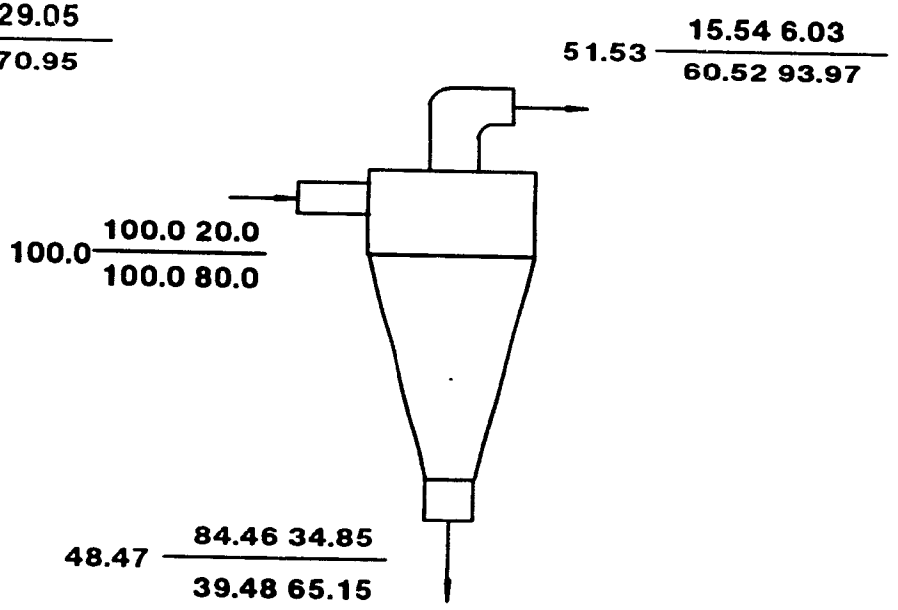

(b) the 16 pole design

$$D\ \frac{E\ F}{G\ H}$$

D - mass recovery of the product,%
E - recovery of magnetite,%
F - grade of magnetite,%
G - recovery of coal,%
H - grade of coal,%

Figure 43. Simulation of magnetic hydrocyclones with a feed of fine magnetite and coal particles

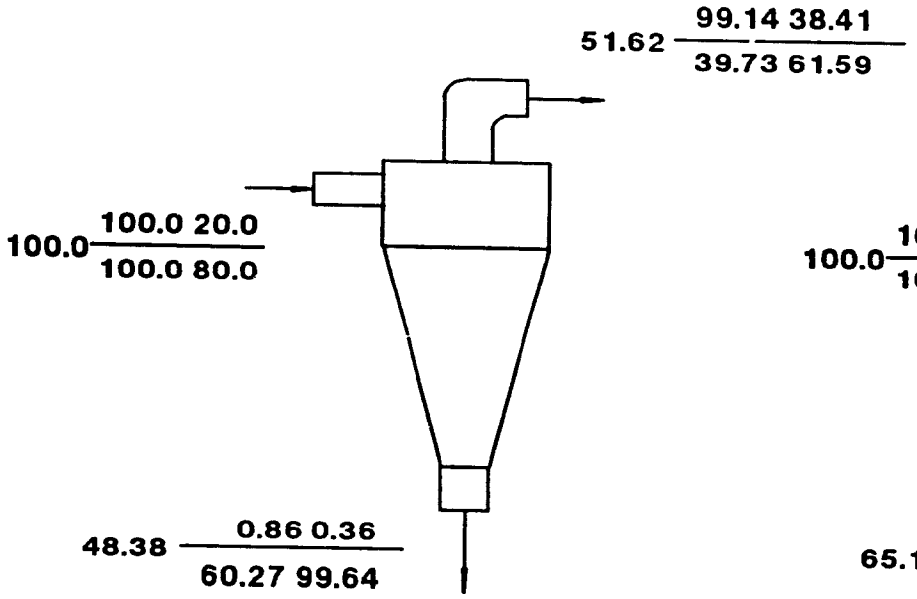

(a) Fricker

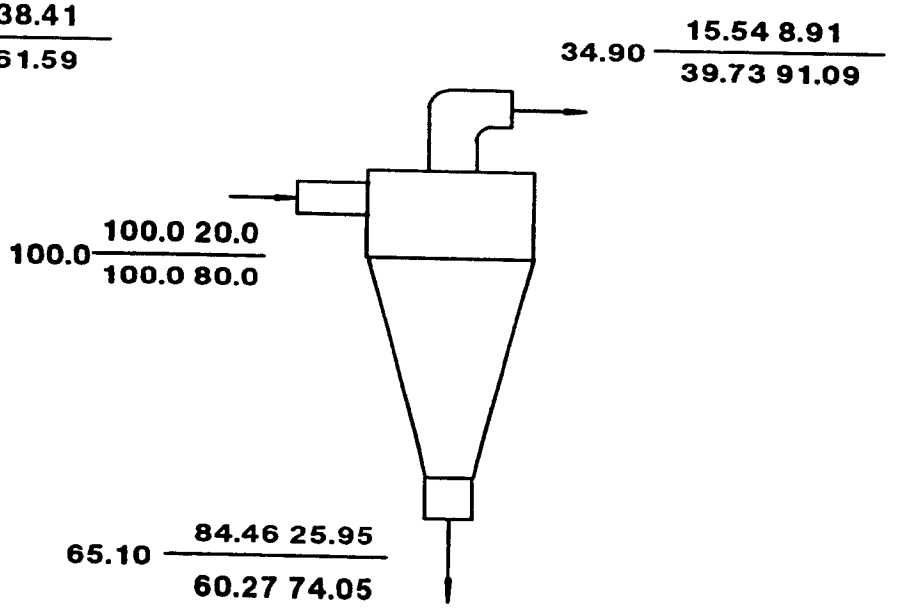

(b) the 16 pole design

$$D \frac{E\ F}{G\ H}$$

D - mass recovery of the product,%
E - recovery of magnetite,%
F - grade of magnetite,%
G - recovery of shale,%
H - grade of shale,%

Figure 44. Simulation of magnetic hydrocyclones with a feed of fine magnetite and shale particles

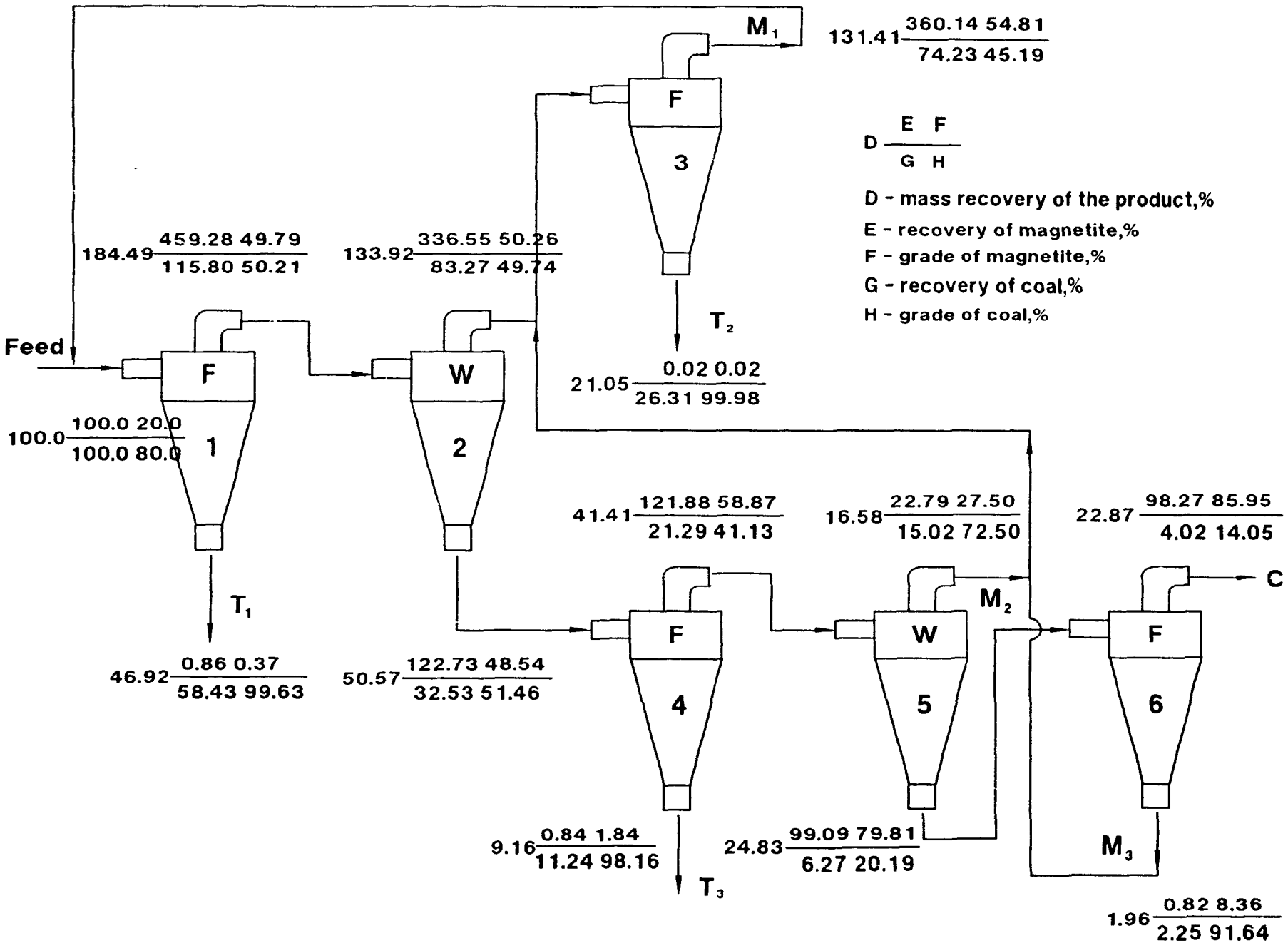

Figure 45. Simulation of a magnetic hydrocyclone circuit with a feed of fine magnetite and coal particles

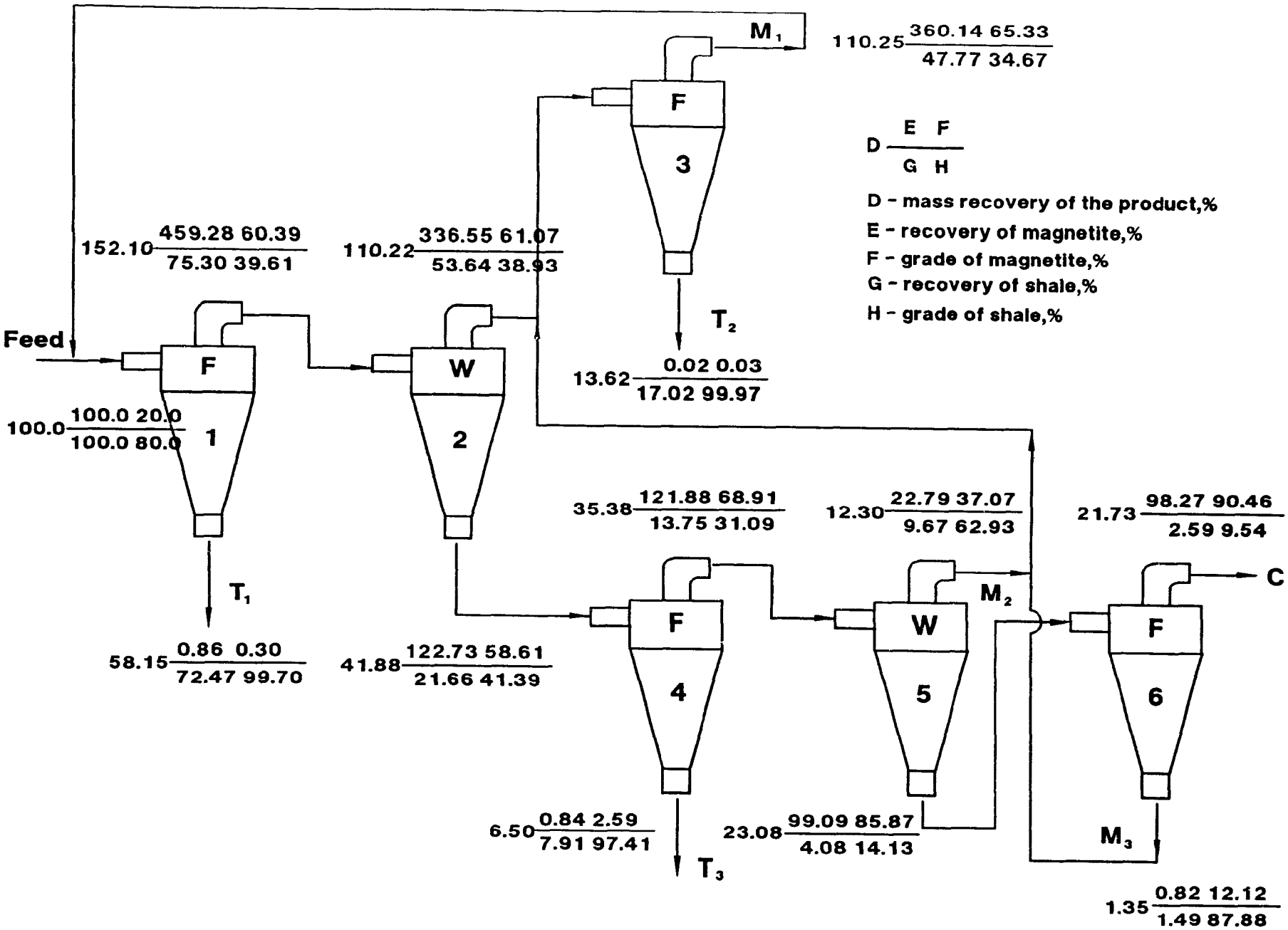

Figure 46. Simulation of a magnetic hydrocyclone circuit with a feed of fine magnetite and shale particles

circuit (Figs. 45 and 46), a high grade magnetite (about 90%) with a high recovery (>98%) may be achieved, although the circuit becomes quite complex.

In this type of circuit, there is one concentrate, three middlings and three tailings. The concentrate is the overflow of the Fricker magnetic hydrocyclone in the sixth stage. With a magnetite grade of 20% in feed, the magnetite concentrate grade is 86% and the recovery over 98% in the magnetite - coal system (Fig.45). From Fig.46, it can be seen that the magnetite concentrate grade is 90.5% with a recovery of over 98% in the magnetite - shale system.

Because the simulations are based only on the corrected performance curves, it is difficult to evaluate some operational characteristics of the magnetic hydrocyclones such as volumetric capacity, feed solids concentration, etc. These operational parameters need to studied in actual tests.

CHAPTER SEVEN

CONCLUSIONS AND SUGGESTIONS FOR FUTURE WORK

7.1. CONCLUSIONS

7.1.1. Numerical Analysis Has Been Applied to The Study of Magnetic Hydrocyclones

1. Five indices of the magnetic field, A.R.F., A.A.R.F., A.T.F., A.A.T.F. and the magnetic energy, have been used to evaluate the magnetic field in the magnetic hydrocyclone.

2. The relationship between the magnetic field and separation has been explored for both Fricker's and Watson's magnetic hydrocyclones.

3. New designs of multipole magnetic circuitry have been developed for the Watson type magnetic hydrocyclone. The optimum design is derived.

7.1.2. Simulation Using Two Types of Magnetic Hydrocyclone Has Been Conducted

1. A single stage Fricker magnetic hydrocyclone may be used for recovering the heavy media (fine magnetite) in a coal washing plant. The possibility of obtaining high recovery and grade of media has been shown. A single stage Watson magnetic hydrocyclone is not suitable in this case.

2. A circuit using combinations of the Fricker magnetic hydrocyclone and the 16 pole Watson magnetic hydrocyclone has been explored for the separation of magnetite from fine coal/shale particles.

7.2. SUGGESTIONS FOR FUTURE WORK

7.2.1. Experimental Work

1. To test the new 16 pole design of the Watson magnetic hydrocyclone.

2. To test the circuit using combinations of the Fricker magnetic hydrocyclone and the new 16 pole design of the Watson magnetic hydrocyclone.

3. To conduct pilot - scale tests using magnetic hydrocyclones for heavy media recovery in a coal washing plant.

7.2.2. Numerical Analysis

1. To develop the three dimensional numerical analysis of the magnetic circuitry into a software package for the design of magnetic hydrocyclones.

2. To construct a mathematical model of the performance of magnetic hydrocyclones.

3. To explore theoretically magnetic hydrocyclones using superconductivity technology.

REFERENCES

1. E.G.Kelly and D.J.Spottiswood, *Introduction to Mineral Processing*, John Wiley & Sons, Inc.(1982)
2. L.Svarovsky, *Hydrocyclones*, Technomic Publishing Co.,Inc.(1984)
3. A.G.Fricker, "Magnetic Hydrocyclone Separator", *Trans. Instn Min. Metall (Sect.C)*, 94, (September 1985)
4. J.L.Watson, "Cycloning in Magnetic Fields", AIME/SME Preprint 83-335. presented at the SME–AIME Fall Meeting and Exhibit, Salt Lake City, Utah, October 19–21, 1983
5. B.C.Flintoff, L.R.Plitt and A.A.Turak, "Cyclone Modelling: a Review of Present Technology", *CIM Bulletin*, 39-50 (September 1987)
6. D.R.Kelland, G.S.Dobby and E.Maxwell, "Efficient HGMS for Highly Magnetic Materials", *IEEE Trans. Magn., Vol. MAG-17, No.6*, 3308 - 3310 (Novenber 1981)
7. J.W.Leonard, etc., *Coal Preparation*, (fourth edition), Port City Press, Inc. (1979)
8. L.R.Plitt, "A Mathematical Model of The Hydrocyclone Classifier" *CIM Bulletin*, 114 - 123 (December 1976)
9. J.A.Finch and M.Leroux, "Selecting Test Condition For High Gradient Magnetic Separation", *Int. J. Miner. Process.* 9, 329 - 341 (1982)
10. J.Svoboda, *Magnetic Methods for The Treatment of Minerals*, Developments in Mineral Processing, Volume 8, Elsevier, (1987)

11. K.J.Binns and P.J.Lawrenson, *Analysis and Computation of Electric and Magnetic Field Problems*, Oxford, Pergamon Press, (1973)

12. S.V.Patankar, *Numerical Heat Transfer And Fluid Flow*, Washington, Hemisphere Publishing Corporation, (1980)

13. D.F.Kelsall, "A Study of the Motion of Solid Particles in a Hydraulic Cyclone", *Trans. Inst. Chem. Eng.*, 30, 87-104 (1952)

14. G.Dobby and J.A.Finch, "Capture of Mineral Particles in a High Gradient Magnetic Field", *Powder Technol.* 17, 73-82 (1977)

APPENDIX A

Units and Conversions [9]

Conversion of magnetic units requires careful attention.

Units

cgs system	SI system
$B = H + 4\pi M$	$B = \mu_o H + \mu_o M^*$
B in gauss	B in webers/meter^2 (or tesla)
H in oersted	H in amperes/meter
M in emu/cm^3	M in amperes/meter
κ = M/H in emu/cm^3 Oe	κ = M/H dimensionless
μ_o (vacuum) = 1	μ_o (vacuum) = 4π X 10^{-7} in webers/ampere meter (or henries/meter, or tesla meter/ampere)

Conversions

B:	1 gauss	= 10^{-4} tesla
H:	1 oersted	= 79.6 amperes/meter
M:	1 emu/cm^3	= 10^3 amperes/meter
κ:	1 emu/cm^3	= 12.56 (dimensionless SI)

* This is sometimes expressed: $B = \mu_o H + M$

APPENDIX B

Cut Sizes d50 and d50c [8]

The d_{50} is that size of particle which has an equal (50 per cent) probability of reporting to either underflow or overflow of the hydrocyclone. As the underflow water entrains feed solids of all sizes which bypass the classification process, the actual classification must be corrected to reveal the true effects of the classification process. The corrected classification is:

$$Y' = \frac{Y - Rf}{1 - Rf}$$

where Y = mass fraction of a given size which actually will report to the underflow;

Y' = mass fraction of a given size which will be directed to the underflow as a result of the classifying action;

Rf = recovery of feed liquid to the underflow;

The d_{50c} is the corrected cut size with $Y' = 0.5$. It is the most important parameter for describing the performance of the hydrocyclone.